Elucidating metabolic alterations in myeloproliferative neoplasms: Implications for treatment

Fei Yan

Thesis submitted to the University of Glasgow in accordance with the requirements for the degree of Doctor of Philosophy

Institute of Cancer Science

College of Medical, Veterinary and Life Sciences

University of Glasgow

October 2024

CRUK Beatson Institute

Garscube Estate

Switchback Road

Bearsden, Glasgow

Abstract

Myeloproliferative neoplasms (MPN) are haematopoietic disorders leading to aberrant expansion of myeloid, erythroid and megakaryocytic lineages, which are classified into three phenotypes namely Polycythaemia Vera (PV), Essential Thrombocythemia (ET) and Primary Myelofibrosis (PMF). The three main somatic mutations leading to MPN are Janus Kinase 2 V617F (JAK2V617F), Janus Kinase 2 exon 12 and Calreticulin (CALR). JAK2V617F was the first driver mutation found in MPNs, with a mutation rate of 95%/60%/55% in PV, ET and PMF respectively. Janus Kinase 2 is one of the four Janus proteins that are constructed to transmit signals from cytokines to downstream pathways. Inside normal cells, Janus Kinase 2 has a dual kinase structure with two domains: an active tyrosine kinase domain JH1 and a catalytically inactive pseudokinase domain JH2. Both domains interact with each other, depending on cellular context with JH2 inhibiting JH1 in the absence of cytokines. In MPN, these mutations lead to the inhibition of JH1 and constitutive activation of downstream signalling pathways including STAT5, RAS/MAPK and PI3K/Akt/mTOR pathways in the absence of growth factors. The discovery of JAK2 inhibitors is beneficial for improving the disease phenotype, but do not eliminate the persistent blood cancer stem cells, which are the cause of the disease. It is therefore important, to find novel therapeutic ways to target blood cancer stem cells. To sustain accelerated growth rate, cancer cells need abnormally high amounts of energy, taken up as nutrients (e.g. glucose), and to increase the breakdown of such nutrients through metabolic pathways. In addition, cancer cells often alter the amount of oxygen they require for the purpose of growing rapidly. Cancer cells therefore alter normal cellular metabolic pathways. Importantly, relying on these alterations makes them vulnerable and targeting altered metabolism and oxygen consumption is an attractive approach to eliminate cancer therapeutically.

My data indicate that metabolic processes are deregulated in MPN. In this thesis, experiments have been performed using advanced assays including Seahorse Metabolic Flux Assay, Liquid Chromatography-Mass Spectrometry, and Flow-cytometry. C57Bl/6 background JAK2V617F mice bone marrow cells were used.

We have found the increased oxidative phosphorylation and glycolysis rates in MPN Homozygous and heterozygous mice c-kit^{+} cells. Furthermore, three solute carriers—SLC25A37, SLC2A4, and SLC43A1—were highly expressed in HSCs from homozygous mice, suggesting that targeting glutamine as an anaplerotic pathway could be a potential therapeutic approach.

Table of Contents

List of Tables

List of Figures

Author’s declaration

I hereby testify that all the work presented in this thesis is my own, unless otherwise stated. I confirm that this work has not been previously submitted for consideration for any other degree.

Fei Yan

Acknowledgments

I would like to begin by expressing my deepest gratitude to my primary supervisor, Professor Kristina Kirschner. From the outset of this PhD journey to its completion, you have consistently provided opportunities for me to challenge myself, offering unwavering support not just in the lab, but in various aspects of my life. Your mentorship has been invaluable to my growth and learning. I also wish to extend my sincere thanks to my second supervisor, Professor Guðmundur Vignir Helgason. Your passion for science and zest for life have profoundly influenced me. Your resilience in the face of challenges has been a source of encouragement, and it has truly inspired me.

I am also immensely grateful to Kevin Rattigan, who, though not officially one of my supervisors, has acted as a third supervisor in so many ways. I deeply admire you—you are a true role model in the scientific world. Whenever I encountered difficulties or made mistakes, you never criticized me negatively. Instead, you encouraged me to learn from every mistake, even paying careful attention to the smallest details of my experiments. Your perseverance has given me hope that we can make meaningful contributions to cancer research. In addition to Kevin, I would like to express my appreciation to all the members in Kristina's lab, including Maria Terada's, Ya-Ching Hsieh, Ruchi Kumari, Neil Robertson, and Shafi Mohammed A Alotaibi. You have all been incredibly helpful. Likewise, I also want to thank the members in Vignir's lab, including Lucie de, Desiree Zerbst, Daniele Sarnello, Bodhayan Prasad, Ekaterini Himonas, Stephen Wilkie, Eric Kalkman, Kiron Roy, Zosmber Kerekes, Martha Zarou, for their assistance when I faced challenges during experiments. A special mention goes to Ahmed Khalaf—I cherished our discussions, and though he has passed away, his impact on me remains.

I am also very thankful for the support of all the technicians who have helped me along the way: Yi-Hsia Liu, Tom Gilbey and Jennifer Cassels from Flow cytometry facility, David Sumpton from Metabolomics facility, Robin Shaw, Ryan Kwan from the Computational biology facility. I am also very grateful to Karen Dunn and all the staff at Beatson BSU mice facility. Your help has been crucial to my work, and I am grateful for all the support you have provided over the years.

Beyond these specific individuals, I would like to extend my thanks to all the

friends and colleagues I've met at the Beatson Institute. It has been a truly wonderful journey, and I am grateful to people like Chris Halsey, Hakem Mohsen M Albilasi, Peggy Paschke, Ed Roberts, Chiara Pirillo, Catherine Cloix, and Boyu Yu. I am also grateful to my three reviewers, Alison Michie, Oliver Maddocks, and Saverio Tardito and especially my convenor Heather Jorgensen, for your patient and constant support.

Lastly, I would like to thank my dear parents, who have stood by me throughout my entire PhD experience. Their understanding and unwavering support mean the world to me. Finally, to my friends, both in China and in the UK, thank you for the care and kindness you've shown during difficult times. Special thanks went to David Blenkinson at Sandyford Memorial Church—your boundless support brought me immense warmth during my time in Glasgow.

To the only wise God, through Jesus Christ— to him be the glory forever! Amen.

Romans 16:27

Abbreviations

ANOVA	Analysis of variance
ATP	Adenosine triphosphate
BIT	Bovine serum albumin, insulin and transferrin
BM	Bone marrow
BSA	Bovine serum albumin
MPN	Myeloproliferative Neoplasms
MPN HSPCs	Myeloproliferative Neoplasms Hematopoietic stem and progenitor cells
CoA	Coenzyme A
DMEM	Dulbecco's Modified Eagle Medium
DMSO	Dimethyl sulfoxide
DNA	Deoxyribonucleic acid
ECAR	Extracellular acidification rate
ETC	Electron transport chain
FACS	Fluorescence-activated cell sorting
FAO	Fatty acid oxidation
FBS	Foetal bovine serum
FSC	forward-angle light scatters
G-CSF	Granulocyte colony-stimulating factor
GLS	Glutaminase
GM-CSF	Granulocyte-macrophage colony-stimulating factor
HIF-1α	Hypoxia-inducible factor 1-alpha
HSC	Haematopoietic stem cell
HSPCs	Haematopoietic stem and progenitor cells
IFN-α	Interferon-alpha
IL-3	Interleukin-3
IL-6	Interleukin-6
IMDM	Iscove's Modified Dulbecco's Medium
LC-MS	Liquid chromatography-mass spectrometry
LDH	Lactate dehydrogenase
Lin	Lineage
LSC	Leukaemic stem cell

LT-HSC	Long-term haematopoietic stem cell
MEP	Megakaryocyte/erythroid progenitor
MPP	Multipotent progenitor
MT-CO1	Cytochrome c oxidase subunit 1
MT-CO2	Cytochrome c oxidase subunit 2
NFκB	Nuclear factor-κB
OCR	Oxygen consumption rate
OXPHOS	Oxidative phosphorylation
PC	Pyruvate carboxylase
PDH	Pyruvate dehydrogenase
PDK	Pyruvate dehydrogenase kinase
PI	Propidium iodide
PI3K	Phosphoinositide 3-kinase
RNA	Ribonucleic acid
RPMI	Roswell Park Memorial Institute
S.D.	Standard deviation
S.E.M	Standard error of the mean
SCF	Stem-cell factor
SDS	Sodium dodecyl sulfate
STAT5	Signal transducer of activation and transcription 5
TCA	Tricarboxylic acid
TMRM	Tetramethylrhodamine, methyl ester

1 Chapter1 Introduction

Myeloproliferative neoplasms (MPNs) are haematopoietic disorders driven by somatically mutated haematopoietic stem cells (HSCs) that lead to the aberrant expansion of myeloid, erythroid and megakaryocytic lineages (Spivak, 2017). They are classified into three types--Polycythaemia Vera (PV), Essential Thrombocythemia (ET), and Primary Myelofibrosis (PMF) --mainly according to the lineages involved in the expansion, with the symptoms not only expressing high erythrocytes, megakaryocytes, platelets, but also include frequent headaches and other symptoms (Spivak, 2017). All three phenotypes carry a risk of progressing into Acute Myeloid Leukemia (AML) with 2-14%, 1-5% and 10-20% of PV, ET, and PMF cases, respectively (Spivak, 2017). In order to prevent the patients from progressing to AML, reduce the symptoms and decrease the blood cell counts, there are ongoing treatments for MPN patients (Greenfield et al., 2021). There are JAK2 inhibitors as the first-line drug like Ruxolitinib and Fedratinib, which are quite common to use to reduce the JAK2 expression level of the cells (How and Hobbs, 2020). Hydroxyurea and interferon are also used either solely or as a combination of JAK2 inhibitors to control the inflammation of the disease (How and Hobbs, 2020). However, the treatments are not specifically targeting mutated hematopoietic stem cells but also could not restrict the expansion of mutated HSCs. So recent years, significant research has focused on identifying characteristics of somatic mutated HSCs that are core for the disease development. As a result of this, the investigation of abnormal mutated HSCs is not only compared to normal HSCs function in the aspect of self-renewal or differentiation (biological process or pathways) but also compared to other cancer stem cells or leukemic stem cells. Cancer cell metabolism is also regarded as one of the hallmarks of cancer. These cells seem quite active in cell metabolism which was also, as seen on Skoda's paper (Nageswara Rao et al., 2019). As a result of this, targeting cancer metabolism becomes a potential target for mutated HSCs in MPN.

Somatic mutations, genetic predisposition, metabolic reprogramming and inflammation/immunity have been investigated as mechanisms favoring the expansion of mutated HSCs (Rumi and Cazzola, 2017). Several signalling pathways underlie the expansion of mutated HSCs in MPN, including the Janus

Kinase 2-Signal Transducer and Activator of Transcription (JAK2-STAT) pathway, Phosphoinositide 3-kinase/mammalian target of rapamycin (PI3K/mTOR) pathway, Ras/mitogen-activated protein kinases/mitogen-activated protein kinase (RAS/MAPK) pathway, and Nuclear factor kappa-light-chain-enhancer of activated B cells (NF-KB) pathway (Ortmann et al., 2015).

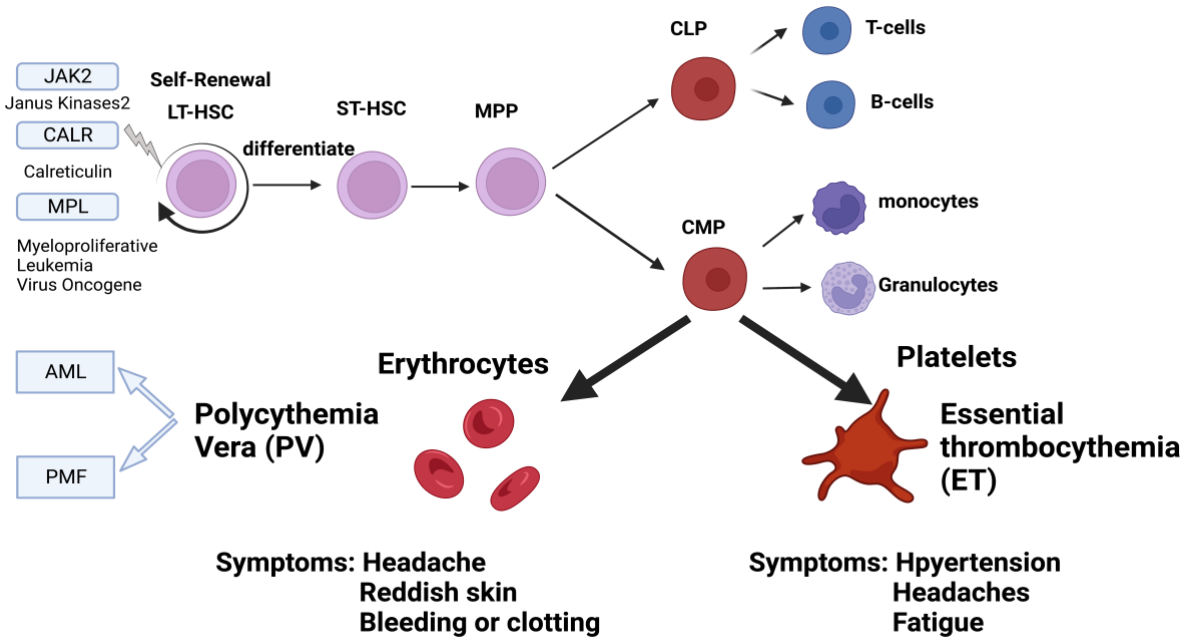

Figure 1.1 Myeloproliferative neoplasms somatic mutations, phenotypes and symptoms

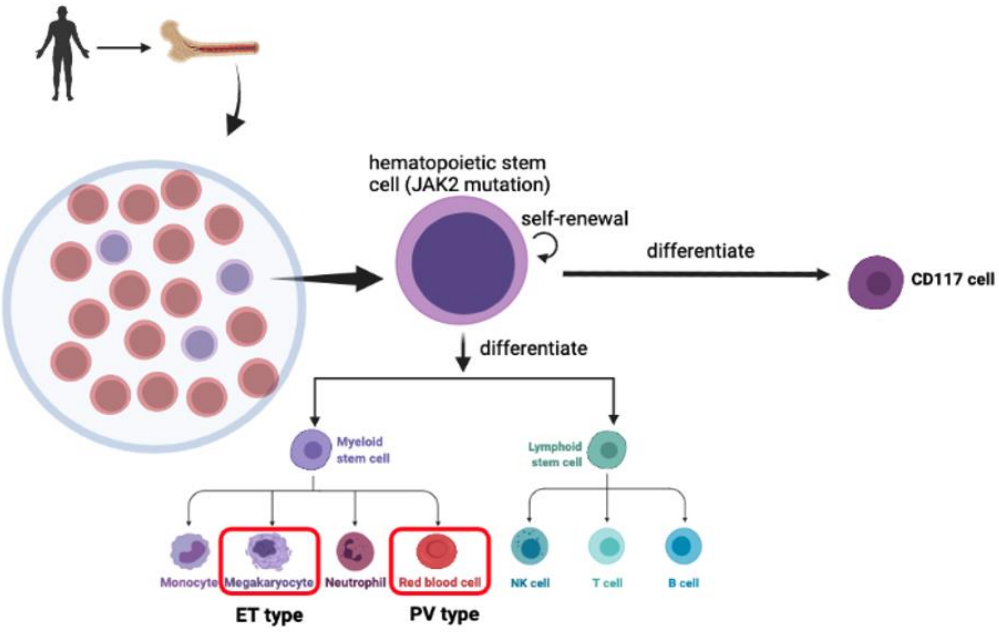

Figure 1.2 Myeloproliferative neoplasms hematopoietic stem cells and phenotypes.

1.1 Myeloproliferative Neoplasms (MPNs)

1.1.1 Clinical Epidemiology of MPN

An estimated incidence of MPN is approximately 1-2 cases per 100,000 individuals annually (Nangalia and Green, 2014). The prognosis and clinical outcomes for MPN patients vary significantly depending on the "subtype, genetic mutations and individual risk factors" (Harrison and Garcia, 2014). For instance, patients with ET and PV generally have a favourable prognosis, with median survival spanning several decades, although they remain at risk for thrombotic events and progression to MF or acute myeloid leukaemia (AML) (Harrison and Keohane, 2013). Conversely, MF is associated with a poorer prognosis, with median survival ranging from 3 to 10 years, depending on risk stratification (Chapman et al., 2018). Advances in molecular understanding, particularly the role of JAK2, CALR and MPL mutations, have improved prognostic accuracy and guided targeted therapies like JAK inhibitors, which have enhanced symptom control and quality of life for many patients (Klampfl et al., 2013). Although patients could get JAK2 inhibitors as a primary therapeutic way to reduce symptoms, disease-associated complications, including cytopenia, constitutional symptoms, and progression to AML, drug resistance and the existence of JAK2 mutation on HSCs remain unsolved, which highlights the importance of ongoing research and personalized patient management (Collotta et al., 2023).

1.1.2 Pathogenesis of MPNs

A mutation in the JAK2 gene replaces the valine with phenylalanine at position 617 (JAK2-V617F) and was the first driver mutation found in MPNs, with a mutation rate of 95%/60%/55% in PV, ET and PMF, respectively (Arranz et al., 2014; Barbui and Tefferi, 2012). Janus Kinase 2 is one of the four proteins constructed to transmit signals from cytokines to downstream pathways(Kubo et al., 2018, p. 2). In normal cells, Janus Kinase 2 has a dual kinase structure with two domains: an active tyrosine kinase domain JH1 and a catalytically inactive pseudokinase domain JH2 (Kubo et al., 2018). Both domains interact with each other, depending on cellular context with JH2 inhibiting JH1 in the absence of cytokines (Greenfield et al., 2021). In MPNs, JAK2V617F, an exon14 point mutation in JAK2 JH2, leads to reduced inhibition of JH1 and constitutive activation of downstream

signalling pathways including STAT5, RAS/MAPK and PI3K/Akt/mTOR pathways in the absence of growth factors (Greenfield et al., 2021). These downstream signalling pathways induce erythropoiesis and thrombopoiesis. Consequently, JAK2 V617F increases progenitor cell production, leading to the expansion of mature hematopoietic lineages (Tefferi and Pardanani, 2015). In addition, scientists have found other driver mutations of MPNs (Skoda et al., 2015). Another driver mutation is myeloproliferative leukaemia virus oncogene (MPL). MPL is a gene that encodes the thrombopoietin receptor. It has an extracellular cytokine-binding domain similar with JAK2, which is involved in MPL-STAT pathway signalling for thrombopoiesis (Bao et al., 2020). A somatic MPL mutation in exon 10, MPLW515, is the most common mutation among all other MPL mutations. MPL mutations have a significant impact on ET and PMF, but is not as vital as JAK2V617F in PV (Skoda et al., 2015). The calreticulin (CALR) mutation is a somatic mutation found in 20% ET and 50-60% PMF (Nangalia and Green, 2014). CALR is a multifunction protein. In the endoplasmic reticulum, CALR functions in calcium homeostasis (Klampfl et al., 2013). On a cellular level, CALR is involved in proliferation, phagocytosis, and apoptosis (Klampfl et al., 2013). CALR mutations consist of deletions or insertions in exon 9 leading to a change in the CALR C terminal domain (Nangalia and Green, 2014). The mechanism of action of CALR mutations in MPNs remains unclear, with one possible explanation being the activation of the MPL receptor, leading to JAK2 signalling pathway activation to drive thrombopoiesis (Klampfl et al., 2013). JAK-STAT signalling inhibitors are effective not only in the context of JAK2V617F mutations in MPNs, but also in CALR mutated MPNs. This indicates that the mechanism of CALR mutation is related to the JAK-STAT signalling pathway.

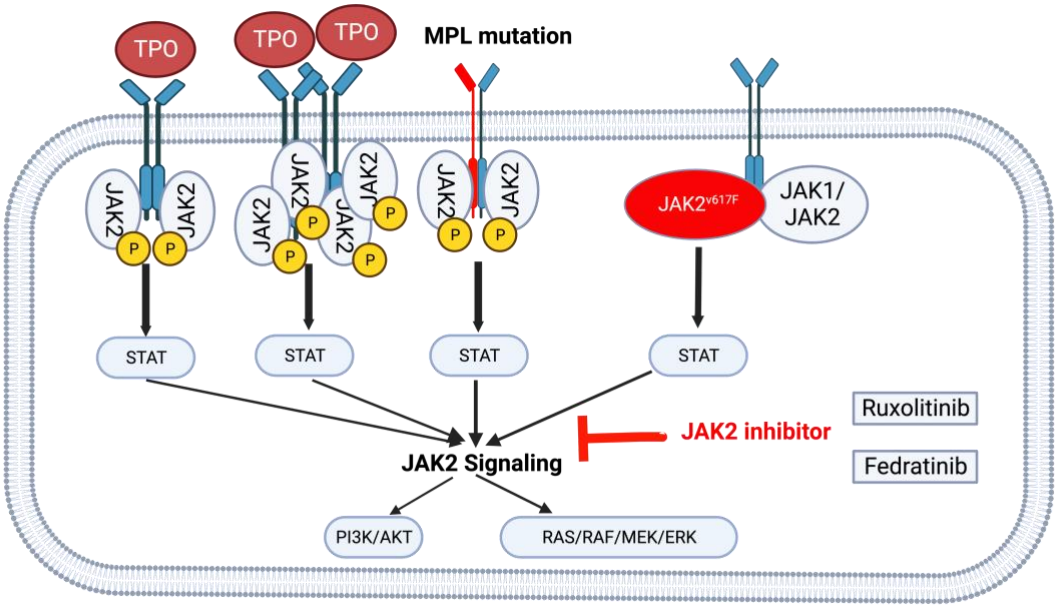

Figure 1.3 Schematic of the JAK/STAT pathway, commonly occurring mutations and JAK2 inhibitors

1.1.3 The molecular basis of Myeloproliferative Neoplasms

1.1.3.1 Normal haematopoiesis and haematopoietic stem cells

Normal haematopoiesis

Normal Hematopoiesis is governed by hematopoietic stem cells (HSCs) which either self-renew or differentiate into lineages of progenitor cells, finally resulted in a production of mature blood cells including erythrocytes, white blood cells and platelets (Olson et al., 2020).

Normal Hematopoiesis is governed by hematopoietic stem cells (HSCs) which are responsible for the production of all the mature blood cells. HSCs are resident in the bone marrow but can also exist in peripheral blood and umbilical cord blood (Olson et al., 2020). HSCs have the remarkable ability to differentiate into lymphoid and myeloid lineages. Myeloid cells are composed of Erythrocytes, Megakaryocytes, Eosinophil, Basophil, Monocytes and Neutrophil, while Lymphoid cells are composed of T cells, B cells and NK cells (Olson et al., 2020).

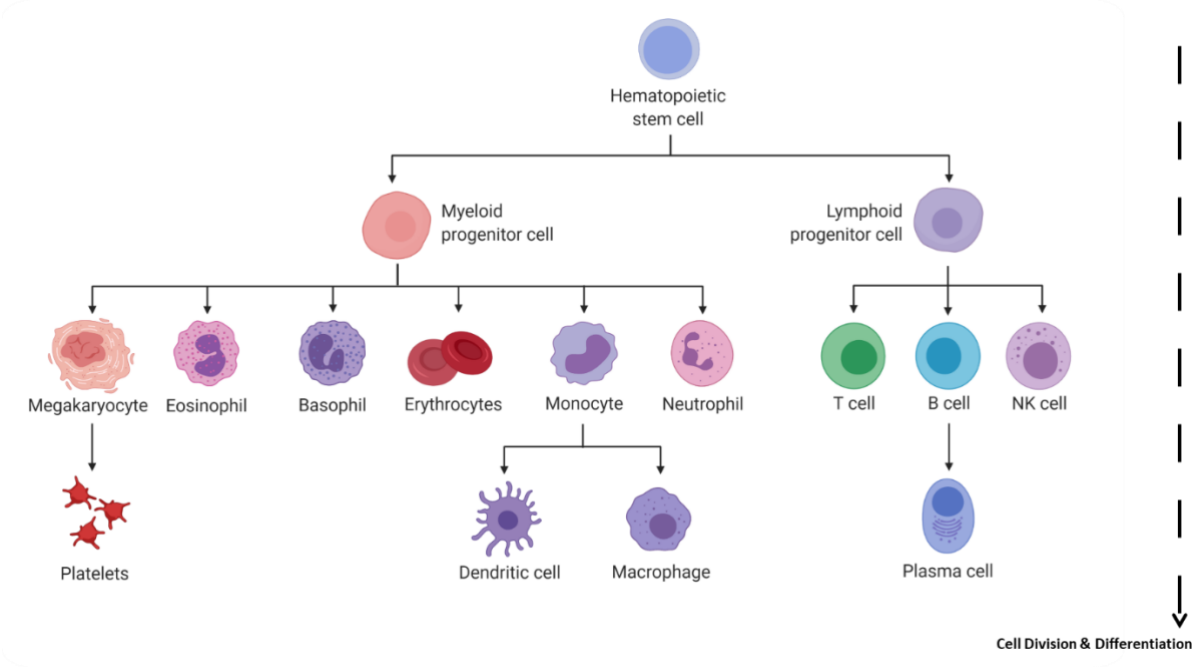

Figure 1.4 Schematic of normal Haematopoiesis showing the main cell types.

1.1.4 Isolation strategies for hematopoietic stem cells

1.1.4.1 Murine HSC Isolation Strategies

Initially, murine hematopoietic stem cells (HSCs) were isolated using $Lin^{-}Scal1^{+}c\text{-}Kit^{+}$ (LSK) markers in mice bone marrow cells, which include all four types of multipotent progenitors (MPP) (Mayle et al., 2013). Different tactics to separate purer HSC populations have evolved throughout time. For instance, $CD11b^{-}CD4^{-}$ CD90low $Lin^{-}Sca1^{+}$markers are used to specifically identify functional long-term HSCs (LT-HSCs) in the bone marrow (Morrison and Weissman, 1994). To further purify LT-HSC populations, $CD150^{+}CD244^{-}CD48^{-}$ markers, also known as SLAM markers, were developed to accurately phenotype stem cells (Yilmaz et al., 2006). Another common marker combination to enrich LT-HSCs is the 34F marker set, which includes $LSK^{+}CD34^{-}FLT3^{-}$ (Challen et al., 2009a).

Additional markers have been reported for functional murine LT-HSC enrichment, such as the LSK markers combined with Hoechst dye efflux, which can distinguish between myeloid and lymphoid-biased HSCs and remains stable with aging (Challen et al., 2009b). Other studies have identified murine LT-HSCs as LSK CD90low, fetal liver kinase 2- (Flk2) or Fms Related Receptor Tyrosine Kinase 3 (Flk3) (Christensen and Weissman, 2001). The diversity in markers used to

identify LT-HSCs highlights the heterogeneity within the LT-HSC compartment and complicates direct comparison across studies.

1.1.4.2 Human LT-HSC Isolation Strategies

Human HSCs with long-term repopulation ability were first identified in a subpopulation of $CD90^{+}CD34^{+}Lin^{-}$ cells (Baum et al., 1992). However, more heterogeneous stem and progenitor populations are often defined as $CD34^{+}CD38^{-}$ cells, which contain only a small fraction of true long-term repopulating HSCs alongside several progenitor cell populations. The addition of several markers has since refined a more purified HSC population in humans, with $Lin^{-}CD34^{+}CD38^{-}CD90^{+}CD45RA^{-}$ markers now commonly used (Ortmann et al., 2015). Since only a subset of $CD90^{+}$ cells demonstrate serial transplantation capacities in humans, (Notta et al., 2011) identified CD49f as a new marker capable of distinguishing long-term multilineage engraftment. The inclusion of $CD49f^{+}$ to $Lin^{-}CD34^{+}CD38^{-}CD90^{+}CD45RA$ further enriches the population of LT-HSCs (Notta et al., 2011).

1.1.5 Treatment of MPN

The aim of MPN treatment is to avoid the formation of thrombosis and the progression of disease to acute myeloid leukaemia (Harrison & Garcia, 2014). PV, ET and PMF patients have increased red blood cells, platelets and primary fibrotic tissues that can easily lead to thrombosis (Harrison & Garcia, 2014). Drugs currently used in the clinic are aimed to reduce the high counts of blood cells, such as phlebotomy, Aspirin, Hydroxyurea, IFN- α and Anagrelide. Phlebotomy and small dose of Aspirin are used to prevent thrombosis, with no effects on the pathogenesis of MPNs (Harrison & Garcia, 2014). Hydroxyurea is frequently used in the clinic to decrease blood counts, but it has no effect on preventing the formation of thrombosis and improving life span (Harrison & Garcia, 2014). IFN- α prohibits the proliferation of hematopoietic progenitors which leads to the decrease in the formation of mature hematopoietic lineages (Harrison & Garcia, 2014). However, immune suppressions have been resorted with IFN- α which some patients cannot tolerant (Harrison & Garcia, 2014). Anagrelide is a second line therapy to reduce platelet counts and it is now recommended for patients who are resistant to hydroxyurea (Harrison & Garcia, 2014). Targeted treatment for MPNs has improved since the discovery of JAK/STAT signalling pathway and the identification of Ruxolitinib, an inhibitor of JAK1 and JAK2. Ruxolitinib can

effectively decrease blood counts and reduce other symptoms like splenomegaly (Barbui, et al., 2013). They are especially targeted for hydroxyurea-refractory PV. However, since mutated HSCs persist, current treatments cannot stop leukemic transformation or fibrosis. Therefore, new treatment avenues must be found to target this disease (Barbui, et al., 2013) Figure 1.3.

1.1.6 MPN mouse models

1.1.6.1 Retroviral MPN mouse models

Soon after the JAK2V617F mutation was discovered, retroviral models were developed to assess its phenotypic effects in vivo. Mice transplanted with bone marrow from JAK2V617F-expressing donors rapidly developed significant polycythemia, with high penetrance following a short latency period. Additional observations included leukocytosis, splenomegaly due to extramedullary hematopoiesis, and the development of myelofibrosis. All studies showed persistent activation of Jak2 kinase signaling, Stat5 phosphorylation, and cytokine-independent colony formation. These models demonstrated that JAK2V617F expression alone is sufficient to induce myeloproliferative neoplasm (MPN) phenotypes and suggested the presence of genetic modifiers influencing JAK2V617F-mediated fibrosis, as more severe fibrosis was seen in the Blab/c strain compared to the C57Bl/6 strain (Molina et al., 2018).

1.1.6.2 Transgenic mouse models

In 2008, Zhao et al. created a transgenic mouse model using a vav gene promoter to express the JAK2V617F mutation specifically in the hematopoietic system, establishing two lines of JAK2V617F-mutated mice. One line expressed a lower level of JAK2V617F, leading to a moderate increase in blood cell counts, while the other expressed a higher level, resulting in a significant rise in blood cell counts that mimicked human ET and PV phenotypes, and even progressed to PMF as the mice aged. This transgenic model offers two main advantages: first, the transgene can be passed down through generations, and second, it can be crossed with other transgenic or knockout mice.

In the same year, two additional transgenic mouse models were developed. Kumano T et al. generated a model using the H-2Kb promoter for stable JAK2V617F expression, and Skoda et al. developed a transgenic model with

marked thrombocytosis (Xing et al., 2008).

1.1.6.3 Knock in MPN mouse models

In 2010, four JAK2V617F knock-in models were published, developed with three primary objectives: (i) to replicate human myeloproliferative neoplasms (MPNs) through physiological expression of Jak2V617F, (ii) to examine the effect of Jak2V617F gene dosage on disease phenotype, and (iii) to study the impact of Jak2V617F on hematopoietic stem and progenitor cells (HSPCs). Models by Akada, Marty, and Mullally all utilized murine Jak2V617F expressed from the endogenous murine Jak2 promoter, though with slight variations. Akada and Mullally designed conditional Jak2V617F knock-in models, while Marty's model had constitutive Jak2V617F expression. Li's model conditionally expressed human JAK2V617F from the murine Jak2 promoter. In all models, the mutant to wild-type Jak2 expression ratio was 1:1 or lower. Akada's model was unique in producing homozygous Jak2 mutant mice, but because the mutant Jak2 allele was expressed at approximately 50% of the wild-type level, Jak2V617F expression in homozygous mice was relatively low.

A summary of the Jak2V617F knock-in models and a schematic of the targeting strategies for each can be found in a recent review by Li (Li et al., 2011). The phenotypes of the three models expressing murine Jak2V617F were largely similar. In each model, mice heterozygous for the Jak2V617F mutation developed severe erythrocytosis, leucocytosis, splenomegaly due to extramedullary haematopoiesis, and, over time, myelofibrosis, though myelofibrosis was observed only in transplant recipients in Mullally's study. Compared to the other models, Li's model showed a relatively mild hematologic phenotype. Mice in this model exhibited only moderate increases in platelets and haemoglobin, more typical of essential thrombocythemia (ET) than polycythaemia vera (PV), and erythropoietin (Epo) levels were not suppressed. With extended follow-up, about 10% of the mice developed significant erythrocytosis. In this model, human JAK2V617F was expressed from the murine Jak2 promoter, though it remains unclear if human JAK2V617F signals differently in murine cells (Li et al., 2014).

1.1.6.4 Xenograft MPN mice models

Xenograft models have been developed to study BCR-ABL-negative MPN cells in vivo, enabling the functional assessment of the repopulating ability of primary human MPN $CD34^+$ cells, which retain both the complete germline and somatic genotypes of human MPN. Peripheral blood $CD34^+$ cells from myelofibrosis patients successfully engraft in NOD/SCID mice and exhibit clonal hematopoiesis with a myeloid cell bias. However, two independent studies have reported relatively poor engraftment of JAK2V617F-mutant $CD34^+$ cells from patients with polycythemia vera (PV) and essential thrombocythemia (ET). Additionally, the ratio of JAK2V617F to JAK2 wild-type SRCs was higher in myelofibrosis compared to PV, and functionally, JAK2V617F SRCs did not demonstrate a long-term proliferative advantage over wild-type SRCs. Key findings from these studies include: (i) JAK2V617F is present in a functionally competent long-term hematopoietic stem cell (LT-HSC) population, (ii) the JAK2V617F LT-HSC compartment is expanded in myelofibrosis compared to PV, and (iii) the poor engraftment of JAK2V617F $CD34^+$ cells in xenografts may be linked to CXCR4 downregulation. It's also important to consider that incompatibilities between human cytokine receptors and murine cytokines in xenograft models might impact the functional analysis of JAK2V617F, which activates cytokine receptor signaling. Overall, further refinement is needed to reliably perform xenotransplantation across a wide range of genetically diverse MPNs (Lukes et al., 2023).

1.1.6.5 The mice model used in this project

To generate mice with homozygous JAK2V617F expression, mice carrying the floxed allele (JAK2V617F, designated as $JAK2^{F/F}$) were crossed with StellaCre mice. This produced offspring with the recombined allele ($JAK2^{R/+}$) and germline heterozygous JAK2V617F expression. Since the StellaCre enzyme is active only during early embryonic development, it does not affect adult mice that carry Cre recombinase. Interbreeding $JAK2^{R/+}$ mice resulted in groups with different genotypes: wildtype ($JAK2^{+/+}$), heterozygous JAK2V617F ($JAK2^{R/+}$), and homozygous JAK2V617F ($JAK2^{R/R}$) (Li et al., 2014).

Figure 1.5 Schematic of normal mouse model generated by Li et al and used in this thesis

1.2 Metabolism and cancer

Metabolism offers basic nutrients and energy for all cell functions including cell growth, cell proliferation and cell differentiation(De Berardinis and Chandel, 2016). Basic nutrients in mammalian cells consist of glucose, amino acids, nucleotides, and lipids (Fahy et al., 2011). Energy in cells is either stored in the nutrient's chemical bones in a stable fashion or in electron transport chain in an active fashion. Energy is transferred between reduction and oxidation processes to accomplish various cell functions. These mechanisms also apply to cancer cells which are characterized by high proliferation and low differentiation(Cluntun et al., 2017). However, as cancer cells are highly proliferative, they can neither survive nor grow without metabolic alterations compared to normal cell metabolism. As metabolic alterations play a vital role in cancer development, they have become one of the hallmarks of cancer and have been targeted therapeutically (DeBerardinis et al., 2008). The key alterations in cancer cell metabolism are replenishment of molecule intermediates, balancing redox oxygen species in hypoxia and a low nutrient tumour microenvironment (Liu et al., 2020). There are two main deregulated signalling pathways leading to majority of cancer cell metabolic alterations: PI3K/AKT/mTOR and Ras/Myc. Both pathways are also altered in MPNs (Boroughs and DeBerardinis, 2015).

1.2.1 Metabolic changes in cancer stem cells

One distinguished characteristic of cancer cells metabolism is increased

biosynthesis (De Berardinis and Chandel, 2016). It requires cancer cells acquiring not only enough energy, but also replete nutrients compared to quiescent cells. Three main classes of biomass proteins, nucleotides and lipids are needed for building daughter cell organelles, cell chromatin and cell membrane respectively (Kang et al., 2018), with the PI3K/AKT/mTORC1 pathway being the main deregulated signalling pathway in increased biosynthesis (De Berardinis and Chandel, 2016).

1.2.2 Metabolic changes in Leukemic stem cells

Hematopoiesis is the process where haematopoietic stem cells differentiate into mature blood cells (Ito and Ito, 2018). Haematopoietic stem cells (HSCs) can also renew themselves to maintain the HSC pool in the mammalian bone marrows (Ito and Ito, 2018). The ratio between hematopoiesis and self-renewal is crucial (Ito and Ito, 2018). An imbalance in this ratio either leads to exhaustion of the HSC pool or generating leukemic haematopoietic stem cell (LSC) (Ito and Ito, 2018). As a result, the fate of HSC has been targeted therapeutically in haematopoietic malignancies (Kuntz et al., 2017). Scientists have attempted to convert uncontrollable LSC into commitment (Kuntz et al., 2017). Metabolism is crucial to the fate of HSCs through mitochondrial autophagy (mitophagy), balance of redox oxygen species and increased anaplerotic pathway (Ito et al., 2019).

1.2.3 Metabolism and MPN

1.2.3.1 Mitophagy and Autophagy

Alterations in metabolism leading to a shift towards anaerobic glycolysis in normal HSCs results from mitophagy. Mitophagy plays a role in clearing damaged mitochondria during HSC division. HSC division consists of symmetric division (SD), asymmetric division (AD) and symmetric commitment (SC) (Ito and Ito, 2018). SD leads to two HSCs, while AD produces one HSC and one mature cell, SC produces two mature cells. In mammary epithelial stem-like cells it has been shown that AD was used to force mitochondria into the differentiated daughter cells to keep the stem daughter cell capacity for renewal (Ito and Ito, 2018). During SD of the same cells, mitochondria were distributed evenly between the

two daughter stem cells (Ito and Ito, 2018). These two mitochondrial division patterns revealed the necessity of damaged mitochondrial clearance to keep HSC self-renewal capacity.

PTEN-induced putative kinase1 (PINK1) degradation decreases when damaged mitochondria are depolarized. PINK1 accumulates to phosphorylate ubiquitin chains recruiting Parkin and resulting in E3 ligase activity. Autophagosomes are generated when mitochondrial proteins are polyubiquitinated (Yang and Suda, 2018). Mitochondria degradation then processes through mitophagy. Because fatty acid oxidation and oxidative phosphorylation both take place in mitochondria, mitochondrial mitophagy shifts HSC cell metabolic traits to anaerobic glycolysis instead of mitochondrial respiration (Simsek et al., 2010). It has been found that both long-term HSCs (LT-HSCs) and cells with low mitochondrial potential have low ATP levels which indicates decreased mitochondrial oxidative phosphorylation (Simsek et al., 2010). These findings are consistent with the microenvironment HSCs are resident in (Simsek et al., 2010). In the hypoxic bone marrow, HSCs keep the capacity to self-renew by shifting their metabolic status to anaerobic glycolysis (Simsek et al., 2010). Some leukemic stem cells (LSCs) keep quiescence through autophagy as normal HSCs do, continuously keep the capacity differentiating to abnormal blood cells which could be one reason for haematological malignancies drug resistance (Baquero et al., 2019). Primitive CML cells have been shown to have high levels of basal autophagy (Baquero et al., 2019). Targeting LSC autophagy has therefore been identified as a therapeutic avenue (Baquero et al., 2019).

1.2.3.2 Balance of haematopoietic stem cell homeostasis

Haematopoietic stem cell homeostasis refers to the maintenance of HSC quiescence. Two main factors will lead to an imbalance of HSC homeostasis imbalance: Increased intracellular redox oxygen species (ROS) and upregulation of oxidative phosphorylation (Oxphos)(De Berardinis and Chandel, 2016). Redox oxygen species refers to intracellular chemicals which contain a superoxide anion (O2-) and a hydroxyl radical (OH-). ROS is produced during the one-electron reduction of oxygen through Nicotinamide adenine dinucleotide phosphate (NADPH) oxidases (NOXs) (De Berardinis and Chandel, 2016). There are NADPH related antioxidant defense systems to counteract the oxidation of lipids,

proteins and DNA by ROS(De Berardinis and Chandel, 2016). However, it has been demonstrated that ROS levels are increased in cancer cells at specific locations compared normal cells, helping to initiate cancer cell signalling pathways such as PI3K, mitogen activated protein kinase/extracellular signal-regulated kinase (MAPK/ERK), transcription factors HIF and nuclear factor (NF-kB) for tumorigeneses (De Berardinis and Chandel, 2016). At the same time, to avoid increased damage by elevated ROS levels, cancer cells increase their antioxidant defense system. One way of increasing the antioxidant defense system is by activating the transcription factor Nuclear Factor (Erythroid-Derived 2)-Like 2 (NRF2)(Ito and Ito, 2018). NRF2 then induces the transcription of antioxidant proteins and activates relevant enzymes increasing the level of cytosolic NADPH(Ito and Ito, 2018). Therefore, targeting cancer cells antioxidant defense system has been suggested as a therapeutic approach, accumulating ROS to damage cancer cells(De Berardinis and Chandel, 2016). Quiescent HSCs have a low ROS level environment. However, increased ROS levels in quiescent HSC lead to HSC differentiation, ultimately causing HSC exhaustion(Ito and Ito, 2018). Because ROS levels are highly related to NADPH metabolic procedures playing a role in the oxidative pentose phosphate pathway (PPP), alterations in IDH1 and one carbon metabolism, have been regarded to be crucial characteristics of LSCs (De Berardinis and Chandel, 2016). Upregulation of oxidative phosphorylation will also accumulate impaired mitochondrial, thereby limits the capacity for HSC self-renewal, shifting HSC fate to differentiation.

1.2.3.3 Increased anaplerotic pathway

One of the metabolic alterations in cancer cells, including LSCs, is an increase in the anaplerotic pathway. It also applies to the leukemic stem cells. Alterations in anaplerotic pathways includes fatty acid oxidation, amino acid synthesis, glycolysis and glutaminase (**Error! Reference source not found.**). It has been found that $CD34^{+}CD38^{-}$ CML cells have increased anaplerotic metabolites like aspartate, glutamate and acetyl-coA which provide enough energy and maintain the carbon and nitrogen pool (Kuntz et al., 2017). It also has been reported that $CD34^{+}CD38^{-}$ CML cells have increased oxidative phosphorylation which is different from normal HSC metabolic traits (Kuntz et al., 2017). Increased oxidative phosphorylation was also found in MPNs by examining JAK2 mutant mice (Nageswara Rao et al., 2019). It was reported that hyperactive erythropoiesis results in hypoglycemia

which indicate high glucose consumption in JAK2 mutant hematopoietic cells (Nageswara Rao et al., 2019). Further studies are needed to clarify these findings and add mechanistic insight.

1.2.4 Metabolic pathway changes in cancer stem cells

1.2.4.1 Glucose and Glutamine pathways changes in cancer stem cells

Glutamine

Glutamine is obtained from the extracellular environment through Alanine-Serine-Cysteine transporter2 (ASCT2) encoded by the Solute Carrier 1A5 (SLC1A5) gene (Liu et al., 2018). ASCT2 is upregulated in most cancers including breast and liver cancer (Liu et al., 2018). Both, the aberrantly activated oncogene c-myc and loss of tumour suppressor gene Retinoblastoma (Rb), participate in inducing transcription of ASCT2 (Reynolds et al., 2014). Loss of Rb indirectly drives transcription of ASCT2 via transcription factor deregulation (Reynolds et al., 2014). Consequently, glutamine intake is significantly increased in tumour cells, followed by glutaminolysis (De Berardinis and Chandel, 2016). The key enzyme that catalyzes glutamine to glutamate is glutaminase1 (GLS1), which is also upregulated by c-myc and through loss of Rb (Pavlova and Thompson, 2016). Glutamate then can be oxidized to α-ketoglutarate which is used as an anaplerotic pathway in the Tricarboxylic acid (TCA) cycle to maintain the carbon pool (De Berardinis and Chandel, 2016).

Glutamate

Glutamate can either proceed with dehydrogenase or amino transferases to generate α-ketoglutarate together with the reduction of NAD(P)+ to NAD(P)H (Choi and Park, 2018). Glutamate dehydrogen relies on Glutamate dehydrogenase (GLUD) whose mRNA is increasingly expressed in many cancer subtypes according to transcriptomic data from The Cancer Genome Atlas (Spinelli et al., 2017). Glutamate amino transferases are catalyzed by Glutamate pyruvate transaminase (GPT), Glutamate oxalate transaminase (GOT) and Phosphoserine amino transaminase1 (PSAT1) generating alanine, aspartate and phosphoserine respectively (Choi and Park, 2018). All three amino acids are either involved in nucleotides or protein synthesis (Choi and Park, 2018), among which aspartate

plays a vital role in asparagine synthetase (Chiu et al., 2020). Aspartate was traced as a metabolite which represents the anaplerotic pathway used in cell metabolism (Kuntz et al., 2017). L-asparaginases (ASNase) has been widely used to target Acute lymphoblastic leukaemia (ALL) since 1970 (Chiu et al., 2020). Consequently, in cancer cells, α-ketoglutarate is replenished from glutamate for use in the TCA cycle while it is normally generated from Acetyl-coA in non-proliferating cells.

α-ketoglutarate

α-ketoglutarate is part of the glutamine anaplerotic pathway and can either generate succinate in the direction of the normal TCA cycle or be reductively carboxylated through mitochondrial IDH2 (isocitrate dehydrogenase2) to isocitrate (Zaidi et al., 2012). From one way, the majority of α-ketoglutarates are oxidized to succinate via succinyl-CoA (Choi and Park, 2018). SDH (Succinate dehydrogenase) and FH (furmarate hydratase) catalyze succinate and furmarate to generate furmarate and malate respectively (De Berardinis and Chandel, 2016). Malate then generates oxaloacetate from which Acetyl-coA is replenished (Choi and Park, 2018). Oxaloacetate is condensed by Acetyl-coA to generate citrate (Zaidi et al., 2012). On the other hand, when hypoxia-inducible factor 1 (HIF-1) is expressed, mitochondrial isocitrate dehydrogenase2 (IDH2) reversely carboxylates α-ketoglutarate to isocitrate (Wise et al., 2011). In both scenarios, citrate is exported to the cytosol (Zaidi et al., 2012).

Citrate

Citrate is vital for the synthesis of both lipids and proteins in the cytosol (Zaidi et al., 2012). After citrate is transported to the cytosol, it either generates an oncometabolite 2-hydroxyglutarate (2-HG) or is catalyzed by ATP-Citrate Lyase (ACL) to generate Acetyl-coA and oxaloacetate (Wise et al., 2011). Acetyl-coA is the main compound for the synthesis of lipids and adds acetyl groups to DNA for epigenetic acetylation (Koundouros and Poulogiannis, 2020). Oxaloacetate and pyruvate generate aspartate, which provides serine and glycine for protein synthesis (Koundouros and Poulogiannis, 2020).

1.3 Flow activated cell sorting assays for mitochondrial function

1.3.1 Oxidation of Haematopoietic stem cells

The presence of oxygen allowed eukaryotic cells to adopt a more efficient metabolic process, which facilitated the rapid advancement of eukaryotic evolution. However, aerobic metabolism also has its drawbacks, including the generation of reactive oxygen species (ROS) because of the partial reduction of oxygen. Examples of these ROS include superoxide (O_2^-), hydrogen peroxide (H_2O_2), and hydroxyl radical (OH^-). Ros were traditionally viewed as harmful by-products of cellular respiration due to their high reactivity, which allows them to modify various biomolecules within cells. Consequently, oxidative stress has been associated with aging and diseases like cancer. However, in recent decades, it has been recognized that moderate ROS production plays an essential role in regulating cellular signaling and gene expression. The term “redox signaling” has gained prominence and is now distinguished from the concept of oxidative stress. Mitochondria are quantitatively the primary source of ROS within cells. Additional enzymatic systems contributing to ROS production include xanthine oxidoreductase (XOR), uncoupled nitric oxide synthase (NOS), cyclooxygenase (COX), cytochrome P450 (monooxygenase), myeloperoxidase (MPO), lipoxygenase, and NADPH oxidases (NOX). Notably, the NADPH oxidase family evolved specifically to generate ROS as its main function. Interestingly, the first discovered member, phagocyte oxidase, was identified in the hematopoietic system, where it produces high levels of ROS needed for pathogen destruction. Genetic disorders affecting this enzyme led to chronic granulomatous disease (CGD), an innate immunity deficiency characterized by recurrent fungal and bacterial infections. Besides NOX2, the catalytic subunit of phagocyte oxidase, there are six other family members: NOX1, NOX3, NOX4, NOX5, Duox1, and Duox2. Duox1 and Duox2 contain a peroxidase-like domain and, along with NOX5, can be activated by calcium (Kauffman et al., 2016).

Haematopoietic stem cell (HSC) homeostasis refers to the maintenance of HSC numbers. Various factors can disrupt HSC homeostasis, including increased levels of intracellular reactive oxygen species (ROS) and elevated oxidative

phosphorylation (Oxphos) activity (De Bernardinis and Chandel, 2016). ROS encompasses intracellular molecules containing superoxide anions (O_2^-) and hydroxyl radicals (OH^-), produced through the one-electron reduction of oxygen mediated by NADPH and oxidases (NOXs) (De Berardinis and Chandel, 2016). NADPH-related antioxidant defense systems counteract the oxidative effects of ROS on lipids, proteins, and DNA (De Berardinis and Chandel, 2016). However, studies have shown that cancer cells have elevated ROS levels in specific cellular regions compared to normal cells, which promotes cancer signaling pathways, including PI3K, MAPK/ERK, and transcription factors like HIF and NF-kB, facilitating tumorigenesis (De Berardinis and Chandel, 2016). To manage elevated ROS and avoid damage, cancer cells upregulate their antioxidant defenses, partly through the activation of the transcription factor NRF2. NRF2 drives the transcription of antioxidant proteins and activates enzymes that boost cytosolic NADPH levels (Ito and Ito, 2018). Targeting the antioxidant defense in cancer cells has been proposed as a therapeutic approach, potentially causing ROS buildup and inducing damage in cancer cells (De Berardinis and Chandel, 2016).

In quiescent HSCs, ROS levels are typically low. However, increased ROS levels prompt HSC differentiation, ultimately leading to a depletion of the HSC pool (Ito and Ito, 2018). Since ROS levels are closely linked to NADPH metabolic pathways, which are involved in the oxidative pentose phosphate pathway (PPP), changes in isocitrate dehydrogenase (IDH), and one-carbon metabolism have been identified as key features of leukemic stem cells (LSCs) (De Berardinis and Chandel, 2016). Furthermore, increased oxidative phosphorylation can lead to the accumulation of damaged mitochondria, impairing the self-renewal ability of hematopoietic stem cells (HSCs) and directing them toward differentiation.

1.3.2 Intracellular Redox Oxygen Species Indicator: 5-(and-6)-chloromethyl-2',7'-dichlorodihydrofluorescein diacetate acetyl ester (CM-H2DCFDA)

CM-H2DCFDA is a commonly used chemical compound in scientific research, especially in the fields of cell biology and fluorescence microscopy. It is a chloromethyl derivative of H_2DCFDA, acting as an effective indicator for reactive

oxygen species (ROS) within cells and offering improved retention in live cells compared to H_2DCFDA. CM-H_2DCFDA passively diffuses into cells, where intracellular esterizes cleave its acetate groups, and its chloromethyl group reacts with intracellular glutathione and other thiols (Oparka et al., 2016).

Once inside the cell, CM-H_2DCFDA is converted to 5-(and-6)-chloromethyl-2',7'-dichlorodihydrofluorescein diacetate (H_2DCF-DA), a non-fluorescent compound. In the presence of ROS, especially hydrogen peroxide, H_2DCF-DA is oxidized to form a highly fluorescent compound, 2',7'-dichlorofluorescein (DCF). As the fluorescence intensity of DCF correlates with ROS levels, CM-H_2DCFDA is a useful tool for measuring intracellular ROS and monitoring oxidative stress.

CM-H_2DCFDA is commonly used in cell culture studies, flow cytometry, and fluorescence microscopy to investigate oxidative stress, analyse cellular responses to oxidative damage, and examine the impact of antioxidants and other compounds on ROS levels. While CM-H_2DCFDA is a valuable tool for detecting reactive oxygen species (ROS), careful consideration is required due to factors such as interference from other fluorophores, as well as the effects of pH and temperature on its fluorescence. To ensure accurate measurements, appropriate controls and calibration are essential. Additionally, various derivatives of H2DCFDA exist, each designed with specific properties to detect distinct types of ROS (Oparka et al., 2016).

In summary, CM-H2DCFDA is a widely utilized fluorescent probe for measuring intracellular ROS levels, particularly hydrogen peroxide. It has played a crucial role in advancing research on oxidative stress, cellular responses to ROS, and the impact of various compounds on ROS production and signaling within cells.

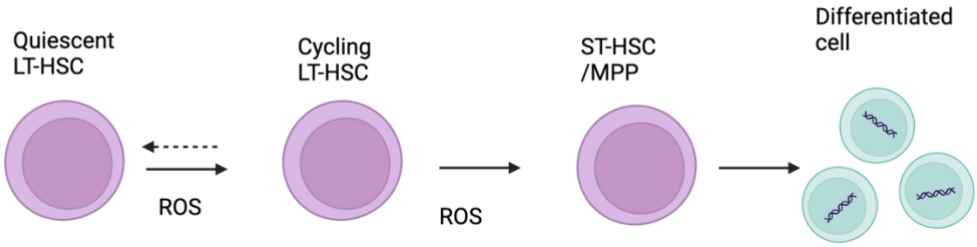

Figure 1.6 LT HSC fate: Self Renewal and Differentiation

1.3.3 Tetramethylrhodamine, Methyl Ester (TMRM) to assess mitochondrial membrane potential

TMRM is a fluorescent dye widely used in cell biology and biochemistry research to stain and visualize mitochondria within cells. Mitochondria are membrane-bound organelles present in most organisms' cells, responsible for generating energy in the form of ATP through cellular respiration. TMRM is a cationic dye that accumulates in the mitochondria due to the negative charge of the inner mitochondrial membrane. Once inside, TMRM fluoresces, enabling researchers to observe and measure mitochondrial activity and health. Variations in TMRM fluorescence can indicate changes in mitochondrial membrane potential, a key marker of mitochondrial function (Mayle et al., 2013).

1.4 Advanced technologies to assess the metabolism of normal and malignant cells in vitro

To assess the mass of mitochondria and the mitochondrial redox oxygen species levels in haematopoietic stem cells (Lineage$^-$ Scal1$^+$ c-kit$^+$ LSK cells) in mice, Mitogreen-FITC (MTG-FITC, Biolegend), Mitochondrial Tetramethylrhodamine (TMRM-PE, Biolegend), Carboxymethyl dichlorodihydrofluorescein derivative (CM-H_2DCFDA-FITC, ThermoFisher) and MitoSox Red (MitoSox-FITC, ThermoFisher) markers were used respectively.

The second energy balance analysis comprises ATP production and consumption, NADH/$FADH_2$ levels, and ADP/ATP Ratio. As stated in the methodology section, the Seahorse XF Analyser can measure the ATP production rate, while LC-MS can measure the NADH/$FADH_2$ levels and ADP/ATP ratio. Liquid chromatography-mass spectrometry (LC-MS) is used to measure NADH/FADH2 levels and the ADP/ATP ratio. The LC-MS results will be demonstrated in the last chapter.

The third mitochondrial function includes the formation of reactive oxygen species (ROS), mitochondrial membrane potential, and oxygen consumption rate (OCR). OCR has been described above, while reactive oxygen species and mitochondrial membrane potential are detected by flow cytometry technology employing TMRM and ROS dyes.

1.4.1 Mass Spectrometry

Mass spectrometry (MS) is an analytical technique used to measure the mass-to-charge ratio of ions. It is extensively applied in chemistry, biology, and various fields to identify a sample's composition, quantify specific substances, and determine molecular structure. MS involves three main steps: ionization, mass analysis, and detection. Firstly, the sample undergoes ionization, where its molecules are converted into charged particles (ions). Common ionization methods include Electron Ionization (EI), Electrospray Ionization (ESI), and Matrix-Assisted Laser Desorption/Ionization (MALDI). In the second step, mass analysis, ions are separated based on their mass-to-charge (m/z) ratio using a mass analyser. Different types of mass analyzers include Quadrupole, Time-of-Flight (TOF), and Ion Trap. Finally, in the detection step, the separated ions are

detected, and the data is used to create a mass spectrum—a graph that plots the relative abundance of ions against their m/z ratio (Nakorchevsky and Yates, 2012).

1.4.2 Seahorse

Cell metabolic functional analysis is based on three key elements: the assessment of metabolic pathways, energy balance analysis, and mitochondrial function evaluation (DeBerardinis and Keshari, 2022).

Common metabolic pathways include glycolysis, oxidative phosphorylation (OXPHOS), fatty acid oxidation, and amino acid metabolism (Boroughs and DeBerardinis, 2015). These pathways are evaluated as follows:

Glycolysis: The rate at which cells convert glucose into pyruvate and lactate. This can be assessed using the Seahorse XF Analyzer, which measures the extracellular acidification rate (ECAR) as an indicator of glycolysis.

Oxidative Phosphorylation (OXPHOS): The Seahorse XF Analyzer measures oxygen consumption rate (OCR), which provides insights into ATP production, the efficiency of the electron transport chain, and overall mitochondrial function.

Fatty Acid Oxidation: While the Seahorse XF Analyzer can also detect fatty acid oxidation using specific reagents, this pathway is not evaluated by our lab on hematopoietic stem and progenitor cells (HSPCs) due to limited experience.

Thus, the Seahorse XF Analyzer is primarily used to quantify glycolysis and OXPHOS in my project.

1.4.3 Bulk RNASeq and Single Cell RNASeq

1.4.3.1 Bulk RNASeq

Bulk RNA sequencing (bulk RNA-seq) is a high-throughput method for analysing the transcriptome, the full set of RNA transcripts generated by a specific cell population at a particular time. Unlike single-cell RNA sequencing, which examines the transcriptomes of individual cells, bulk RNA-seq provides an averaged expression profile of the entire cell population under study.

1.4.3.2 Single Cell RNASeq

Single-cell RNA sequencing (scRNA-seq) is a powerful and cutting-edge technique that allows researchers to examine the gene expression profiles of individual cells. Unlike bulk RNA-seq, which provides an average expression profile of a mixed population of cells, scRNA-seq enables the study of cellular heterogeneity, identifying distinct cell types, states, and their roles in biological processes.

1.5 Aims

As JAK2 inhibitors are unable to eliminate Jak2V617F-mutated hematopoietic stem cells (HSCs) in MPN, it is important to find novel stem cell-directed therapeutic approaches. Our previous single-cell RNA-sequencing data showed that 8% of genes that differ in Jak2V617F LSCs compared to wild-type (WT) LSCs are involved in metabolic processes. Pathway analysis in Jak2V617F-positive LSCs compared to WT revealed a multitude of upregulated metabolic pathways, such as glutathione metabolism, oxidative stress, and phosphatidylinositol lipid metabolism. This provides a strong rationale for searching for targetable metabolic vulnerabilities in MPN.

Therefore, firstly, we aimed to investigate cell survival mechanisms in MPN using robust pre-clinical Jak2V617F mice models.

Secondly, we aimed to conduct transcriptomic analysis to identify deregulated pathways in MPN among both patients and mice compared to their normal counterparts.

Thirdly, we aimed to perform functional assays to document changes in deregulated pathways within primitive mouse MPN cells.

2 Chapter 2 Materials and Methods

2.1 Materials

2.1.1 General reagents

$^{13}C_6$-labelled glucose	Cambridge Isotope Laboratories	50-99-7
Ammonium acetate	Sigma	A1542
Antimycin A	Sigma	A8674
BIT 9500 Serum Substitute	Stem Cell Technologies	9500
Bovine Serum Albumin (BSA) Fatty Acid Free	Sigma	A8806
CD117 (c-Kit) Positive Selection Kit	Stem Cell Technologies	18757
Cell Tak	Thermo Fisher Scientific	10317081
DAPI	Sigma	D9542
Dimethyl Sulfoxide (DMSO)	Fisher Scientific	D/4121/PB08
DNase I Solution (1 mg/mL)	Stem Cell Technologies	7900
Ethanol	Chemical Stores	L/278/01
FCCP	Sigma	C2920
Foetal bovine serum (FBS)	GIBCO	10270
Hydrocortisone	Sigma	H0888
IMDM	Life technologies	21980
Isopropanol	Chemical Stores	L/585
L-Glutamine 100x (200mM)	Gibco	25030
Methanol	Chemical Stores	L/425/IE
Methanol (HPLC grade)	Fisher Scientific	67-56-1
MethoCult^{TM}H4034	Stem Cell Technologies	4034
MitoTracker Green FM	Life technologies	M-7514
Mouse IL-3	Biolegend	575504
Mouse IL-6	Biolegend	575704
Mouse SCF	Biolegend	579704
PBS	Homemade	N/A
Penicillin-Streptomycin	GIBCO	15140
Pierce Bovine Serum Albumin Potassium bicarbonate	Sigma	60339
RNeasy Mini Kit	Qiagen	74106
Rotenone	Sigma	R8875
RPMI 1640 Medium, no glutamine	Life technologies	3187005
SCF CARRIER FREE	Biolegend	579704
Seahorse Base Medium	Agilent Technologies	102353

Sodium bicarbonate ($NaHCO_3$)	Sigma	S5761
Sodium dodecyl sulfate (SDS)	Sigma	L5750
Sodium pyruvate	Gibco	11360070
Streptavidin, Pacific Blue	Life technologies	S-11222
Tetramethylenediamine (TEMED)	Sigma	T9281
TMRM	Life technologies	T-668
XF Calibrant	Seahorse Bioscience	
β-Mercaptoethanol	Sigma	M3148

2.1.2 Flow cytometry reagents

4',6-diamidino-2-phenylindole (DAPI)	D9542	Sigma
7-AAD staining solution	559925	BD Biosciences
APC anti-mouse c-kit	135107	Biolegend
FC block	553142	BD Pharmigen
FITC anti-human CD45	555842	BD Biosciences
FITC anti-mouse CD45.1	110706	Biolegend
FITC anti-mouse TER-119	116206	Biolegend
Mitotracker green (MTG)	M-7514	Life Technologies
Pacific Blue™ anti-mouse CD45.2	109820	Biolegend
PE anti-human CD133	372803	Biolegend
PE anti-mouse CD48	103406	Biolegend
PE/Cy7 anti-mouse Scal1	122514	Biolegend
PE/Cy7 anti-mouse/human CD11b (Mac-1)	101216	Biolegend

2.1.3 Equipment

7500 Fast Real-Time PCR System	Applied Biosystems
Mastercycler™ PCR machine	Eppendorf UK Ltd
FACSAria™ Fusion sorter	BD Biosciences
FACSFortessa™	BD Biosciences
FACSCalibur™ Z6003	BD Biosciences
Seahorse flux analyser XF96	Agilent Seahorse Technologies
Q Exactive Orbitrap Mass Spectrometer	Thermo Fisher Scientific
NanoDrop™ 2000 Spectrophotometer	Thermo Fisher Scientific
ddPCR system	Qiagen
CASY cell counter and analyser	Roche Applied Science
SpectraMax Plus 384 Absorbance Microplate Reader	Molecular Devices
UltiMate 3000 HPLC system	Thermo Fisher Scientific

2.1.4 Composition of tissue culture media, solutions and buffers

RPMI^{+}

RPMI 1640	500ml
FBS Heat inactivated	10%

Red blood cell lysis

Ammonium acetate	8.02 g
$KHCO_3$ potassium bicarbonate	1 g
EDTA	0.02g
H_2O	to 1L

c-kit^{+} cells medium

IMDM	
0.2% 2 Mercaptoethanol (50mM)	100ul
Low Density Lipoprotein (10mg/ml)	200ul
1% Penicillin-Streptomycin (10,000 U/ml)	500ul
20% BIT	10ml
Murine IL-3 (10ng/ml)	2.5ul
Murine IL-6 (25ng/ml)	6.25ul
Murine SCF (50ng/ml)	25ul

Freezing cells medium (primary human)

DPBS	15ml
DMSO	3ml
Albunorm (5% stock)	12ml
500mM EDTA	30ul

Freezing cells medium (Primary mouse)

DMSO	5ml

FBS	25ml
IMDM	20ml

LC-MS medium

Alumax II (Gibco)	50ul
Human insulin (10mg/ml)	10ul
Glutamine (1.66 mM)	33.13ul
Pen/Strep	100ul
Transferrin (25mg/ml)	3ul
Beta Mercaptoethanol (50mM)	20ul

XF Assay Media for primary mouse cells

XF Base Media	24.3 ml
Glucose (1.66 M)	167 µl
L-Glutamine (200 mM)	250 µl
Mouse IL-3	2.5ul
Mouse IL-6	6.25ul
Mouse SCF	25ul

XF Assay Media for cell lines

XF Base Media	24.3 ml
Glucose (1.66 M)	167 µl
L-Glutamine (200 mM)	250 µl
Pyruvate (100 mM)	250 µl
Fc block*	
Fc block	1 µl
PBS, 2% FBS (v/v)	49 µl

Lin cocktail

Biotin anti-mouse CD4	3.2 µl

Biotin anti-mouse CD5	6.4 µl
Biotin anti-mouse CD8a	6.4 µl
Biotin anti-mouse Mac-1	24.8 µl
Biotin anti-mouse B220	24.8 µl
Biotin anti-mouse TER119	100 µl
Biotin anti-mouse GR-1	50 µl
PBS	284.4 µl
Murine ST/LT HSC mix	
Pacific Blue Lin cocktail	22 µl
Sca anti-mouse PeCy7	1 µl
cKit anti-mouse APC/780	1 µl
CD48 anti-mouse PE	3.2 µl
CD150 anti-mouse APC	1 µl
FITC anti-mouse CD45.1	1 µl
PerCP/Cy5.5 anti-mouse CD45.2	3 µl
PBS	17.8 µl
Murine myeloid mix	
FITC anti-mouse CD45.1	0.5 µl
PerCP/Cy5.5 anti-mouse CD45.2	1.5 µl
APC anti-mouse GR-1	1 µl
PeCy7 anti-mouse Mac-1	0.5 µl
FITC anti-mouse TER119	1 µl
Streptavidin*	
Streptavidin	1 µl
PBS, 2% FBS (v/v)	100 µl
Myelocult*	
Myelocult™	100 ml
Hydrocortisone hem succinate ($1x10^{-4}$ M)	1 ml
Human HSC/LSC staining	
APC anti-human CD34	3 µl

PerCP anti-human CD38	3 µl
FITC anti-human CD45	10 µl
PBS	84 µl

2.2 Methods

2.2.1 Mice bone marrow samples c-Kit$^+$ selection

Murine bone marrows were harvested from C57BL/6 WT (n=3), HOM (n=3), and HET (n=3) mice aged 10 to 11 weeks. The bone marrows were crushed using a mortar and pestle in 30 ml of Dulbecco's Phosphate Buffered Saline (DPBS) (Sigma) containing 0.5% of bovine serum albumin (BSA) (Sigma). The cell suspensions were filtered through a 70 µm mesh nylon strainer to eliminate remaining aggregates and debris.

BM cells were enriched for c-Kit$^+$ cells using EasySep Mouse CD117 Positive Selection Kit (StemCell Technologies). BM cell suspensions were counted using a haemocytometer/Cell drop (DeNovix) and centrifuged at 350g 5min. Cell pellets were resuspended at 10^8 cells/ml concentration by adding appropriate 0.5%BSA+DPBS. Cell suspensions were transferred into FACS tubes for c-Kit$^+$ selection. c-Kit$^+$ cells were firstly incubated with 50ul/ml PE-labelled CD117 antibody for 15min at room temperature. Then c-Kit$^+$ cells were selected by using 70ul/ml of selection cocktail directed against PE and dextran for 15min at room temperature. 50ul/ml RapidSpheres were added to the samples evenly for 10min at room temperature. Samples were topped up to 2.5ml with 0.5% BSA+DPBS. FACS tubes were placed into the magnet without the lid and incubated 5min at room temperature. The magnet was picked up and inverted in a continuous motion to pour off the supernatant. The FACS tube was removed from the magnet. The c-Kit$^+$ cells were left in the tube. Steps from topping up 2.5ml with 0.5% BSA+DPBS to pour off the supernatant were repeated three more times. c-Kit$^+$ cell medium (see reagents part) below for culturing medium- was added to FACS tubes with isolated c-Kit$^+$ cells. c-Kit$^+$ cells were cultured in 6 well plates at 10^5 cells/ml to 10^6 cells/ml overnight at 37 °C 5% CO_2. c-Kit$^+$ cells were cultured in Iscove's modified Dulbecco's medium (IMDM) supplemented with 20% BIT (bovine serum albumin/insulin/transferrin; StemCell Technologies), 0.2% Mercaptoethanol (Invitrogen), 10mg/ml Low-Density Lipoprotein LDL (SIGMA), 1% Penicillin-Streptomycin (Invitrogen), 10ng/ml Murine Interleukin3 IL-3 (Biolegend), 25ng/ml Murine Interleukin6 IL-6 (Biolegend), 50ng/ml Murine Stem Cell Factor SCF (Biolegend).

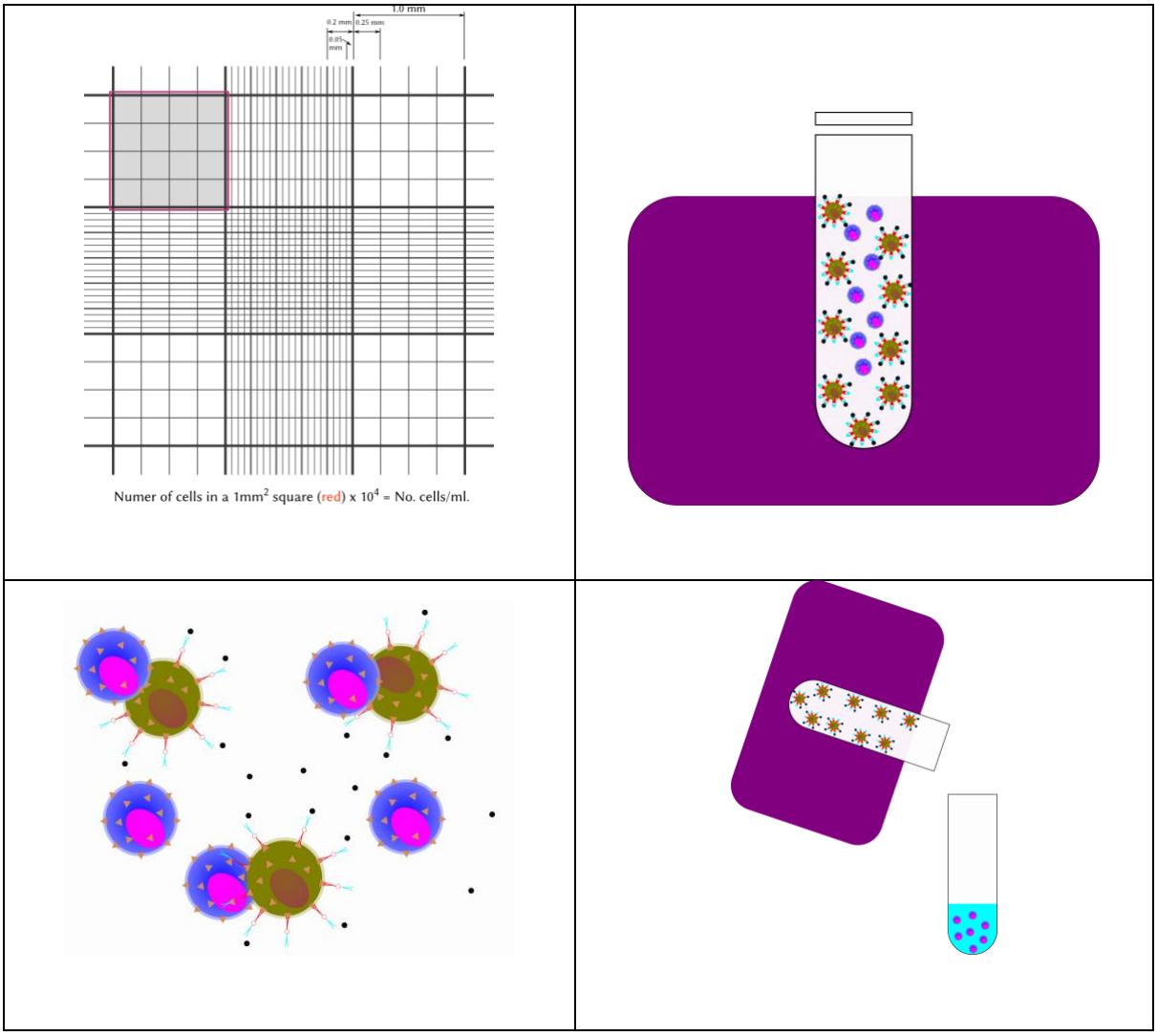

Figure 2.1 Method for cell purification.

Using a haemocytometer to count cell numbers, and magnetic beads for magnetic cell purification.

2.2.2 RNASeq of c-Kit⁺ cells

Before RNA extraction, a clean lab coat and gloves were donned, and pipettes as well as the working area were cleaned with RNaseZAP (Sigma). The RNeasy Plus mini kit (Qiagen) was employed for RNA extraction. After overnight culture, c-Kit⁺ cells were counted again. 1 ml of c-Kit⁺ cells from each well was transferred from the 6-well plates into 1.5 ml RNase-free Eppendorf tubes. The cells in the Eppendorfs were centrifuged at 350 g for 5 minutes and left as cell pellets at the bottom of the Tubes. The supernatants were carefully pipetted off without disturbing the cell pellets. For a c-Kit⁺ cell count at or below 5 × 10^6 cells, 350 µl of Buffer RLT Plus was added directly to the cell pellets. The cells were then vortexed for 30 seconds to homogenize the lysate, which was transferred to a gDNA

eliminator spin column placed in a 2 ml collection tube. The gDNA eliminator spin column with a collection tube was centrifuged for 30 seconds at 10,000 rpm; the flow-through was retained, and the column was discarded. 350 µl of 70% ethanol was added to the flow-through and mixed by pipetting. A total of 700 µl of the sample was transferred to an RNeasy spin column positioned in a 2 ml collection tube. The lid of the spin column was closed and centrifuged for 15 seconds at 10,000 rpm, and the flow-through was discarded. 700 µl of Buffer RW1 was added to the RNeasy Mini spin column, the lid was shut, and it was centrifuged for 15 seconds at 10,000 rpm, with the flow-through discarded. 500 µl of Buffer RPE was added to the RNeasy spin column and centrifuged for 15 seconds at 10,000 rpm, after which the flow-through was discarded. Another 500 µl of Buffer RPE was added to the column and centrifuged for 2 minutes at 10,000 Rpm. The RNeasy spin column was placed in a new 2 ml collection tube and the sample was centrifuged at 13,000 rpm for 1 minute to further dry the membrane. The RNeasy spin column was then placed into a new 1.5 ml collection tube, and 30 µl of RNase-free water was added directly to the spin column membrane. The column lid was closed and centrifuged at 10,000 rpm. RNA was eluted in 30 µl of RNase-free water. Using a Nanodrop Spectrophotometer, the extracted RNA was kept on ice for quality control and concentration measurements.

2.2.2.1 Establish RNA quality by Nanodrop Spectrophotometer

The Nanodrop software was launched, and the nucleic acid option was selected. The Nanodrop was gently wiped with double-distilled water. One microliter of RNase-free water was pipetted onto the sensor pedestal of the Nanodrop, ensuring it was fully covered without producing any bubbles to initialize the instrument. Next, one microliter of RNase-free water was used to set the blank sample, and the blank measurement was taken. Subsequently, one microliter of extracted RNA was placed onto the sensor pedestal for measurement. The 260/280 ratio was used to determine protein contamination, while the 260/230 ratio was used to determine organic contamination.

2.2.2.2 Library Preparation and sequencing

The quality of the RNA samples was re-checked using the Tapestation (Agilent). This was done with the High Sensitivity RNA Screen Tape (Agilent), which utilizes the RNA Integrity Number (RIN) to indicate RNA degradation. The RIN is calculated through the ratios of 28S to 18S ribosomal bands, which were analyzed by gel electrophoresis. RIN values range

from 1 to 10, with higher RIN values indicating lower RNA sample degradation. One microgram of RNA was subjected to Ribo-depletion to eliminate ribosomal RNA (rRNA) before generating RNA-Seq libraries using the Truseq Stranded Total RNA Library Prep Gold Kit (Illumina). Paired end (PE) sequencing of 36 base pairs was performed on the NextSeq 500 sequencer (Illumina). All steps were carried out by William Clark at the Molecular Technologies Core Facility at CRUK Beatson Institute, adhering to the manufacturer's instructions.

2.2.2.3 RNA-Sequencing Data Analysis Workflow

The pipeline for RNA sequencing data analysis comprises five steps: processing raw reads, aligning reads, quantifying genes, testing for differential expression, and testing for functional enrichment. Firstly, to process the raw reads, the quality of the FASTQ-format raw reads is assessed using FastQC software (URL_1). Secondly, STAR 2.7.3a (Dobin et al., 2013), one of the RNA-Seq alignment tools, was utilized to align the raw reads to the reference genome Mus musculus GRCm39.104. STAR is time saving and can align the reads across splice junctions. For the third step, the Feature Counts function from the Rsubread 2.4.3 package was invoked to generate a count matrix. To eliminate batch effects due to the different processing dates of samples, the Combat function from the Sva package 3.38.0 was applied (Leek et al., 2021), resulting in a new expression matrix for all downstream analyses. Lastly, the Limma package 3.46.0 was employed for the normalization of the counts. For differential expression analysis, we are comparing gene expression changes between phenotypes (WT, HOM, and HET), rather than comparing expression across multiple genes. As a result, gene length normalization is unnecessary. The Counts per Million (CPM) function is used to normalize library size. The log of CPM is typically applied to generate plots. After library size normalization, it is necessary to filter out and remove lowly expressed genes to eliminate genes with no biological significance in the context of the study. The filtering employs CPM instead of counts, prioritizing samples with large library sizes. The filterByExpr function retains genes with approximately 10 read counts or more.

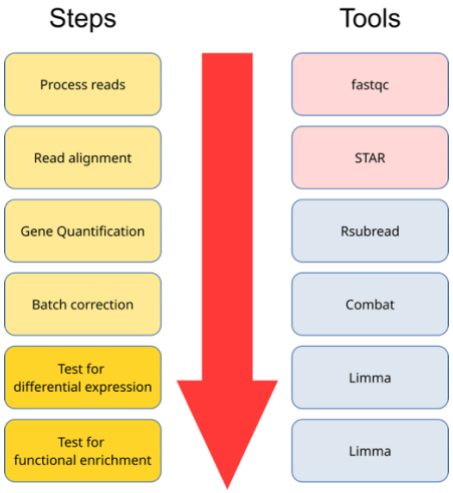

Figure 2.2 RNA-seq data analysis workflow.

2.2.3 Seahorse assay for measuring oxygen consumption rate (OCR) and extracellular acidification rate (ECAR).

2.2.3.1 The principle and calculation of seahorses

The Seahorse XF96 analyser (Seahorse Bioscience) can simultaneously measure the cellular oxygen consumption rate (OCR) and the extracellular acidification rate (ECAR). Cells utilize two methods of respiration. One is mitochondrial respiration, which occurs in mitochondria within a high-oxygen environment; the other is glycolysis, which takes place in a hypoxic environment. During mitochondrial respiration, electrons are transported through the inner mitochondrial membrane's electron transport chain (ETC). Oxygen is consumed during the process of electron transport, and hydrogen ions are pumped into the mitochondrial intermembrane space. ATP is also generated in the ETC. To assess mitochondrial respiration and metabolic traits, including basal mitochondrial respiration, ATP-linked respiration, proton leak, maximal respiration rate, mitochondrial reverse, and non-mitochondrial respiration, we employ three drugs to inhibit different complexes on the inner mitochondrial membrane. The first drug used is the ATP-synthase inhibitor oligomycin (1 µM), which is added after 15 minutes of basal mitochondrial OCR measurements.

The second drug introduced is carbonyl cyanide-4-(trifluoromethoxy) phenylhydrazone (FCCP) at a concentration of 0.6 uM, which functions as a mitochondrial uncoupler. Oxygen consumption is linked to hydrogen via ion pumps before the addition of FCCP. Consequently, the oxygen consumption rate peaks following the addition of FCCP, indicating the maximal respiration rate. The reverse capacity of cells is calculated by subtracting the

basal oxygen consumption rate from the maximal respiration rate, highlighting the cell's capability for oxidative phosphorylation. Lastly, Rotenone and Antimycin A (Rot+AA) are introduced; they act as inhibitors of complex III and complex I, respectively. Once Rot+AA are added, the entire electron transport chain is inhibited, causing a decrease in the oxygen consumption rate. This is referred to as the non-mitochondrial respiration rate.

The extracellular acidification rate (ECAR) indicates the level of glycolysis. As 2-Deoxy-D-glucose (2-DG) was not utilized in our experiment, only the basal glycolysis rate and the glycolytic reversal rate were assessed. Glucose was added after 15 minutes; however, our Seahorse media recipe already contained glucose. Consequently, our basal ECAR already characterized glycolysis. The glycolytic reversal was calculated as the ECAR measured after FCCP addition minus the basal ECAR.

2.2.3.2 Seahorse cells counting and seeding

After overnight culture, c-Kit$^+$ cells were counted using Celldrop (DeNovix). The c-Kit$^+$ cells were transferred from 6-well plates to 10ml tubes, centrifuged, and resuspended in Seahorse Medium (Agilent) supplemented with 1.6M glucose (SIGMA), 200mM glutamine (SIGMA), 10ng/ml Murine IL-3 (Biolegend), 25ng/ml Murine IL-6 (Biolegend), and a cocktail of 50ng/ml Murine SCF (Biolegend). The volume of Seahorse Medium added was calculated based on the c-Kit$^+$ cell concentration for each mouse and the replicate well numbers on the Seahorse plates. A total of 100,000 cells were seeded per well of a Seahorse XF96 cell culture plate (175 µl volume). The cells were incubated for 30 minutes in a CO_2-free incubator at 37℃ before being transferred to the Seahorse XF96 analyser. A calibration plate was placed in the CO_2-free incubator overnight for calibration. Measurements of OCR were taken at baseline and following injections of (i) oligomycin (1µM), an ATP synthase inhibitor, (ii) carbonyl cyanide-4-(trifluoromethoxy) phenylhydrazone (FCCP) (1.8µM), a mitochondrial uncoupler, and (iii) antimycin A (1µM) and rotenone (1µM; all Sigma-Aldrich), which are inhibitors of complex III and complex I, respectively.

WT c-Kit$^+$ cells and HOM or HET c-Kit$^+$ cells were compared in terms of basal mitochondrial respiration, ATP-linked respiration, proton leak, maximal respiration rate, reverse capacity, non-mitochondrial respiration, glycolysis, and glycolytic reverse rate.

2.2.4 Flow cytometry

2.2.4.1 Antibodies panel design

To assess the mass of mitochondria and the mitochondrial redox oxygen species levels in hematopoietic stem cells (Lineage^{-}Scal1^{+} c-Kit^{+} LSK cells) in mice, the markers Mitogreen-FITC (MTG-FITC, Biolegend), Mitochondrial Tetramethylrhodamine (TMRM-PE, Biolegend), Carboxymethyl dichlorodihydrofluorescein derivative (CM-H_2DCFDA-FITC, ThermoFisher), and MitoSox Red (MitoSox-FITC, ThermoFisher) were used, respectively.
TMRM-PE was not directly used to stain purified c-Kit^{+} cells because the selected c-Kit^{+} cells showed the same color of PE (CD117) on their surface. Unfortunately, the c-Kit^{+} selection kit from StemCell Technologies features only PE as a marker. Therefore, a different panel was devised to visualize c-Kit^{+} cells from the same bone marrow fraction, employing Zombie-BUV395, Lineage-Pacific Blue, Scal1-PerCP-Cy5.5, and c-Kit-APC-Cy7 to assess TMRM levels. Zombie-BUV395 was included to separate live and dead cells. For MTG, CM-H_2DCFDA, and ROS, another panel consisting of Zombie-NIR-R780/60, Lineage-Pacific Blue, Scal1-APC, and c-Kit-PE was utilized to stain LSK cells. LSK cells were characterized as Lin^{-}Scal1^{+}c-Kit^{+}. After gating the LSK cells, histograms for MTG, TMRM, CM-H_2DCFDA, and ROS were generated to display mitochondrial functions.
As efflux pumps are present on the cell membrane of Lin^{-} cells to expel the MTG and TMRM dye, verapamil was added as needed to inhibit the efflux pump(de Almeida et al., 2017).

2.2.4.2 Procedure of staining panel for flow-cytometry

Cells were initially stained with MTG, TMRM, CM-H_2DCFDA, and ROS dyes, as the staining procedure for these three antibodies should be completed under 37℃ incubations to allow the colour to be absorbed into the live cell membrane.

Pre-warmed media at 37℃ should be prepared for the mixing of MTG and TMRM dyes. Because the ROS dye is the same color as the MTG dye, it is added to a separate pre-warmed Medium. The media volume was calculated using the counts of BM cells to obtain 50,000,000 cells. The Mitogreen working concentration was 100 nM. Ten microliters were taken from the 100X stock solution and added to the pre-warmed media containing 50,000,000 BM cells. For TMRM staining, the stock concentration was 10 mM, and the working concentration was 100 nM. A small vial of TMRM stock was diluted 100X. For ROS staining, both Redox oxygen species Red and CM-H_2DCFDA had a stock concentration of 5 mM and a working concentration of 5 µM.

After incubation at 37℃ for 30min, BM cells were already stained with the MTG, TMRM and ROS dyes. The next step was c-Kit$^+$, LSK markers staining. Antibodies were added according to Table 3 to make a 50ul staining solution per sample. 50,000,000 BM cells solution were centrifuged and stained with 50ul antibodies on ice for 30 min.
Samples were washed with PBS three times to eliminate the unspecific antibody binding. Then 500ul PBS was added to the sample ready for the flow cytometry.

Table 2.1 c-Kit$^+$, LSK staining antibodies panel for MTG, CM-H_2DCFDA and ROS

Antibody	Colour	Volume	Fortessa channel	Cat. Number
Lineage (-)	Pacific Blue	5ul	V 450/50	Biolegend 133310
Scal1 (+)	APC	2ul	R 670/14	Biolegend 108124
C-kit (+)	PE	2ul	YG586/15	Biolegend 105826
Zombie	APC-cy7	1ul	R 780/60	Biolegend 423101

2.2.5 ddPCR

The ddPCR workflow utilized the Bio-Rad QX200 system with the ddPCR™ Mutation Assay: for detecting the Mt-Nd1 mutation. The assay employed a FAM-labelled probe targeting the mutant JAK2 and a HEX-labelled probe targeting the wild type (WT). Prior to each experiment, a master mix was prepared, comprising 10 µl of 2X ddPCR Supermix for Probes (No dUTP) and 1 µl of the ddPCR™ Mutation Assay. Variable volumes of DNA were added, and nuclease-free water was used to adjust the total reaction volume to 20 µl. Samples were thoroughly mixed by pipetting up and down. The reactions were prepared in ddPCR™ 96-Well Plates, skipping the first row.

After adding all reagents and samples, the plate was sealed using the PX1 PCR Plate Sealer and Heat Seal Foil at 180°C for 6 seconds. The plate was briefly vortexed and centrifuged at 500 rpm for 30 seconds. It was then loaded into the AutoDG system along with Automated Droplet Generation Oil for Probes, AutoDG pipette tips, DG32 Droplet Generator cartridges, and another ddPCR™ 96-Well Plate placed on the cooling block. The AutoDG was set up according to the instrument's instructions.

Once droplets were generated, the second plate was sealed as before and subjected to thermal cycling in the C1000 Touch Thermal Cycler using the following program:

1. 95°C for 10 minutes
2. 94°C for 30 seconds
3. 55°C for 1 minute (repeated for 40 cycles)
4. 98°C for 10 minutes
5. 12°C hold

The plates were left at 12°C for at least 3 hours or overnight, as recommended by (Rowlands et al., 2019) before reading. Droplet fluorescence was analysed using the QX200 Droplet Reader, set to the Rare Event Detection (RED) Assay parameters with FAM and HEX probes. Data were processed using Bio-Rad's Quantasoft (Version 1.7).

Inclusion criteria for data analysis required:

- Each well to contain >10,000 droplets.
- Controls to display expected clusters (Negative, Mutant Positive, WT Positive) on the 2D amplitude plot.

Thresholding was performed manually for each experiment using the 2D amplitude plots of PC and NTC/NC results to define thresholds for WT, Mutant, and Negative clusters.

2.2.6 Liquid chromatography-tandem mass spectrometry (LC-MS)

2.2.6.1 Preparation of Extraction Solvent

The extraction solvent was prepared with 50% methanol (HPLC grade), 30% acetonitrile (HPLC grade), and 20% water (HPLC grade).

2.2.6.2 LC-MS on murine bone marrow hematopoietic stem cells (LSK cells)

2.2.6.2.1 Isolation and culture of LSK cells

Murine bone marrow was harvested from C57BL/6 WT (n=3), HOM (n=3), and HET (n=3) mice aged 10-11 weeks. The bone marrows (BM) were crushed using a mortar and pestle in 30 ml of Dulbecco's Phosphate Buffered Saline (DPBS) (Sigma) containing 0.5% bovine serum albumin (BSA) (Sigma). The cell suspensions were filtered through a 70 µm mesh nylon strainer to remove any remaining aggregates and debris. BM cells were enriched for c-Kit$^+$ cells using the EasySep Mouse CD117 Positive Selection Kit (StemCell Technologies). c-Kit$^+$ cells were then re-suspended in 50 µl of 0.5% BSA + DPBS, stained

with Scal1-APC (3 µl) (Biolegend) and Linage-Pacific Blue (5 µl) (Biolegend) in 42 µl of 0.5% BSA + DPBS for 15 minutes on ice. After staining, the cells were washed twice with 0.5% BSA + DPBS and re-suspended in 600 µl of 0.5% BSA + DPBS. Cells were prepared for sorting, and following sorting, LSK cells were washed, counted, and cultured in c-Kit^{+} media for overnight (O/N) recovery.

2.2.6.3 Cell tracing and preparation for LC-MS

After O/N recovery, cells were washed with DPBS and re-suspended in ^{13}C6 Glucose (Cambridge Isotopes) tracing media (**Error! Reference source not found.**) for 24h incubation.

After cells were traced 24h, cells were counted using a hemacytometer and using trypan blue before counting, washed with DPBS, and centrifuged at 350g for 5 min. The supernatant was removed, and cells were re-suspended in 1ml ice-cold DPBS in small Eppendorf tubes and centrifuged 12,000g for 15 seconds. Cells were re-suspended in 1ml ice-cold DPBS and again centrifuged at the same conditions. The supernatant was removed, and extraction solvent was added according to the cell numbers added per sample. The extraction solvent was mixed 5 times by pipetting and Eppendorf tubes were vortexed for 2-3 seconds and left in the centrifuge for 4 min. Debris was pelleted at 16100g for 10min at 40C. The supernatant was transferred to a glass vial and stored at -800C. Samples were analyzed on a Liquid chromatography tandem mass spectrometry (LC-MS). All data were analyzed and TOXID was used to generate accurate retention time for each metabolite. Trace finder (ThermoFisher) software was used to further compare carbon isotopes labelling among WT, HOM and HET mice.

Table 2.2 Mass-Spectrometry Medium components

	Stock	Volume for 10mL (uL)	Want (concentration)
Alumax II (Gibco)	100%	50[&]	0.5%
Human insulin (Sigma)	10mg/mL	10	10ug/mL
Gln (Sigma/Cambridge isotopes)	200mM* or non*	32.5 (* or non*)	0.65M

Glc (Sigma/Cambridge isotopes)	1M* (1.66mM for non*)	55* (33.13 for non*)	5.5mM
Pyruvate (Sigma)	100mM	10	100uM
P/S (Gibco)	100%	100	1%
Transferrin (Sigma)	25mg/mL	3ul	7.5ug/mL
Beta Mercaptoethanol (Sigma)	50mM	20	100uM
Murine IL-3 (10ng/ml)	Biolegend (Cat: 575502)	2.5ul of 200ug/ml IL-3	
Murine IL-6 (25ng/ml)	Biolegend (Cat: 575702)	6.25ul of 200ug/ml IL-6	
Murine SCF (50ng/ml)	Biolegend (Cat: 579702)	25ul of 100ug/ml SCF	

2.2.7 Statistical analyses

We did not use any statistical method to predetermine sample size. For in vitro experiments, a minimum of 4 mice per phenotype were chosen as a sample size to ensure adequate power, unless stated otherwise. Data obtained from each mice sample represents an independent experiment. We were not blinded to mice allocation during in vivo experiments. No method of randomization was used. All mice were cared for equally in an unbiased fashion by animal technicians and investigators. No animal was excluded from the analysis.

P values were calculated by two-tailed paired or unpaired Student's t-test using GraphPad Prism software (GraphPad Software 9.0) as indicated in the figure legends. Where indicated, variables were transformed using the natural logarithms before t-tests were performed to meet the assumption of equal variances.

3 Chapter 3 Metabolism related changes in the transcriptome of MPNs

3.1 Introduction

Bulk RNA sequencing (Bulk RNAseq) reveals the average gene expression of a group of cells which may come from the same tissues or organ (Li and Wang, 2021). This group of cells is often heterogenous, containing various cell types. Bulk RNA-seq therefore only reflects the average expression profile among a group of cells, identifying the most highly differentially expressed genes. Differentially expressed genes can be analyzed for molecular pathway changes and various biological processes such as metabolism. Bulk RNASeq varies from single Cell RNA sequencing (Sc-RNASeq). Single Cell RNASeq captures the transcriptome of individual cells coming from the same or different tissues. For Sc-RNAseq clustering of cells helps to identify cell types and subpopulations. As a result, single cell RNASeq is utilized to reveal cell heterogeneity while bulk RNASeq is utilized to assess the biological process and downstream pathway analysis overall.

CD117 cells (c-Kit$^+$ cells) are a group of cells that represents hematopoietic stem and progenitor cells (HSPCs) in murine bone marrow (Shin et al., 2014). It is a heterogenous group of cells, including long term hematopoietic stem cells (LT-HSCs) and short-term hematopoietic stem cells (ST-HSCs). To learn more about metabolic processes in c-kit+ cells, I performed bulk RNASeq for downstream metabolic molecular pathway analysis. I investigated Jak2V617F homozygous and heterozygous MPN mice for this purpose. Previous reports in human stem and progenitor cells reported metabolic reprogramming in MPN patients driven by a different burden of the JAKV617F mutation (Sappington et al., 2016).

In Tong et al, JAK2V617F positive essential thrombocythemia (ET) patients were assessed using single-cell gene expression profiling and parallel mutation detection (Nageswara Rao et al., 2019). They found hematopoietic stem cell heterogeneity between homozygous mutant HSCs and heterozygous mutant HSCs. Interestingly, homozygous mutant HSCs are induced into quiescence while heterozygous mutant HSCs underwent apoptosis. In addition, fatty acid metabolism showed differences between homozygous JAK2V617F mutant HSCs and heterozygous JAK2V617F mutant HSCS. The homozygous mutant HSCs additionally showed higher Glucose metabolic compared to heterozygous mutant HSCs.

Another paper highlights the limitations of conventional single cell RNA Sequencing (ScRNA-Seq) protocols in reliably analyzing mutation status in patient (Rodriguez-Meira et al., 2019). It introduces TARGET-Seq, a method that integrates high-sensitivity genomic DNA and cDNA genotyping with ScRNA-Seq. TARGET-seq enables the resolution of distinct transcriptional signatures of tumour genetic subclones. The paper demonstrated that there is no difference in gene transcription between WT JAK2V617F mutated cells in terms of oxidative phosphorylation pathways compared to homozygous and heterozygous JAK2V617F mutated cells, hinting at the tumour microenvironment to alter even WT cells. Lastly, single-cell transcriptome and whole-genome sequencing were conducted on hematopoietic stem and progenitor cells (HSPCs) from individuals with myeloproliferative neoplasms (MPNs)(Van Egeren et al., 2021). The JAK2V617F mutation was detected in a single hematopoietic stem cell (HSC) many years before the clinical diagnosis of MPNs. HSCs carrying the JAK2V617F mutation exhibited enhanced fitness in the natural human hematopoietic system. The proportion of JAK2 mutant cells varied among different myeloid progenitor compartments within the same individuals.
In this chapter, I interrogated the transcriptional changes in metabolism between mouse Jak2V617F mutated and WT mice in the stem and progenitor cell compartment.

3.2 Results

To determine metabolic changes in MPN mice, c-Kit^{+} cells were isolated from Jak2V617F WT, HOM and HET mice. Standard Ribo-depletion to eliminate ribosomal RNA (rRNA) was deployed followed by generating RNA-Seq libraries using the Truseq stranded total RNA library prep gold kit (Illumina, Table 3.1).

Table 3.1 Sample overview for bulk-RNA-sequencing

Sample_ID	Cell Type	I7_Index_ID	index
WT2-ckit	c-Kit positive	AR018-A	GTCCGC
WT3-ckit	c-Kit positive	AR019-A	GTGAAA
WT4-ckit	c-Kit positive	AR016-A	CCGTCC
HOM1-ckit	c-Kit positive	AR020-B	GTGGCC
HOM2-ckit	c-Kit positive	AR021-B	GTTTCG
HOM3-ckit	c-Kit positive	AR022-B	CGTACG
HET1-ckit	c-Kit positive	AR023-B	GAGTGG
HET2-ckit	c-Kit positive	AR025-B	ACTGAT
HET3-ckit	c-Kit positive	AR027-B	ATTCCT

To assess c-Kit^{+} cell differences in transcription compared to WT, differentially regulated genes between HOM and WT or HET and WT were calculated and displayed as a Venn diagram Figure 3.1 Venn Diagram showing the overlap between differentially expressed genes. Overall, I found 478 genes that were specifically deregulated in HOM mice when compared to WT, 38 genes that were commonly differentially regulated in HOM and HET when compared to WT and only 2 genes that were specific to HET mice Figure 3.1 Venn Diagram showing the overlap between differentially expressed genes.

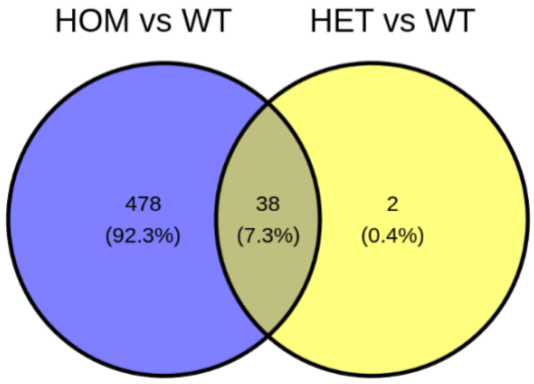

Figure 3.1 Venn Diagram showing the overlap between differentially expressed genes.

Differentially expressed genes for HOM versus (vs) WT and HET vs WT were overlaid.

Additionally, Volcano plots were generated to assess commonly upregulated genes between HOM and HET and for HOM when compared to WT alone. Some of the top regulated HOM specific genes play a role in metabolic pathway regulation and amino acid transport such as Slc43a and Slc24a37 Figure 3.4. The SLC43a family consists of L amino acid transporters, which include the structurally and functionally distinct LAT1 and LAT2 from the SLC7 family. LAT3 and LAT4 have 12 predicted transmembrane domains with both N and C termini inside the cell. They transport neutral amino acids without the need for Na+ or Cl-, and exhibit two kinetic behaviors. LAT3 (SLC43A1) is highly expressed in the pancreas, liver, skeletal muscle, and fetal liver, while LAT4 (SLC43A2) is mainly found in the placenta, kidney, and peripheral blood leukocytes. A full table denoting al differentially expressed genes is attached as an appendix.

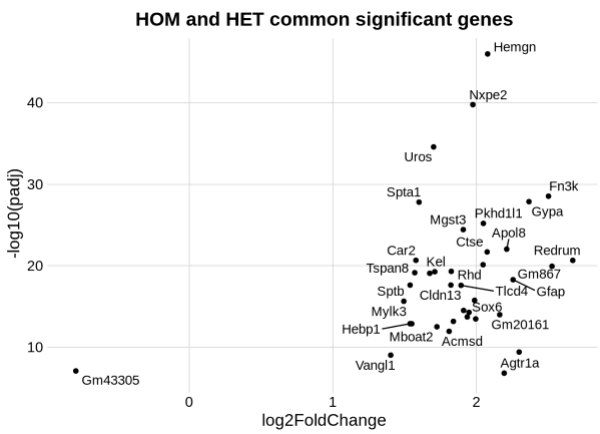

Figure 3.3 Volcano plots between HOM and HET differentiated expressed genes

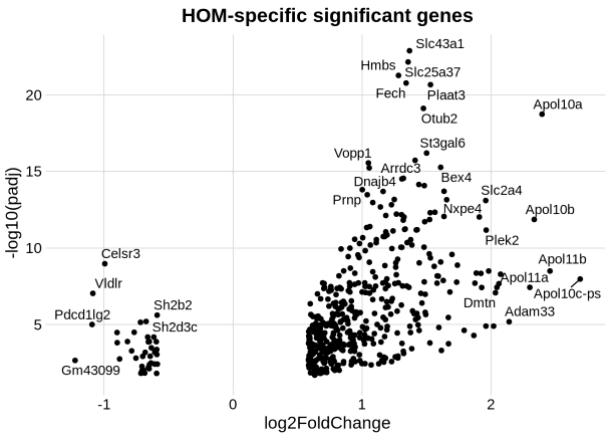

Figure 3.2 HOM-specific significant genes

Differentially expressed genes that are HOM specific or common for HOM and HET are denoted.

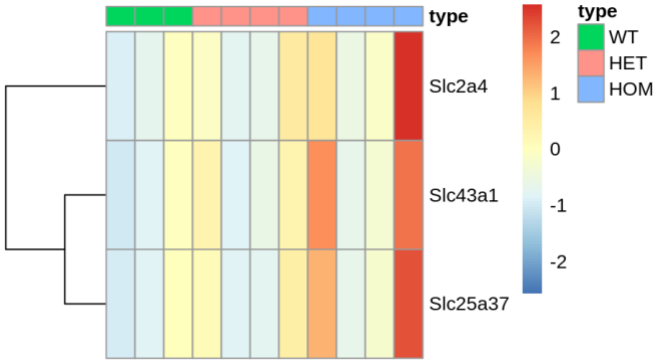

Figure 3.4 Heatmap summarising amino acid transport genes specifically upregulated in HOM Jak2V617F mutated c-kit+ cells.

Scale shows upregulated pathways in orange/ red and downregulated pathways in blue. HOM marked with blue, HET marked in orange and WT marked in green.

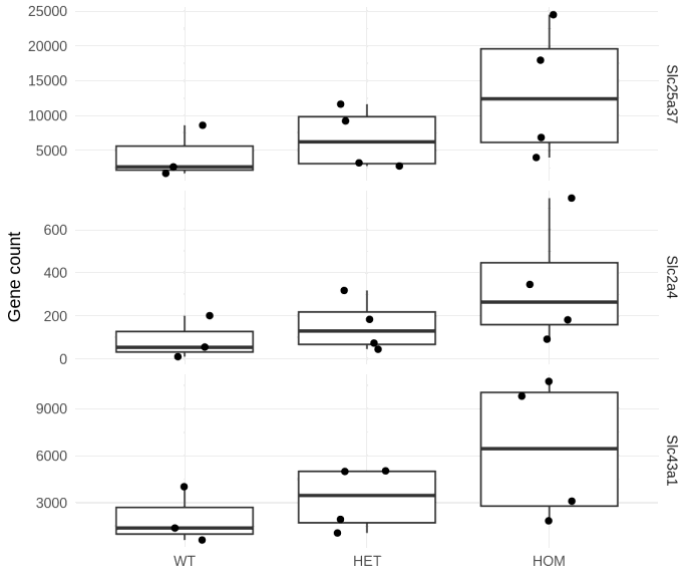

Figure 3.5 Box plots showing gene counts for amino acid transport genes specifically upregulated in HOM Jak2V617F mutated c-kit+ cells.

Individual samples are marked by dots and the average is indicated with a line.

I next went on to assess metabolic pathway regulation in the MPN mice. I wanted to focus on pathways that were upregulated in HOM or HET c-Kit cells when compared to WT. I used KEGG pathway analysis to create a heatmap of differentially regulated metabolic pathways. HOM and HET c-Kit cells equally upregulate many metabolic pathways such as

oxidative phosphorylation, pyruvate, sphingolipid and fatty acid metabolism. However, several HET-specific pathways, such as fructose and mannose metabolism and galactose metabolism, could be identified in Figure 3.6 Heatmap summarising KEGG pathway analysis of metabolic transcriptional changes in Jak2V617F mutated c-kit+ cells., with HOM-specific pathways being the glycine, serine and threonine pathways and the one-carbon metabolism pathway in Figure 3.6 Heatmap summarising KEGG pathway analysis of metabolic transcriptional changes in Jak2V617F mutated c-kit+ cells. Overall, my data showed metabolic upregulation in Jak2V617F mutated c-Kit^{+} cells. In addition, some pathways were commonly downregulated in HOM and HET c-Kit^{+} cells, such as steroid biosynthesis and biosynthesis of unsaturated fatty acids Figure 3.6 Heatmap summarising KEGG pathway analysis of metabolic transcriptional changes in Jak2V617F mutated c-kit+ cells.

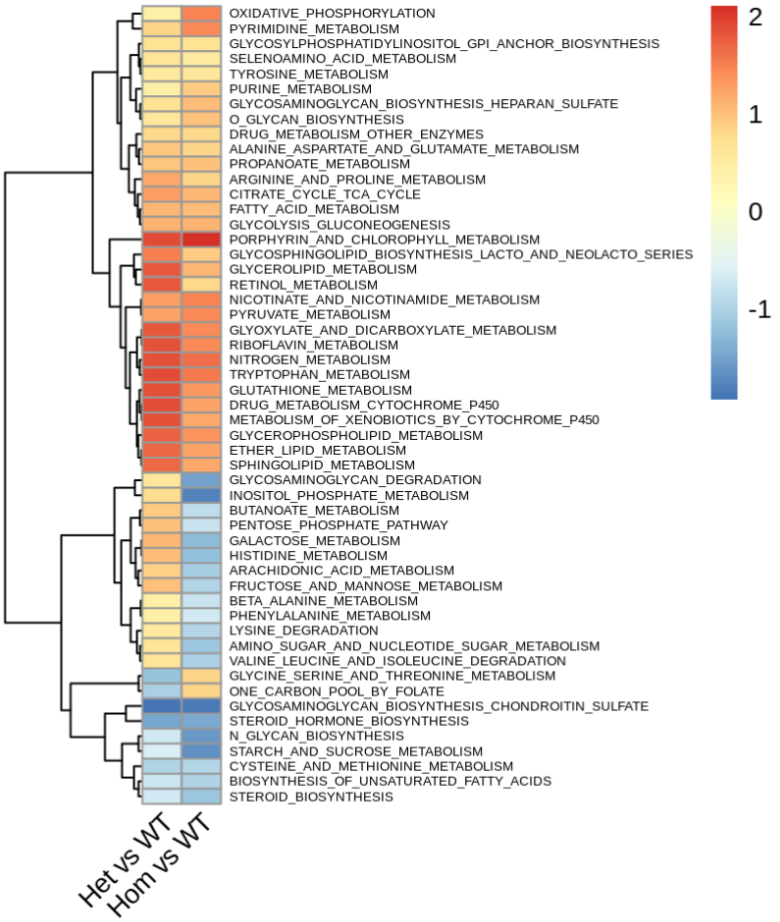

Figure 3.6 Heatmap summarising KEGG pathway analysis of metabolic transcriptional changes in Jak2V617F mutated c-kit+ cells.
Scale shows upregulated pathways in orange/ red and downregulated pathways in blue.

Next, I wanted to assess metabolic pathway deregulation in human primitive cells, namely Lin$^-$, CD34$^+$ cells. I re-analyzed publicly available single cell Target-seq data, providing genotype and transcriptome data from a single cell (Rodriguez-Meira et al., 2019) from MPN patients. Seurat was used to produce a UMAP (Uniform Manifold Approximation and Projection) cluster analysis. Overall, I identified 7 different clusters in the data, which I annotated to diagnose the status of the samples. Overall, normal donors and ET samples were more closely related with each other with PV samples clustering more separately and more advanced disease in form of MDS/MPN giving rise to yet another cluster.

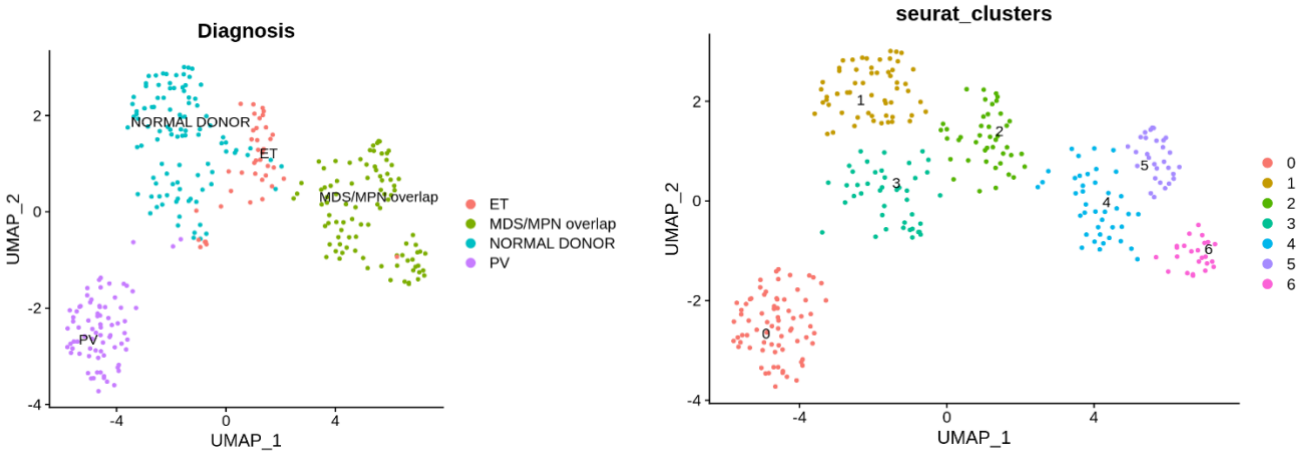

Figure 3.7 UMAPs displaying single cell Target-Seq data from CD34+ normal donors, ET, PV and MPN/MDS patients.

Samples were clustered in an unsupervised manner and disease phenotype annotated.

I then assessed the Target-seq data for metabolic pathway deregulation according to genotype and disease status. The majority of metabolic pathway changes could be observed in CD34$^+$ cells that were HET for JAK2V617F and belonged to ET patients (Figure 3.8 Heatmap summarising KEGG pathway analysis of metabolic transcriptional changes in JAK2V617F mutated CD34+ cells.). Again, fatty acid metabolism was upregulated in ET HET and PV HOM CD34$^+$ cells, with Oxphos, galactose, fructose and mannose metabolism being highly upregulated in ET HET CD34$^+$ cells. These data indicate a deregulation of similar pathways in mice and human primitive cells. However, sphingolipid metabolism in PV HOM CD34+ cells was highly upregulated, which differs from the results in mice. Figure 3.8 Heatmap summarising KEGG pathway analysis of metabolic transcriptional changes in

JAK2V617F mutated CD34+ cells.

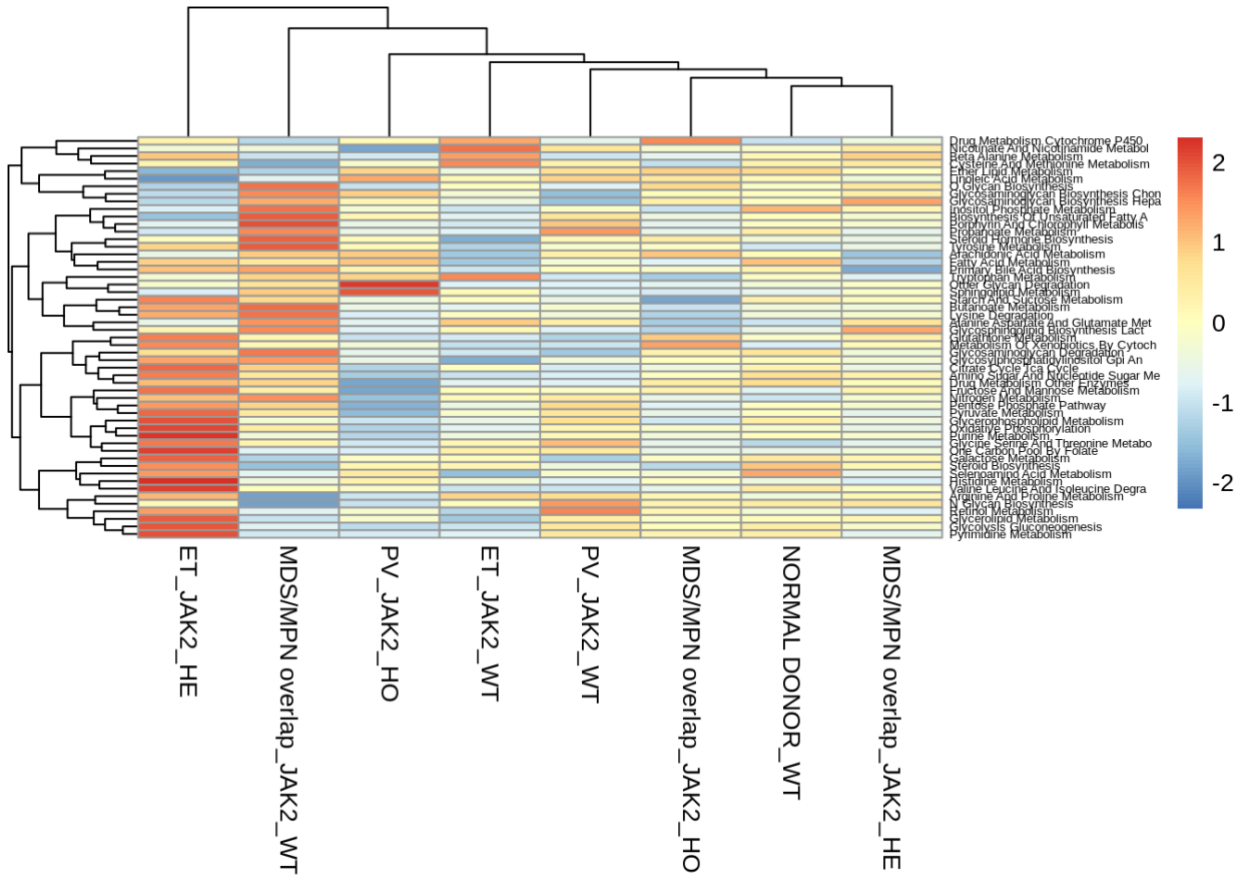

Figure 3.8 Heatmap summarising KEGG pathway analysis of metabolic transcriptional changes in JAK2V617F mutated CD34+ cells.

Scale shows upregulated pathways in orange/ red and downregulated pathways in blue. Disease subtype and JAK2V617F genotype is indicated.

3.3 Discussion

My gene expression data shows many downregulated genes when comparing HOM versus WT Jak2V617F mutated HSPCs. In the downregulated genes, several metabolism genes are apparent, such as Hk3 and mt-Nd5 and mt-Nd6. We now saw a downregulation of both Mitochondrially Encoded NADH Dehydrogenase 5 (mt-Nd5) and Mitochondrially Encoded NADH Dehydrogenase 6 (mt-Nd6), genes which play a role in mitochondrial electron transport chain, enabling NADH dehydrogenase (ubiquinone) activity. Whether mitochondrial function is impaired in Jak2V617F mutated HSPCs needs to be elucidated which I will do in chapter5 where I utilized Seahorse assays to determine OXPHOS activity.

Moreover, the Hk3 gene produces Hexokinases which phosphorylate glucose to produce glucose-6-phosphate which is the first step in the glucose metabolism pathway. Downregulation of the HK3 gene may be related to the decreased oxidative phosphorylation in HOM mice which is in accordance with a low OCR result in HOM mice using Seahorse (see chapter 5 results).

(Rao et al., 2019) reported that the expression of mutant JAK2V617F cells leads to metabolic reprogramming, including an increase in fatty acid catalysis, high level of glycolysis and an increase of ROS levels in their Myeloid and Erythroid progenitor (MEP) cells from a JAK2V617F conditional mouse model. In this study, authors found several metabolic pathways that are deregulated, including Alanine, Aspartate and Glutamate metabolism. Because of the different mice models used, my results were different from them. However, I did identify fatty acid metabolism changes in Hom vs WT comparison, like studies in human ET (Tong et al., 2021).

Several amino acid transporter genes were deregulated between WT vs Het and WT vs Hom *Jak2V617F* mutated cells. Seven families of amino acid transporters in the SLC gene superfamily have been identified to date. Examples are the SLC1A family which are high-affinity glutamate and neutral amino acid transporters, the SLC6A family responsible for Na^+ dependent neurotransmitter transporters, the SLC7A family genes regulating cationic and neutral amino acid transporters. Other important players in this superfamily of genes are SLC16A which regulate monocarboxylate, such as lactate, pyruvate, and others and aromatic amino acid transporters, SLC36A which is involved is H^+ dependent amino acid transport. The exact contributions of the amino acid transporter genes I identified in this study remain to be elucidated.

4 Chapter 4 Characterising the metabolic profile of hematopoietic stem cells in two phenotypes, PV and ET of myeloproliferative neoplasms (MPN)

4.1 Introduction

Patients with Polycythemia Vera (PV) or Essential thrombocythemia (ET) display different clinical manifestations (Barbui and Tefferi, 2012). Haematopoietic stem cells (HSCs) in these two phenotypes show various STAT1 levels, which hinted a possibility of metabolic profile differences between these two phenotypes (Greenfield et al., 2021). HSC's function depends on the cell metabolic levels, including HSC quiescence, renewal and differentiation (Guglielmelli et al., 2014). Therefore, metabolic changes may occur in HSCs of two phenotypes, which influence the HSCs function, leading to the progression of MPN. So, targeting metabolic changes in the HSCs of two phenotypes of MPN may be a potential treatment for MPN except for the existing treatment methods JAK2 inhibitor ruxolitinib and interferon-α.

Mitochondria is the main organelle that is responsible for the oxidative phosphorylation of glucose, transference of electrons to produce H_2O and production of Adenosine triphosphate (ATP) when oxygen is sufficient during cell respiration (De Almeida et al., 2017). Also, when HSC cells are lack of oxygen or in low oxygen levels, mitochondria still get some alternative ways to produce ATP to acquire energy to provide for HSCs function (Chen et al., 2008). As a result of that, mitochondria are the main part that influence cell metabolic profiles. So, it's vital that we have an investigation of mitochondrial profiles of HSC cells in two phenotypes of MPN.

In this thesis, I will study both the HSC and HSPC populations of two phenotypes PV and ET in MPN as defined in and determine how their metabolic profiles change with phenotypes of MPN.

To assess the mass of mitochondria and the mitochondrial redox oxygen species levels in hematopoietic stem cells (Lineage$^-$ Scal1$^+$ c-kit$^+$ LSK cells) in mice, Mitogreen-FITC (MTG-FITC, Biolegend), Mitochondrial Tetramethylrhodamine (TMRM-PE, Biolegend), Carboxymethyl dichlorodihydrofluorescein derivative (CM-H_2DCFDA-FITC, ThermoFisher) and MitoSox Red (MitoSox-FITC, ThermoFisher) markers were used respectively. TMRM-PE was not directly used to stain purified c-Kit$^+$ cells because the selected c-Kit$^+$ cells contain the same cooler of PE (CD117) on the cell surface. The c-Kit$^+$ selection kit

from StemCell Technologies unfortunately only has PE as a marker. Thus, a different panel was designed to visualize c-Kit$^+$ cells from the same bone marrow fraction, using Zombie-BUV395, Lineage-Pacific blue, Scal1-PerCP-cy5.5, c-Kit-APC-cy7 to assess TMRM level. Zombie-BUV395 was included for live/dead cells separation. For MTG, CM-H_2DCFDA and ROS, another panel Zombie-Nir-R780/60, Lineage-Pacific blue, Scal1-APC, c-Kit-PE were used to stain LSK cells. LSK cells were characterized as Lin$^-$Scal1$^+$c-Kit$^+$. After LSK cells were gated, histograms for MTG, TMRM, CM-H_2DCFDA and ROS were generated to show mitochondria mass, mitochondrial membrane potential and mitochondrial ROS levels respectively.

As efflux pumps exist on the cell membrane of Lin$^-$ cells membrane to extrude the MTG and TMRM dye from cells, efflux pumps blockage verapamil was added where appropriate(de Almeida et al., 2017).

Cell metabolic functional analysis is based on three key elements: the assessment of metabolic pathways, energy balance analysis, and mitochondrial function evaluation (DeBerardinis and Keshari, 2022).

Mitochondrial function includes the formation of reactive oxygen species (ROS), mitochondrial membrane potential, and oxygen consumption rate (OCR). OCR has been described above, while reactive oxygen species and mitochondrial membrane potential are detected by flow cytometry technology employing TMRM and ROS dyes. To assess the mass of mitochondria and the mitochondrial redox oxygen species levels in haematopoietic stem cells (Lineage$^-$ Scal1$^+$ c-kit$^+$ LSK cells) in mice, Mitogreen-FITC (MTG-FITC, Biolegend), Mitochondrial Tetramethylrhodamine (TMRM-PE, Biolegend), Carboxymethyl dichlorodihydrofluorescein derivative (CM-H_2DCFDA-FITC, ThermoFisher) and MitoSox Red (MitoSox-FITC, ThermoFisher) markers were used respectively.

In this chapter, I intend to investigate the metabolic shifts in HSCs and HSPCs, specifically analysing mitochondrial alterations within these cell populations in relation to two MPN phenotypes. That is to assess the numbers of mitochondria, the mitochondrial membrane potential and the levels of mitochondrial oxidative phosphorylation among WT, HOM and HET progenitor (Lin$^-$c-Kit$^+$ or Lin$^-$Scal1$^+$c-Kit$^+$) cells. Furthermore, I will also examine whether mitochondrial function can be used to define sub populations of HSCs with different functional profiles.

4.2 Results

4.2.1 Characterisation of MPN mice HSPCs and HSCs mitochondrial activity by flow cytometry

For my experiments, I used LSK cells to interrogate mitochondrial function and ROS levels since those cells represent a more primitive progenitor population. In the gating strategy for LSK cells is shown with a representative example for each experiment Figure 4.1.

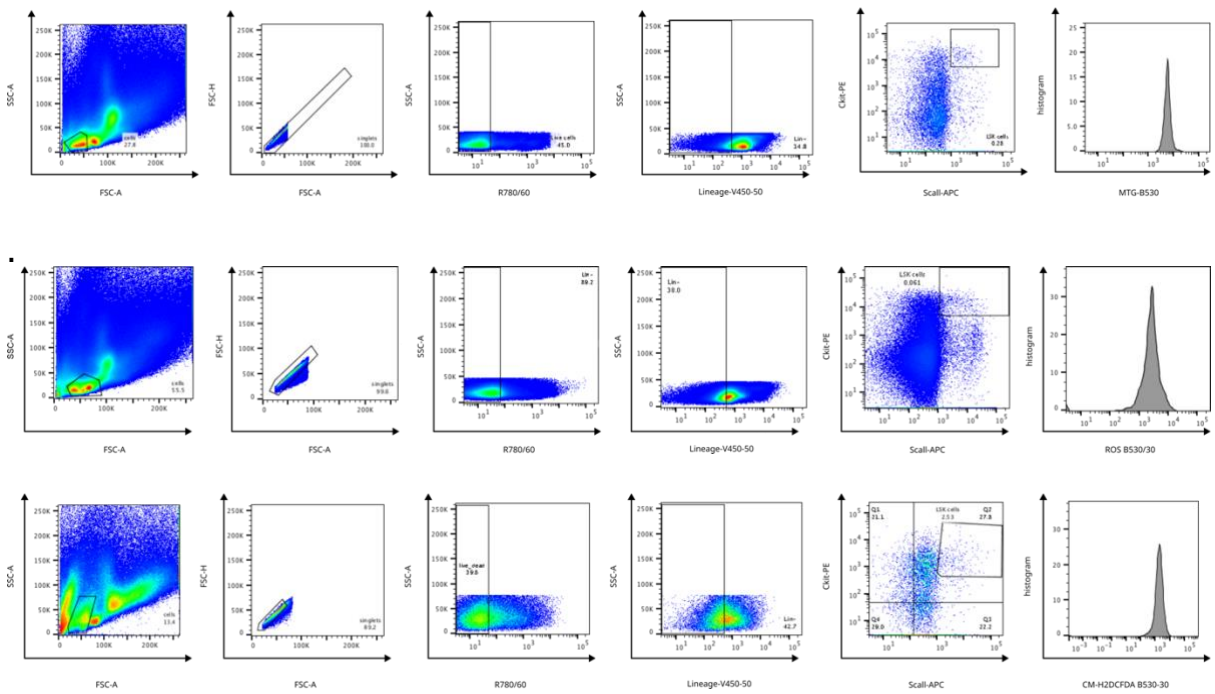

Figure 4.1 Example of LSK gating strategy for Mitotracker Green-FITC A, ROS-FITC B, CM-H2DCFDA-FITCC experiments. Dye colours are indicated in the Y and X axes respectively.

I first wanted to assess the mitochondrial content of LSK cells in our Jak2V617F mouse model. I therefore stained LSK cells for MTG, a marker for mitochondrial mass Figure 4.2. The mean fluorescence intensity of the MTG dye for LSK cells indicated the highest mitochondrial mass in HOM, followed by HET, with the lowest mitochondrial mass being present in WT. The results showed a significant difference among each group, indicating increased numbers of mitochondria in Jak2V617F mutated cells.

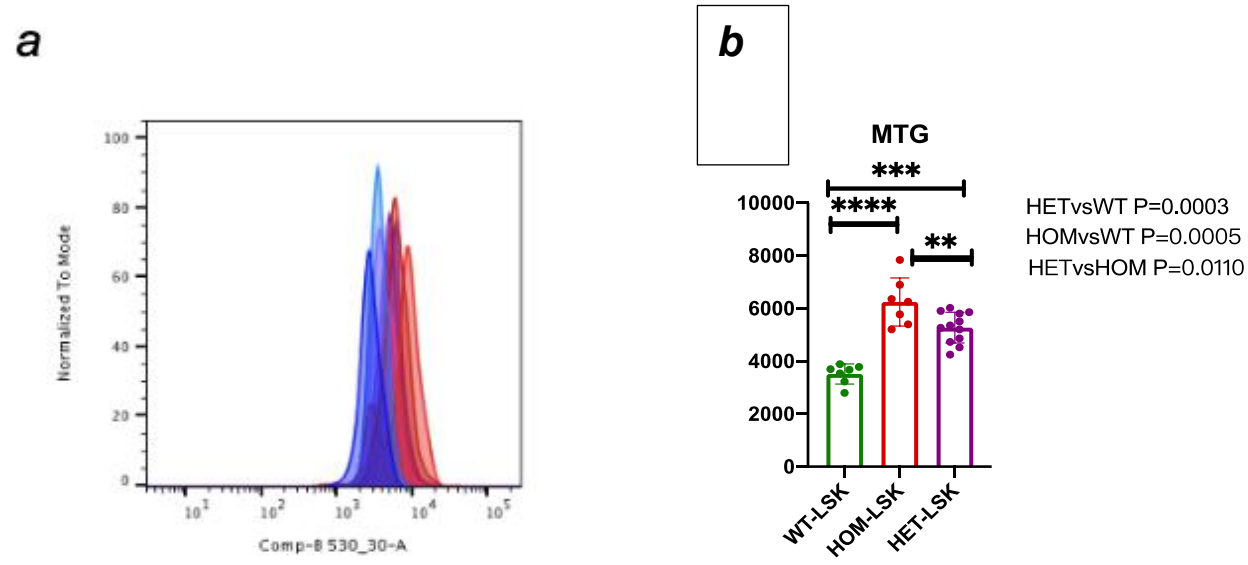

Figure 4.2 MTG histogram and Bar Chart

a) Histograms of Mitochondrial green (MTG) labelled MPN WT, HOM and HET LSK cells. Blue represents WT, Purple represents HET and Red represents HOM. Mean fluorescence intensity (MFI) is used to assess the MTG levels and has been normalized.

b) Bar chart of MTG MFI, Comparisons between HET and WT, HOM and WT, and HET and HOM all have significant differences, with P values 0.0003, 0.0005, 0.0110. P value is calculated using multiple unpaired t-test.

To use a different method for mitochondrial mass content quantification in slightly less primitive cells, namely c-Kit$^+$ cells from our mouse model, I used ddPCR. The *MT-ND1* copy numbers are representing absolute numbers of mitochondrial DNA (mtDNA) to assess the different levels of mitochondria in LSK cells of MPN different phenotypes. The *MT-ND1* copy numbers for c-Kit$^+$ cells from three mice are shown in Table 4.1 The MT-ND1 gene copy numbers representing absolute numbers of mitochondrial DNA (mtDNA) for c-Kit positive cells.. Using this method, the results indicate that the WT1 mtDNA number is higher than HET mtDNA number. Moreover, the WT mtDNA is almost double the value of the HOM, which shows the lowest mt-ND1 copy number change. These results differ from the FACS MTG results above.

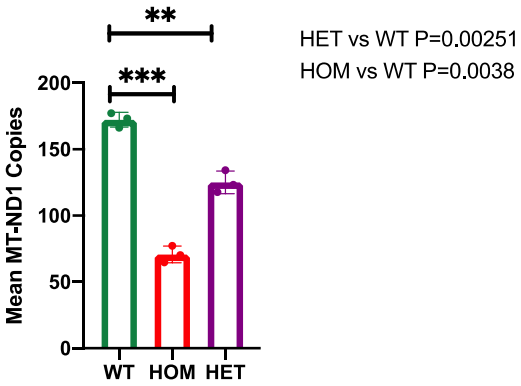

Error! Reference source not found. **Bar chart MT-ND1. Comparisons between HET and WT, HOM and WT both have significant difference, with P values, 0.0251, 0.0038, the p value was calculated using one-way ANNOVA.**

Table 4.1 The MT-ND1 gene copy numbers representing absolute numbers of mitochondrial DNA (mtDNA) for c-Kit positive cells.

Sample	*MT-ND1 Copies/ul*	*MT-ND1 Copies/ul*	*MT-ND1 Copies/ul*	*Mean MT-ND1 Copies/ul*
WT1	160	177	195	177.33
WT2	157	180	183	173.3
WT3	145	175	179	166.3
HOM1	69	68	74	70.33
HOM2	65	60	69	64.67
HOM3	75	80	77	77.33
HET1	103	124	143	123.33
HET2	100	115	138	117.67
HET3	128	130	145	134.33

Next, I wanted to assess the amount of ROS levels in our Jak2V617F mutated mouse model. I therefore used two dyes to assess ROS levels (Table 4.1 The MT-ND1 gene copy numbers representing absolute numbers of mitochondrial DNA (mtDNA) for c-Kit positive cells. Assessment of the mean fluorescence intensity of CM-H_2DCFDA indicated higher mitochondrial ROS levels in HOM and HET compared with WT. These findings confirm previous data showing elevated ROS levels in the context of mutated Jak2V617F in primitive cell types (Lee et al., 2018).

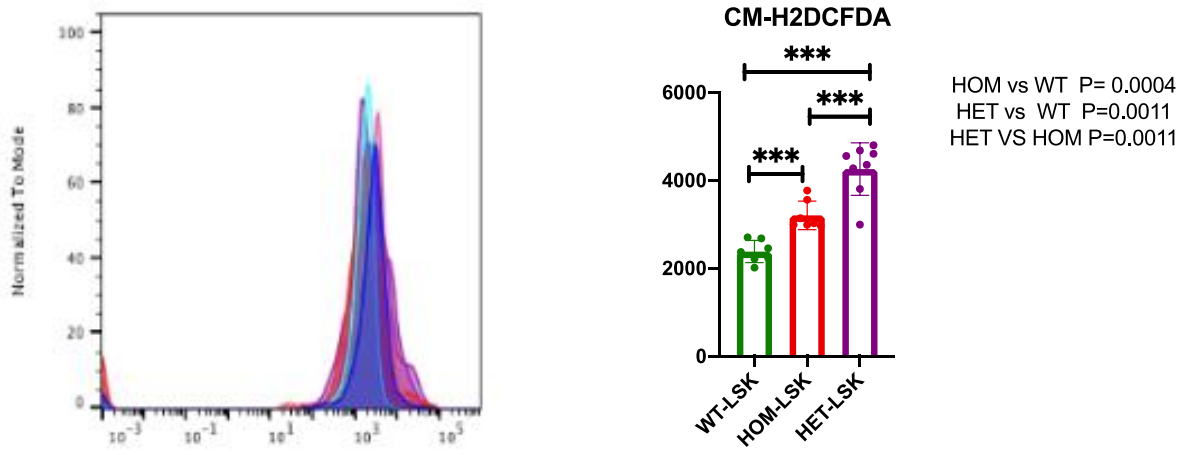

Figure 4.3 Histogram and Bar chart of CM-H_2DCFDA in LSK cells.

a) Histograms of Carboxymethyl dichlorodihydrofluorescein derivative (CM-H_2DCFDA) labelled MPN HET, HOM and WT LSK cells. Mean fluorescence intensity (MFI) is used to assess the CM-H_2DCFDA levels and has been normalized.

b) Bar chart of CM-H_2DCFDA MFI, Comparisons between HET and WT, HOM and WT both have significant difference, with P values 0.0011, 0.0004, the p value was calculated using 2-way ANNOVA.

I then decided to use a different method to assess ROS levels. I therefore stained LSK with using Cell Redox Red dye. This dye stains all redox oxygen species inside all cellular compartments of the cell compared CM-H_2DCFDA which only stains intracellular ROS levels (Oparka et al., 2016). This method confirms my findings in CM-H_2DCFDA, where ROS increases in HOM and HET LSKs compared to WT cells.

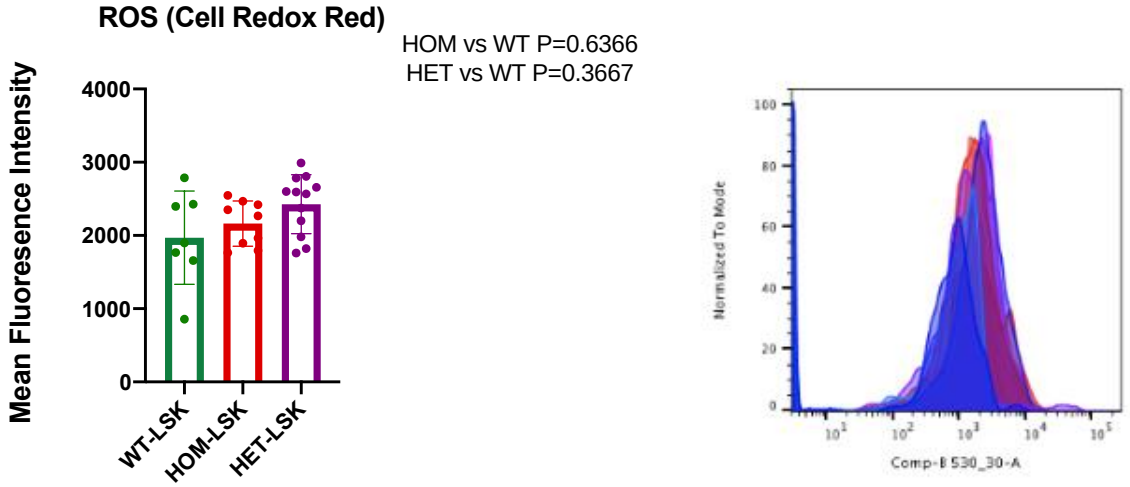

Figure 4.4 Histogram and Bar chart of ROS levels in LSK cells.

a) **Bar chart of mean fluorescence intensity of Cell Redox Red, comparisons between HET and WT, HOM and WT both have significant difference, with P value 0.3667, 0.6366, the p value is calculated using 2-way ANNOVA.**

b) **Histograms of Redox oxygen species (ROS)using Cell Redox Red dye labelled MPN WT, HOM and HET LSK cells. Mean fluorescence intensity (MFI) is used to assess the ROS levels and has been normalized.**

Lastly, I aimed to assess the membrane potential of mitochondria using TMRM to characterize the health of all mitochondria in LSKs with different genotypes. The histogram is a representative image of one set of comparisons with high TMRM being assessed between genotypes (Figure 4.4). My data showed that HET LSK cells had the highest mitochondrial membrane potential, followed by WT, with HOM LSK cells showing the lowest potential.

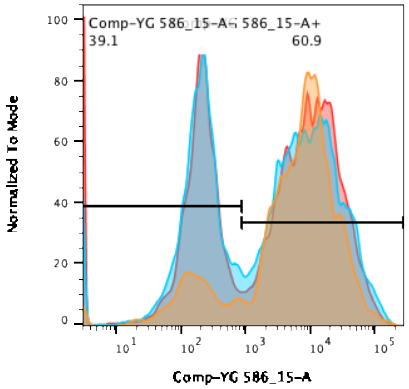

Figure 4.2.6 Histogram and Bar chart of TMRM in LSK cells.

a) Representative Histograms of TMRM labelled MPN LSK cells. Blue represents WT, Purple represents HET and Red represents HOM.

Table 4.2: High TMRM percentage and average in LSK cells

	HIGH	Average High TMRM
WT1	83.8	
WT2	79	
WT3	84.4	
WT4	41.1	
WT5	70.8	71.82
HOM1	44.4	
HOM2	60.8	
HOM3	88.3	64.5
HET1	64.5	
HET2	35	

HET3	60.9	
HET4	81.9	80.77

4.3 Discussion

Verapamil acts as the efflux pumps and is commonly used in hematopoietic stem cells when staining for metabolic related assays, such as mitochondrial dyes (Morganti and Ito, 2021). Verapamil is a type of drug known as calcium channel blockers (Morganti et al., n.d.). Calcium channel blockers are a type of drugs that prohibit the entry of calcium ions into the cells, particularly in the muscle cells of the heart and blood vessels. By inhibiting calcium channels, these drugs alter the intracellular movement of calcium, resulting in a range of physiological effects leading to various physiological effects. I therefore used it for all my experiments.

Mitochondrial dyes are not limited in MTG, TMRM and ROS, there are some more mitochondrial dyes which are commonly used such as DilC1 (50nM, ThermoFisher) or JC-1 (2uM, ThermoFisher) which can indicate mitochondrial fission and fusion.

JC-1 is commonly used as a marker for mitochondrial membrane potential (Jiang et al., 2015). It is a positively charged dye that accumulates in mitochondria in a manner dependent on membrane potential. One of the unique features of JC-1 is its dual-emission capability (Sivandzade et al., 2019). In high mitochondrial membrane potential healthy cells, JC-1 forms aggregate and emits red fluorescence. In depolarized or unhealthy cells, JC-1 remains in its monomeric form, emitting green fluorescence. This enables radiometric analysis, offering a quantitative assessment of membrane potential. JC-1 is widely used in various assays, including flow cytometry, fluorescence microscopy, and plate reader-based assays, making it highly adaptable to different experimental setups. JC-1 only focuses on mitochondrial membrane potential; it could not estimate other aspects of mitochondrial function. JC-1 is often utilised in combination with other assays to obtain a more comprehensive understanding of cellular processes. In summary, JC-1 is a valuable tool for assessing mitochondrial membrane potential, but the limitations and optimised experimental conditions should be obtained to get accurate results.

ddPCR for MT-ND1 is a more concise method to determine the mitochondrial amount compared to MTG staining. ddPCR allows for the absolute quantification of nucleic acid targets without the need for standard curves. It provides an absolute count of the number of target molecules in the sample. It is particularly useful when quantifying low-abundance

targets or when dealing with samples with a limited amount of starting material. The partitioning of the sample into droplets reduces competition for reagents and amplification bias, leading to improved accuracy in quantification. The "digital" aspect of ddPCR, where each droplet is treated as an independent reaction, makes the technique robust against PCR inhibitors and allows for more accurate detection of rare mutations or low-abundance targets. Since I used ddPCR for the more heterogeneous cell population of a mix of primitive and more mature progenitor cells, namely c-Kit$^+$ cells, for the ddPCR experiment, compared to the MTG experiment where is used more primitive LSK cells, my results are difficult to compare and discrepancies in my findings are most likely due to the different cell populations I examined.

Overall, mitochondria have complex biological activities, including mitochondrial fission and fusion. Since the dye only shows one time point as a snapshot of the mitochondrial state, it is influenced by the cell status. For example, if mitochondria are in the fission state, higher amounts of TMRM and ROS species can be detected. Consequently, stress avoidance by direct evaluation immediately after bone marrow crushing is important. Moreover, redox oxygen species are sensitive to the time cells are exposed to oxygen, therefore requiring simultaneous sample processing of all comparison groups. These additional factors may influence discrepancies in results reported between different methods in this chapter.

4.4 In summary

In this chapter, we performed the metabolic functional analysis of c-Kit$^+$ bone marrow cells from MPN three phenotypes' mice. For the first time, we identified different mitochondrial amount and mitochondrial membrane potential between them. MPN *Jak2V617F* homozygous mice c-Kit$^+$ cells have less functional mitochondria with higher numbers of mitochondria, while *Jak2V617F* heterozygous mice c-Kit$^+$ cells have more functional mitochondria with less numbers of mitochondria.

5 Chapter 5 Metabolic profiling of hematopoietic stem and progenitor cells in MPN mice

5.1 Introduction

In metabolic labelling studies using stable isotopes like ^{13}C-labeled glucose, the term "second pass" for citrate describes how carbon atoms can cycle through the tricarboxylic acid (TCA) cycle multiple times, adding additional ^{13}C labelling to citrate with each round (Grankvist et al., 2024).

In the first pass, ^{13}C-labeled acetyl-CoA (derived from labelled substrates like glucose or pyruvate) enters the TCA cycle, producing citrate with a specific labelling pattern. As the TCA cycle progresses, carbons from acetyl-CoA are incorporated into various intermediates and ultimately recycled into oxaloacetate (OAA), which then combines with another acetyl-CoA molecule. This process forms citrate again, now with more ^{13}C atoms added, leading to a "second pass" of labelling (Nakorchevsky and Yates, 2012)

Each additional pass allows more labelled carbons to accumulate in citrate and other intermediates, revealing details about cycle turnover rates and fluxes through various pathways. This repeated labelling can help scientists track metabolic fluxes in detail, which is valuable in studies of cellular metabolism (Ma et al., 2019).

In metabolism, 'redundancy' is a key characteristic of cells, reflecting the existence of multiple metabolic pathways (Boroughs and DeBerardinis, 2015). In other words, metabolites can be synthesized or converted through various pathways (Koundouros and Poulogiannis, 2020). If one pathway is inhibited, an anaplerotic pathway can compensate by filling the gaps(Kang et al., 2018). This redundancy ensures flexibility, enabling cells to meet their energy demands under different environmental conditions (Finley et al., 2013).

For ^{13}C metabolic flux analysis (^{13}C-MFA), this redundancy means that solely relying on external metabolites' uptake and secretion rates (such as glucose uptake rate or lactate secretion rate) cannot accurately distinguish which specific metabolic pathways are driving particular reactions (Long and Antoniewicz, 2019). Therefore, researchers need to use more precise analytical methods, such as stable isotope labelling, to reveal the specific contributions of different intracellular metabolic pathways (Arkoun et al., 2022).

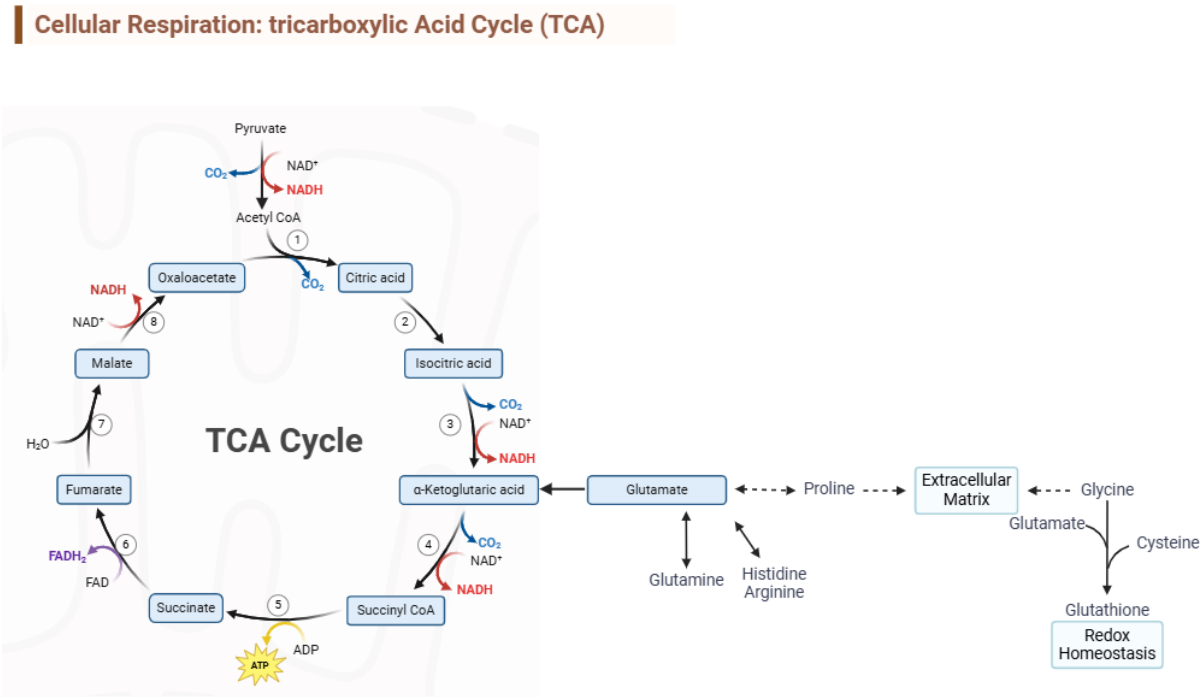

Figure 5.1 Summary of TCA cycle and Glutamate/Glutathione metabolic pathways.

Metabolic functional analysis of metabolites derived from mass spectrometry provides insights into the biochemical roles and functions of various metabolites within biological systems (Oguro, 2019). This analysis involves the following key steps: metabolite identification, quantification, pathway mapping, functional inference, bioinformatic analysis and visualization (Nakorchevsky and Yates, 2012). Mass spectrometry (MS) is first used to identify and quantify the metabolites in a sample. Using mass spectrometry (MS), researchers can acquire high-resolution data across a diverse range of metabolites, such as amino acids, lipids, carbohydrates, nucleotides, and organic acids (Nakorchevsky and Yates, 2012). As for pathway mapping, identified metabolites are mapped onto known biochemical pathways (Boroughs and DeBerardinis, 2015). This can help reveal how changes in metabolite levels are associated with certain metabolic processes, such as glycolysis, the tricarboxylic acid (TCA) cycle, fatty acid oxidation, or amino acid metabolism. When the step comes to Functional Inference, metabolite profiles are analyzed under varying conditions to determine how metabolic functions are modified (Ma et al., 2024). For instance, an increase in glycolytic intermediates might suggest a shift toward glycolysis over oxidative phosphorylation, as seen in rapidly proliferating cells or in immune cells during activation. For the last step, bioinformatic analysis and visualization: computational tools and software help visualize and interpret the data, enabling researchers to model metabolic

networks and predict functional relationships or bottlenecks within metabolic pathways (Shastry and Sanjay, 2020).

In this chapter, I will use ^{13}C-labelled Glucose to culture LSK cells for 24 hours to trace the metabolic pathways by utilizing LC-MS and characterize anaplerotic pathways involved (Grankvist et al., 2024).

5.2 Results

5.2.1 Assessing oxidative phosphorylation and glycolysis in HSPCs from MPN mice using the Seahorse XF analyser

To evaluate oxidative phosphorylation and glycolysis pathways in HSPCs from MPN mice, c-Kit$^+$ cells from *Jak2V617F* WT, *Jak2V617F* HOM and *Jak2V617F* HET murine bone marrows were analysed using the Seahorse XF96 Analyzer (Plitzko and Loesgen, 2018). The Seahorse XF96 Analyzer tracks mitochondrial respiration and glycolysis in cells by continuously monitoring oxygen and proton levels in the cell supernatant (Plitzko and Loesgen, 2018). The mitochondrial respiration and glycolysis rates were measured after isolating c-Kit$^+$ cells from mouse bone marrow using a c-Kit$^+$ cell selection kit. Injections of mitochondrial complex V inhibitor oligomycin, mitochondrial uncoupler FCCP, mitochondrial complex III inhibitor Antimycin A and mitochondrial complex I inhibitor Rotenone were administered sequentially to further evaluate the functional metabolic profiles of the mitochondria (Plitzko and Loesgen, 2018). Previous studies have documented the seahorse method's notable inter-assay variability (Mercier-Letondal et al., 2021). This variability can complicate the analysis of experiments conducted on different plates and at varying times (Mercier-Letondal et al., 2021).

As a result, we analyzed 4 *Jak2V617F* HOM and 3 *Jak2V617F* WT mice simultaneously on a single Seahorse plate. All mice were aged between 8-11 weeks. The overall trend showed that the oxidative phosphorylation rate of HOM c-Kit$^+$ cells was lower compared to that of WT mice. c-Kit$^+$ cells from all four HOM mice exhibited significantly lower oxygen consumption rates compared to all three WT mice across various parameters, including basal mitochondrial respiration, ATP-linked respiration, proton leak, maximal respiration rate, reserve capacity, and non-mitochondrial respiration rate, with P-values of 0.02, 0.04, 0.01, 0.03, 0.09 and 0.17, respectively. All four HOM mice and three WT mice exhibited

nearly identical extracellular acidification rates. Basal ECAR and Glyco-reverse rates showed no significant differences between HOM and WT c-Kit$^+$ cells. These findings suggest that there is reduced respiration of HOM c-Kit$^+$ cells under specific medium conditions, compared to WT c-Kit$^+$ cells, which indicates mitochondrial dysfunction in HOM *Jak2V617F* c-Kit$^+$ cells. This dysfunction could be related to the JAK2 mutation burden in c-Kit$^+$ cells from HOM mice (Li et al., 2014; Nageswara Rao et al., 2019).

The same protocol was applied to 6 *Jak2V617F* HET and 4 WT mice, all aged between 8 and 11 weeks. The overall trend indicated that the respiration rate of c-Kit$^+$ cells from HET mice was higher than that of WT mice. All six HET mice exhibited higher oxygen consumption rates than all four WT mice with c-Kit$^+$ cells. This was observed across various parameters, including basal mitochondrial respiration, ATP-linked respiration, proton leak, maximal respiration rate, reserve capacity, and non-mitochondrial respiration rate, with P values of 0.01, 0.01, 0.046, 0.01, 0.86, 0.33, respectively. All six HET mice and four WT mice exhibited similar extracellular acidification rates. Basal ECAR and Glyco-reverse rates showed no significant differences between HET and WT c-Kit$^+$ cells. These findings suggest that HET c-Kit$^+$ cells have higher respiration rates under specific medium conditions compared to WT c-Kit$^+$ cells, indicating a stronger reliance on oxidative phosphorylation in HET c-Kit$^+$ cells compared to WT and HOM cells. This could be linked to the JAK2 mutation burden in c-Kit$^+$ cells of HET mice, along with possible dysregulation of other metabolic pathways in these mice (Li et al., 2014; Nageswara Rao et al., 2019).

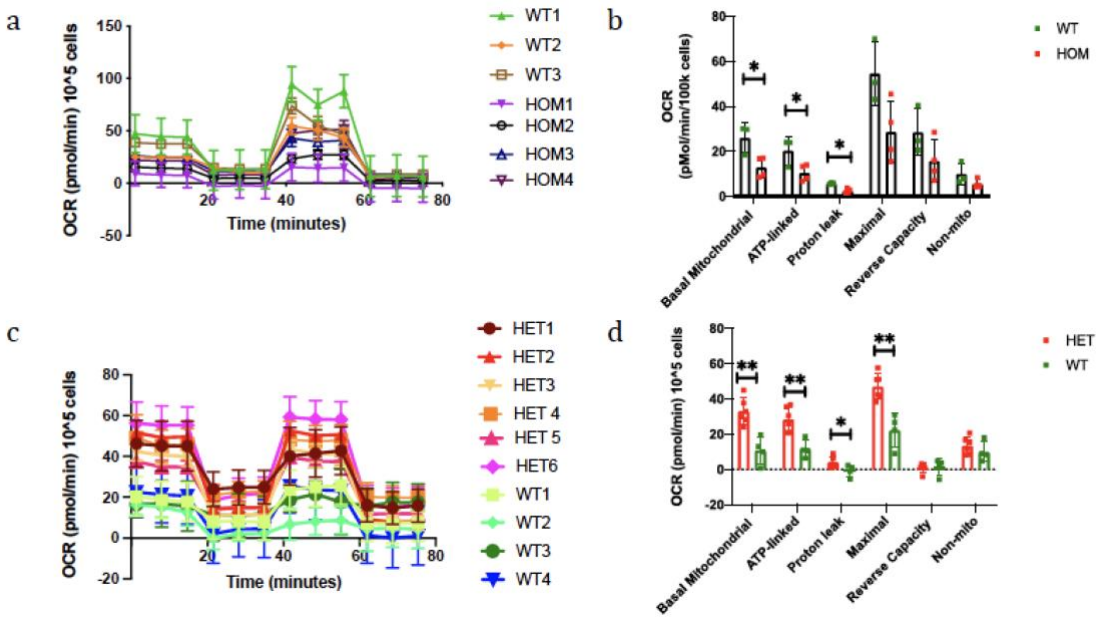

Figure 5.2 Seahorse assay in MPN bone marrow cells.
a) Oxygen Consumption Rate (OCR) was measured in murine c-Kit positive cells in mice with PV(HOM) and WT littermates using Seahorse to assess mitochondrial respiration. Genotypes are indicated. Control is Seahorse media with growth factors. b) Bar chart summary of all seahorse replicates shown in Figure a. Significant results are indicated with *. Red=PV, Green=ET. c) Oxygen Consumption Rate (OCR) was measured in murine c-Kit positive cells in mice with ET (HET) and WT littermates using Seahorse to assess mitochondrial respiration. Genotypes are indicated. d) Bar chart summary of all Seahorse replicates shown in Figure c. Significant results are indicated with *, Red=ET, Green=WT.

5.2.2 Titration of IACS-010759 concentration in hematopoietic stem and progenitor cells from MPN mice

One highly potent and specific small-molecule inhibitor of complex I is IACS-010759 (Yap et al., 2023). For ex vivo applications, it has been tested across a concentration range of 0 nM to 100 nM (Molina et al., 2018). To establish the optimal concentration for our MPN mouse model, we conducted a titration experiment using concentrations of 30 nM, 45 nM, 60 nM, 75 nM, and 90 nM in ^{13}C-glucose tracing studies with c-Kit$^+$ cells from MPN heterozygous HET mice. Each condition included 100,000 HET c-Kit$^+$ cells per well. Following a 24-hour incubation with ^{13}C-glucose, intracellular metabolites were extracted and analysed using LC-MS. Metabolite Autoplotter 2.6 was then employed to determine absolute and relative peak areas for TCA cycle metabolites (Pietzke and Vazquez, 2020). The results indicated that, in the absence of IACS, c-Kit$^+$ cells from HET mice primarily utilized glucose as their

main energy source. Most of the glucose entered the TCA cycle, generating labelled metabolites, particularly citrate, α-ketoglutarate (AKG), and glutamate. The absolute and relative peak areas confirmed this finding. All TCA cycle metabolites were labelled as expected, indicating that the complete TCA cycle was actively utilized in c-Kit^{+} cells initially.

All IACS concentrations from 30nM to 90nM were effective, showing a reduction in isotopologue labelling across all TCA cycle metabolites. To minimize the excessive impact of IACS, we selected 30nM as the concentration for all subsequent experiments Figure 5.3.

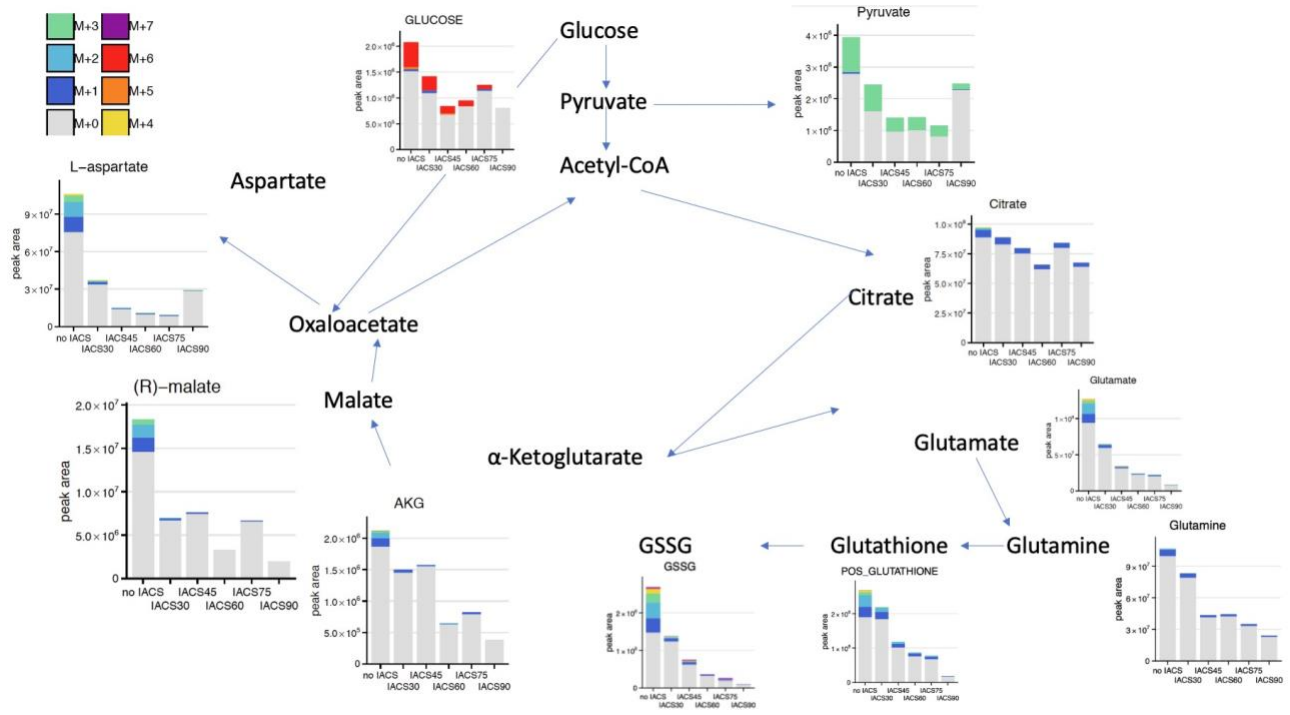

Figure 5.3 Absolute Peak Areas of TCA cycle Metabolites in 24h ^{13}C-Glucose Tracing

LC-MS Analysis of c-Kit^{+} cells in MPN Jak2V617F HET Mice at Varying IACS levels.

The absolute peak areas of TCA cycle metabolites were measured in MPN HET c-Kit^{+} cells cultured for 24 hours with ^{13}C-labeled glucose under conditions of no IACS, 30 nM IACS, 45 nM IACS, 60 nM IACS, 75 nM IACS, and 90 nM IACS.

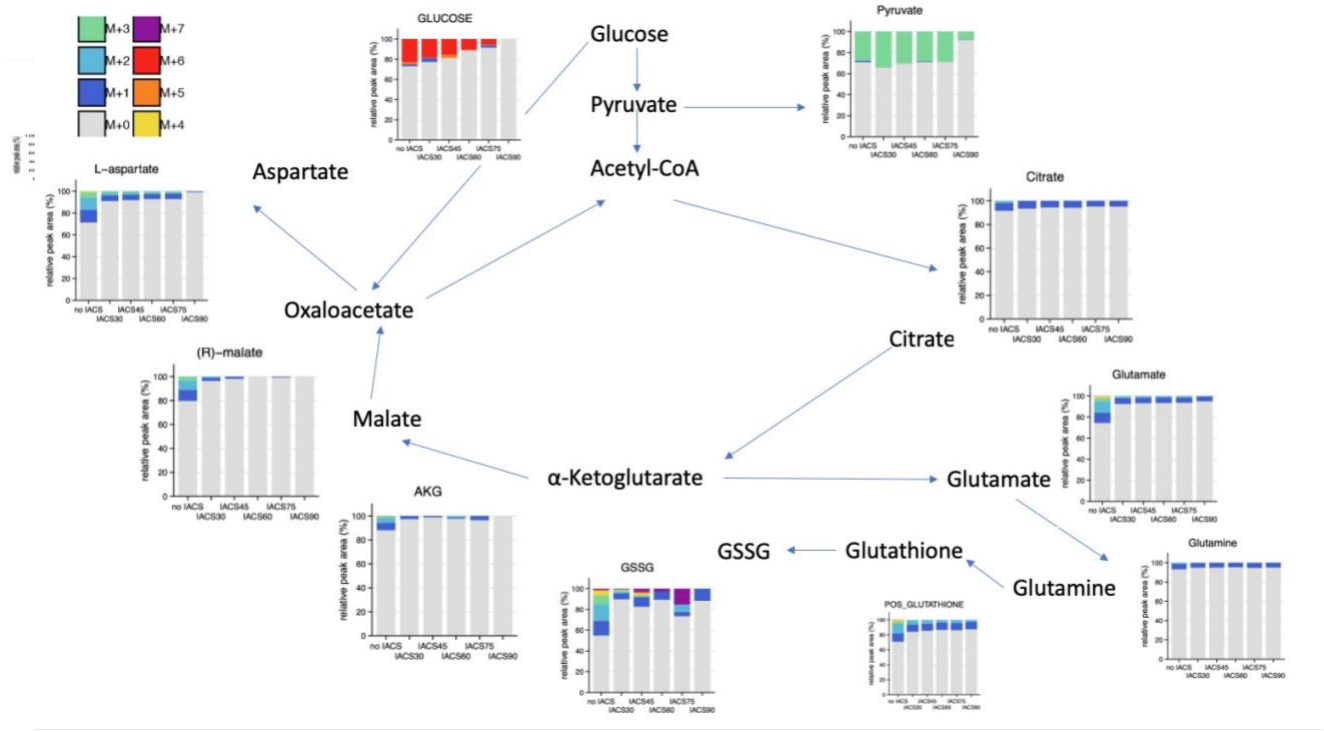

Figure 5.4 Relative Peak Areas of TCA cycle Metabolites in 24h ^{13}C-Glucose Tracing
LC-MS Analysis of c-Kit^{+} cells in MPN Jak2V617F HET Mice at Varying IACS levels.

The relative peak areas of TCA cycle metabolites were measured in MPN HET c-Kit^{+} cells cultured for 24 hours with ^{13}C-labeled glucose under conditions of no IACS, 30 nM IACS, 45 nM IACS, 60 nM IACS, 75 nM IACS, and 90 nM IACS.

5.2.3 Metabolic profiling of WT, HOM and HET LSK cells Using ^{13}C-labeled glucose tracing

5.2.3.1 MPN HOM and HET LSK cells rely on the TCA cycle, targeted by IACS.

In experiment 1, after 24 hours of culturing LSK cells in a medium containing uniformly labelled ^{13}C-glucose, the cell numbers varied across the genotypes. Of note, all the metabolites in the TCA cycle were labelled with varying numbers of ^{13}C carbons. For intracellular metabolite ^{13}C tracing after 24h, glucose was labelled as M+6 in WT, HOM and HET LSK cells, and its relative peak area of glucose showed a decreasing trend when treated with IACS-010759. A small fraction of M+1 glucose was detected, which can be attributed to natural isotopic abundance. Pyruvate was predominantly labelled as M+3 across WT, HOM and HET LSK cells, and its relative peak area percentage also decreased with IACS-010759 treatment. Citrate showed labelling from M+1 to M+5 in HOM and HET LSK cells. The proportions of M+1, M+2, M+3 and M+4 were similar between HOM and HET LSK cells. However, the HET-IACS group exhibited a lower proportion of M+2

compared to the HOM-IACS group. This reduction in M+2 suggests increased flux toward anaplerotic pathways in HET cells. However, the relative peak area of glutamine remained stable across all three phenotypes and was only labelled as M+1, suggesting that glutamate was not being converted into glutamine within the cells. In contrast, the glutathione and GSSG peak areas showed extensive labelling from M+1 to M+6, indicating the involvement of glutamate in anaplerotic pathways.

In the ^{13}C tracing of extracellular metabolites, glucose in the medium was consistently labelled as M+6 across all six samples, with similar relative peak area percentages. For pyruvate, almost all six samples showed heavy labelling with M+3, indicating pyruvate excretion from the cells. Interestingly, the WT-IACS sample exhibited an increased relative peak area compared to the WT sample, whereas the HOM-IACS sample showed a decreased relative peak area compared to the HOM sample. This suggests that with the complex I inhibitor (IACS), cells were partially utilizing glucose for anaplerotic pathways. If cells relied solely on glycolysis, the pyruvate levels would be expected to remain consistent. However, the observed differences indicate that WT cells may predominantly follow the glycolysis pathway, while HOM cells are less reliant on glycolysis. A possible explanation is that HOM cells utilize the pentose phosphate pathway (PPP), which diverts labelled glucose into glucose-6-phosphate.

In experiment 2, after 24 hours of intracellular ^{13}C tracing, the overall metabolite trends were like those observed in experiment 1. However, some differences were noted in specific metabolites. For instance, D-glucose-6-phosphate was labelled as M+6 in the HOM and HET samples, indicating the presence of the pentose phosphate pathway (PPP). Additionally, the detection of M+3 pyruvate in HOM and HET samples with IACS treatment suggests that these cells were not solely relying on the glycolysis pathway. Furthermore, the heavy labelling observed in glutamate, glutathione, and GSSG indicates the activation of another anaplerotic pathway.

In experiments 3 and 4, the trend of both the metabolites from inside the cells and medium showed similar trends compared to experiments 1 and 2, although the percentage of relative peak area varied between samples. However, the data revealed the same anaplerotic pathway, both PPP and glutamate-glutathione and GSSG pathways.

After 24 hours of culturing cells in a medium containing uniformly labelled Carbon 13 labelled glucose, one would expect most glucose to be fully labelled as M+6 (all six carbons labelled with ^{13}C) due to the initial addition of ^{13}C-glucose in the media. However, the presence of M+1 glucose, as well as M+3 pyruvate, indicates that there is some unlabelled carbon entering the glucose pool and glycolytic pathway (Figure 5.5)

The presence of M+1 glucose could result from metabolic recycling. Cells may release unlabelled carbon sources (e.g., through the breakdown of other macromolecules or metabolic by-products) back into the media, where they mix with the labelled glucose (Martin et al., 2016). For instance, cells can synthesize glucose from partially labelled intermediates, which can dilute the fully labelled ^{13}C-glucose pool and produce glucose molecules with one or a few ^{13}C atoms. The presence of M+1 could also indicate some levels of glucose synthesis or exchange with other carbon sources over time, such as through gluconeogenesis pathways or the incorporation of one unlabelled carbon.

As for M+3 Pyruvate**,** normally, glycolysis of M+6 glucose would produce M+3 pyruvate, as each molecule of glucose (6 carbons) splits into two molecules of pyruvate (each with 3 carbons) containing three ^{13}C atoms. This labelled pyruvate in the media likely reflects incomplete uptake by cells or partial release after glycolysis. Alternatively, it could arise if cells release some of the labelled pyruvate back into the media as they metabolize glucose. Another proper explanation maybe the potential Metabolic Exchange and Release: Cells could be taking up glucose, metabolizing it, and releasing labelled metabolic by-products, which re-enter the media and dilute the isotopic labelling pattern. This release and re-uptake process can lead to mixed labelling patterns, especially over extended culture times like 24 hours. The third reason for that maybe the incomplete glucose uptake or exchange with the media: Cells might not fully consume the M+6 glucose, leaving some ^{13}C-glucose in the media. Some exchange with other metabolic sources (e.g., amino acids or other carbohydrates) could result in mixed isotopologue, such as M+1 glucose or partially labelled pyruvate.

In summary, the observed M+6 and M+1 glucose and M+3 pyruvate after 24 hours in ^{13}C-glucose media suggest a combination of factors, including: Metabolic recycling and exchange of intermediates, Incomplete or variable uptake and utilization of the labelled glucose, release of labelled intermediates like pyruvate back into the media.

These complex interactions between cellular metabolism and media components over time create mixed isotopologue patterns in the extracellular metabolites.

The four experiments also revealed a role for glutamate, glutamine, Gluthothine, GSSG metabolic pathways. In comparing the metabolic labelling patterns between HET (heterozygous) and HOM (homozygous) conditions, I noticed some key points:

Glycolytic and TCA Cycle Metabolites: The HET samples generally showed higher labelling (e.g., M+2, M+3, etc.) across various intermediates like pyruvate, citrate, and malate compared to the HET samples. This suggests an increased flux of labelled carbons (possibly from labelled glucose) through glycolysis and the TCA cycle in HOM samples, indicating a possible upregulation in these pathways. In HOM samples, there appears to be a higher incorporation of labelled carbons in both aspartate and AKG compared to HET. This could indicate an enhanced activity of pathways related to amino acid synthesis or anaplerotic reactions (replenishing TCA intermediates). Aspartate, derived from oxaloacetate, shows increased labelling in HOM, which may reflect greater TCA cycle activity or shuttling of intermediates towards amino acid biosynthesis. Both glutamate and glutamine show slightly higher levels of labelled carbons in HOM than in HET samples. Since glutamate and glutamine are closely linked to TCA cycle intermediates (via α-ketoglutarate), this also supports the idea that HOM samples may have increased TCA cycle activity or altered amino acid metabolism. The increased labelling in GSSG (M+5, M+6, and M+7) in HOM samples compared to HET suggests a higher synthesis rate of glutathione, possibly in response to oxidative stress or increased cellular demand for antioxidant protection. Elevated labelling in GSSG in HOM may imply that HOM cells are under a higher oxidative burden, necessitating more glutathione turnover to manage reactive oxygen species. HOM samples showed a broader distribution of labelled isotopologue (e.g., higher M+ forms across multiple metabolites), indicating enhanced metabolic fluxes and possibly a shift in metabolic programming compared to HET samples.

The altered labelling patterns in TCA cycle intermediates and downstream metabolites (like glutamate and GSSG) in HOM suggest that these cells may be adapting their metabolism to meet different bioenergetic or biosynthetic demands, possibly due to genetic differences associated with the homozygous mutation.

In summary, this comparison suggests that HOM cells have an increased metabolic activity, particularly in pathways associated with the TCA cycle, amino acid biosynthesis, and glutathione metabolism, relative to HET cells. This might reflect differences in metabolic reprogramming or stress response due to genetic variation between the two groups.

The labelling patterns and relative intensities of metabolites in this metabolic map indicate metabolic differences. For Glutamate Transporters: Cells have specific transporters for glutamate, such as SLC1A family transporters, particularly EAAT (excitatory amino acid transporters) in neurons and other tissues. These transporters are responsible for the uptake of glutamate into cells, preventing excessive extracellular accumulation, which can be toxic, especially in neural tissue. In non-neuronal cells, other transporters (like SLC7A11, which functions in the antiporter system) mediate the exchange of glutamate with other amino acids, such as cystine. This exchange plays a role in redox regulation and glutathione synthesis. For Glutamine Transporters: Glutamine is transported through various transporters, including SLC1A5 (also known as ASCT2) and SLC38 family transporters (like SNATs). ASCT2 is a prominent transporter involved in glutamine uptake, especially in rapidly proliferating cells (e.g., cancer cells) that use glutamine as a fuel source and nitrogen donor. Some transporters, like SLC7A5/LAT1, function as antiporters that exchange glutamine for other amino acids (like leucine), facilitating nutrient signalling and metabolic regulation. For Glutamate-Glutamine Cycle: In certain tissues, particularly in the brain, there is an essential glutamate-glutamine cycle between neurons and astrocytes. Neurons release glutamate as a neurotransmitter, which is then taken up by astrocytes. In astrocytes, glutamate is converted to glutamine and subsequently released back to neurons, where it can be converted back to glutamate. This cycle helps regulate neurotransmitter levels and maintain cellular health. In cancer cells and other rapidly proliferating cells, the exchange of glutamine and glutamate across the membrane is especially important. These cells often rely on glutamine for energy production (via glutaminolysis) and biosynthesis. They may release glutamate as a byproduct or exchange it to maintain intracellular glutamine levels, supporting growth and survival. The exchange of glutamate and glutamine across the membrane allows cells to adapt to varying metabolic conditions. For example, during nutrient stress, cells may uptake more glutamine to fuel the TCA cycle and produce α-ketoglutarate, which can be further metabolized into other intermediates.

In summary, glutamate and glutamine are indeed exchanged across the cell membrane, and this process is tightly regulated by various transporters. This exchange allows cells to manage nitrogen metabolism, maintain redox balance, participate in intercellular signalling (particularly in the brain), and support biosynthetic and energy needs in proliferative states.

The data suggest that HET cells, rather than HOM, exhibit increased metabolic flux through the TCA cycle, higher glutathione turnover, and possibly enhanced amino acid metabolism. This metabolic reprogramming in HET cells could reflect adaptations or responses to unique metabolic demands or stressors associated with their genetic makeup.

Table 5.1 Cell counting after sorting and O/N culture for Experiment1

LSK cell number	WT (M, 7w)	HOM (M, 7w)	HET (M, 7w)
After Sorting	330,812	331,520	350,000
After O/N culture	400,000	350,000	500,000

Table 5.2 Experiment1 Cell counting before and after ^{13}C6 Glucose* Trace

LSK cells number	WT	WT-IACS	HOM	HOM-IACS	HET	HET-IACS
Before Glucose* Tracing	200,000	200,000	175,000	175,000	250,000	250,000
After Glucose* Tracing	85,000	85,000	155,000	100,000	500,000	187,500

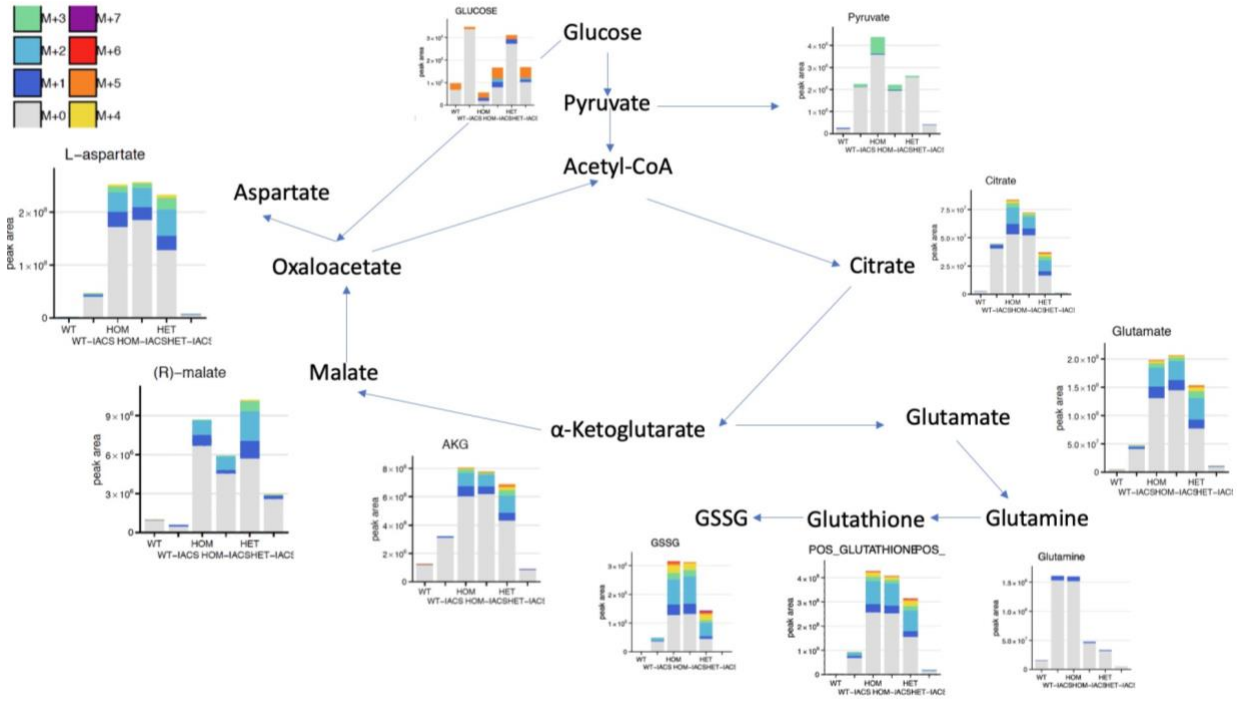

Figure 5.5 LC-MS profiles of LSK MPN cells.

Absolute isotope distribution of indicated metabolites of TCA cycle in WT, HOM and HET LSK cells from experiment1 (The order is WT, WT-IACS, HOM, HOM-IACS, HET, HET-IACS).

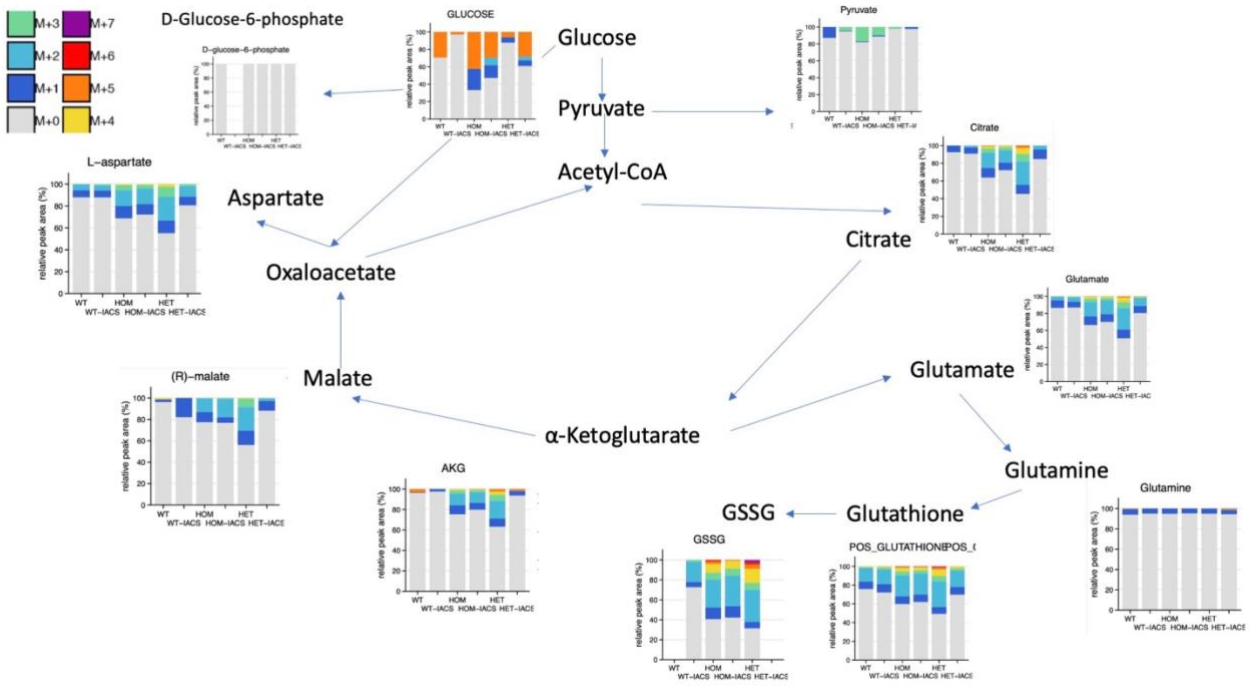

Figure 5.6 Experiment1-LC-MS profiles of LSK MPN cells.

Relative isotope distribution of indicated metabolites of TCA cycle in WT, HOM and HET LSK cells from experiment1 (The order is WT, WT-IACS, HOM, HOM-IACS, HET, HET-IACS).

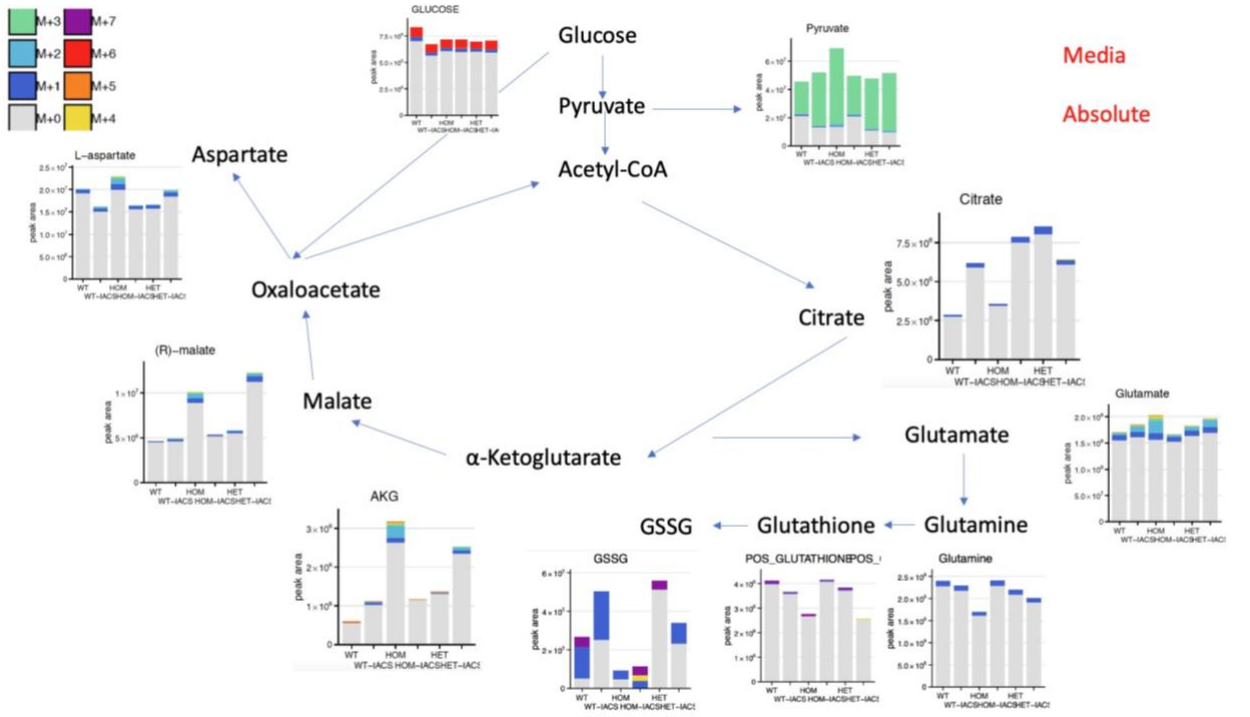

Figure 5.7 Experiment1-LC-MS profiles of culture Media after 24 hour incubation of LSK cells

Absolute isotope distribution of indicated metabolites of TCA cycle in the media of WT, HOM and HET LSK cells after 24h incubation from experiment1 (The order is WT, WT-IACS, HOM, HOM-IACS, HET, HET-IACS).

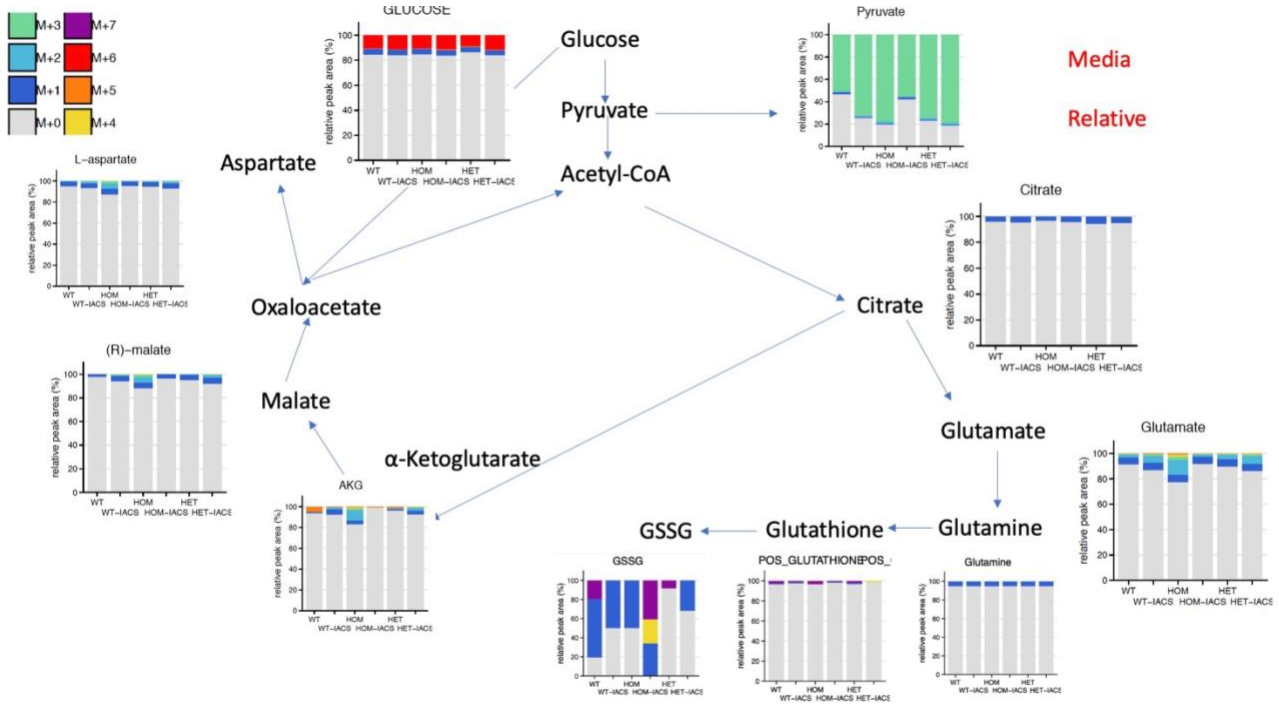

Figure 5.8 LC-MS profiles of culture Media after 24-hour incubation of LSK cells

Relative isotope distribution of indicated metabolites of TCA cycle in the media of WT, HOM and HET LSK cells after 24h incubation from Experiment1 (The order is WT, WT-IACS, HOM, HOM-IACS, HET, HET-IACS).

Experiment 2

Table 5.3 Experiment2 cell counting after sorting and O/N culture

LSK cells number	WT (F, 8w)	HOM (M, 6w)	HET (M, 6w)
After Sorting	38,000	52,000	120,000
After O/N culture	74,000	55,750	75,500

Table 5.4 Experiment2 cell counting before and after [$^{13}C_6$] Glucose* Trace

LSK cells number	WT	WT-IACS	HOM	HOM-IACS	HET	HET-IACS
Before Glucose* Tracing	37,000	37,000	27,875	27,875	37,750	37,750

After Glucose* Tracing	77,400	77,400	44,000	56,000	80,500	77,000

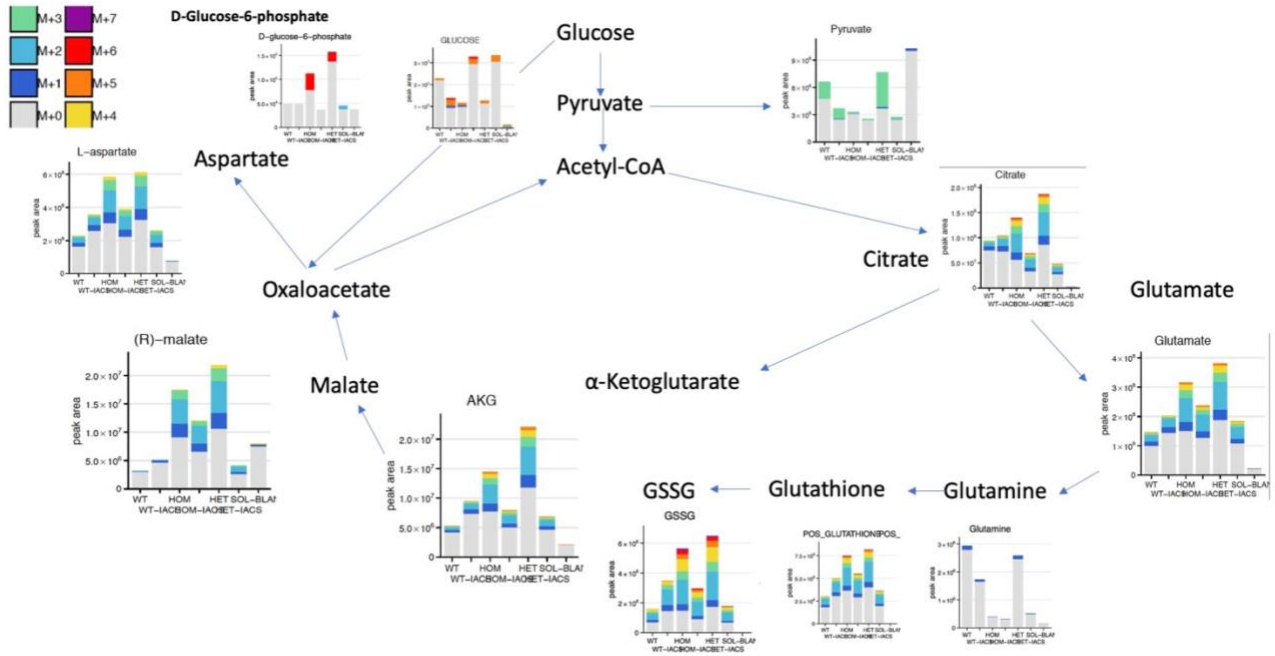

Figure 5.9 Experiment2, LC-MS profiles of LSK MPN cells

Absolute isotope distribution of indicated metabolites of TCA cycle in WT, HOM and HET LSK cells from experiment 2.

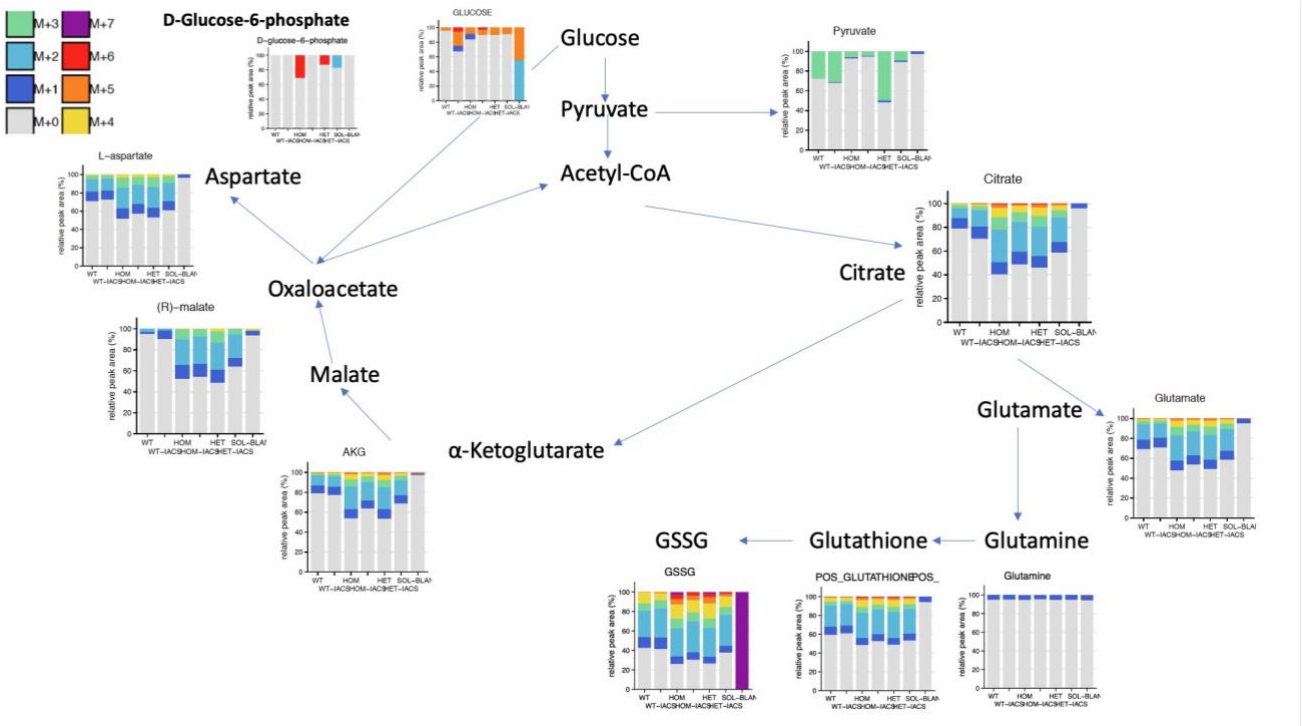

Figure 5.10 Experiment2, LC-MS profiles of LSK MPN cells

Relative isotope distribution of indicated metabolites of TCA cycle in WT, HOM and HET LSK cells from experiment 2.

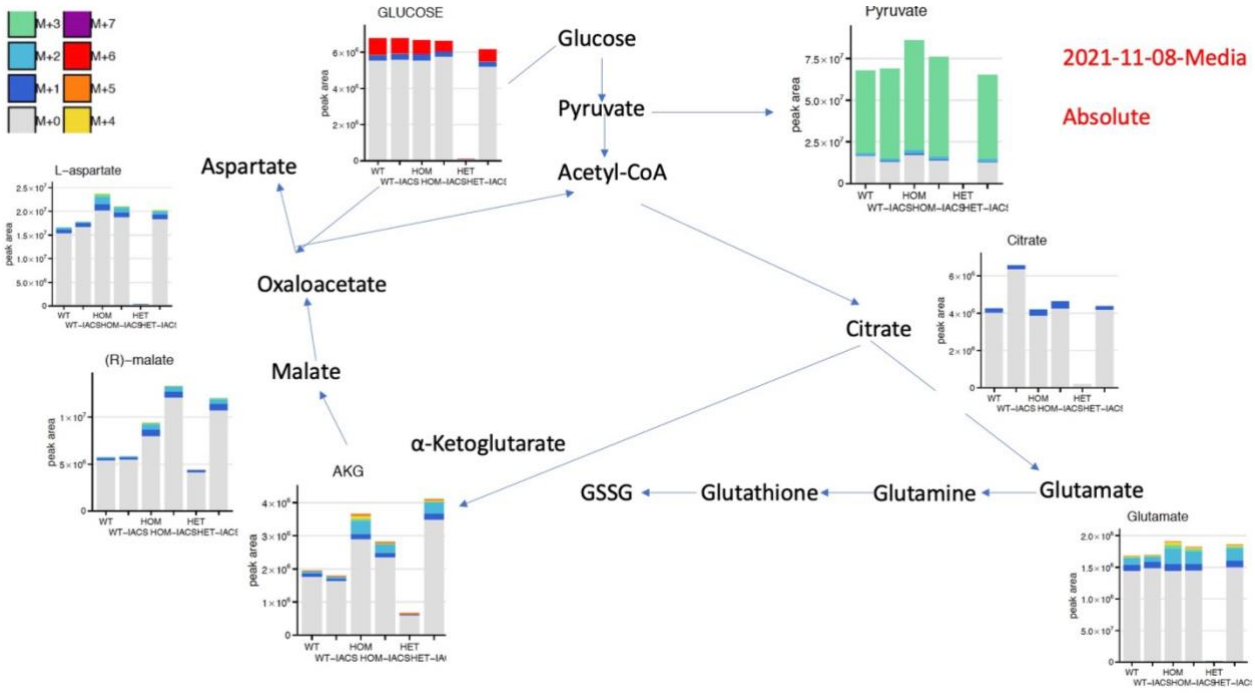

Figure 5.11 Experiment 2-LC-MS profiles of culture Media after 24-hour incubation of LSK cells. Relative isotope distribution of indicated metabolites of TCA cycle in the media of WT, HOM and HET LSK cells after 24h incubation from Experiment1 (The order is WT, WT-IACS, HOM, HOM-IACS, HET, HET-IACS).

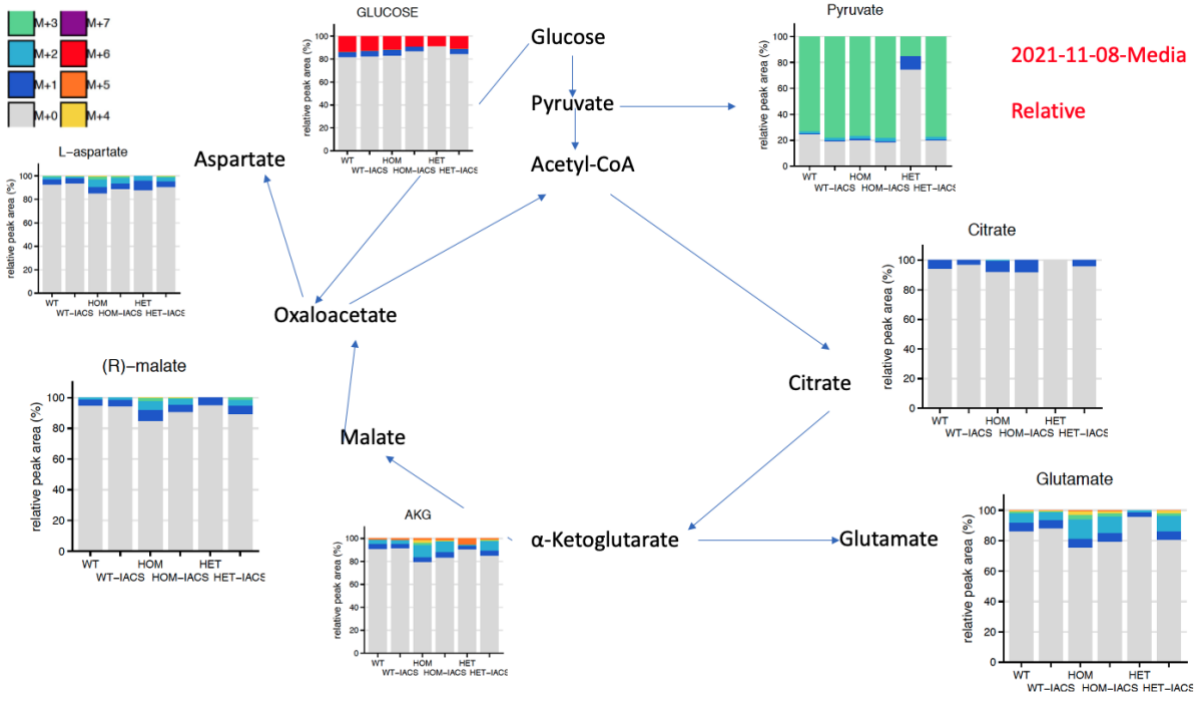

Figure 5.12 Experiment 2-LC-MS profiles of culture Media after 24-hour incubation of LSK cells.

Experiment 3

Table 5.3 Experiment3 cell counting after sorting and O/N culture

LSK cells number	WT (M, 10w)	HOM (M, 10w)	HET1 (M, 10w)	HET2 (M,10w)
After Sorting	338,000	441,627	351,000	562,470
After O/N culture	140,000	180,000	200,000	240,000

Table 5.4 Experiment3 cell counting before and after [$^{13}C_6$] Glucose* Trace

LSK cells number	WT	WT-IACS	HOM	HOM-IACS	HET1	HET1-IACS	HET2	HET2-IACS
Before Glucose* Tracing	70,000	70,000	90,000	90,000	100,000	100,000	120,000	120,000
After Glucose* Tracing	50,000	50,000	130,000	100,000	40,000	50,000	130,000	100,000

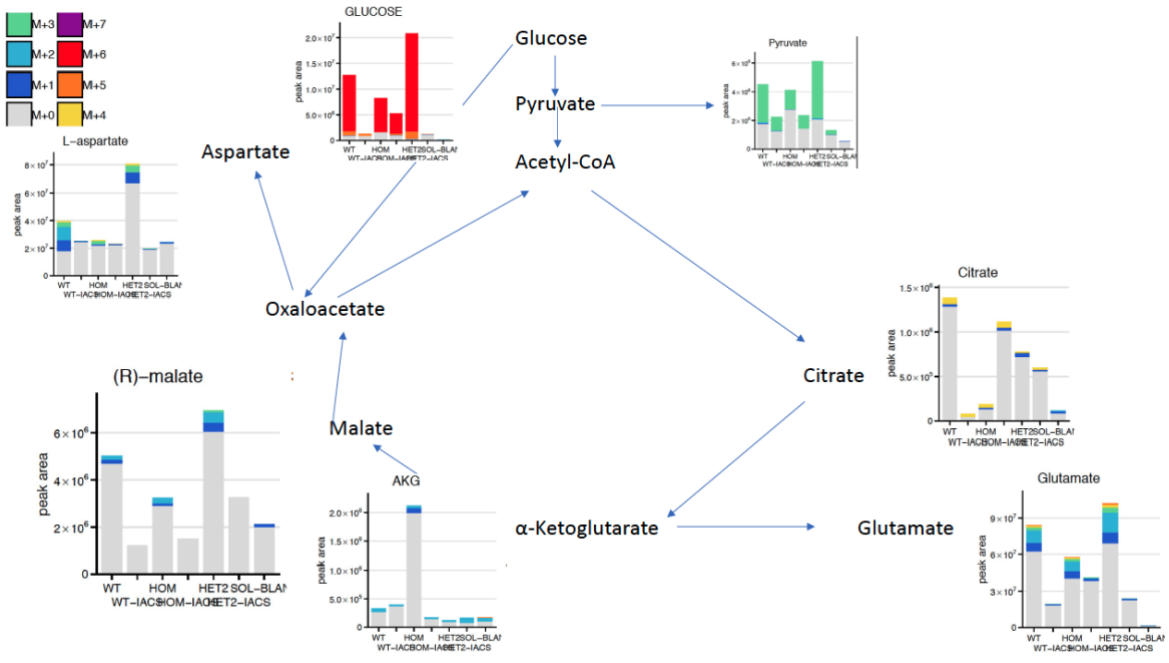

Figure 5.13 LC-MS profiles of LSK MPN cells

Absolute isotope distribution of indicated metabolites of TCA cycle in WT, HOM and HET LSK cells from experiment 3.

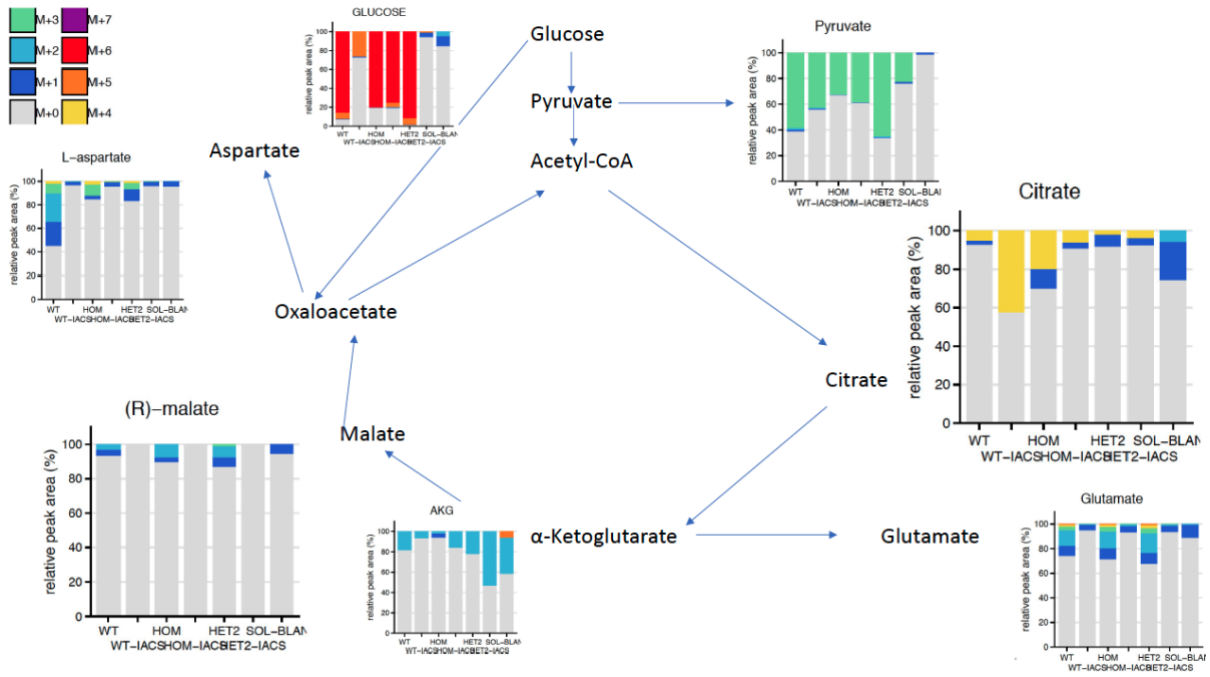

Figure 5.14 LC-MS profiles of LSK MPN cells

Relative isotope distribution of indicated metabolites of TCA cycle in WT, HOM and HET LSK cells from experiment3.

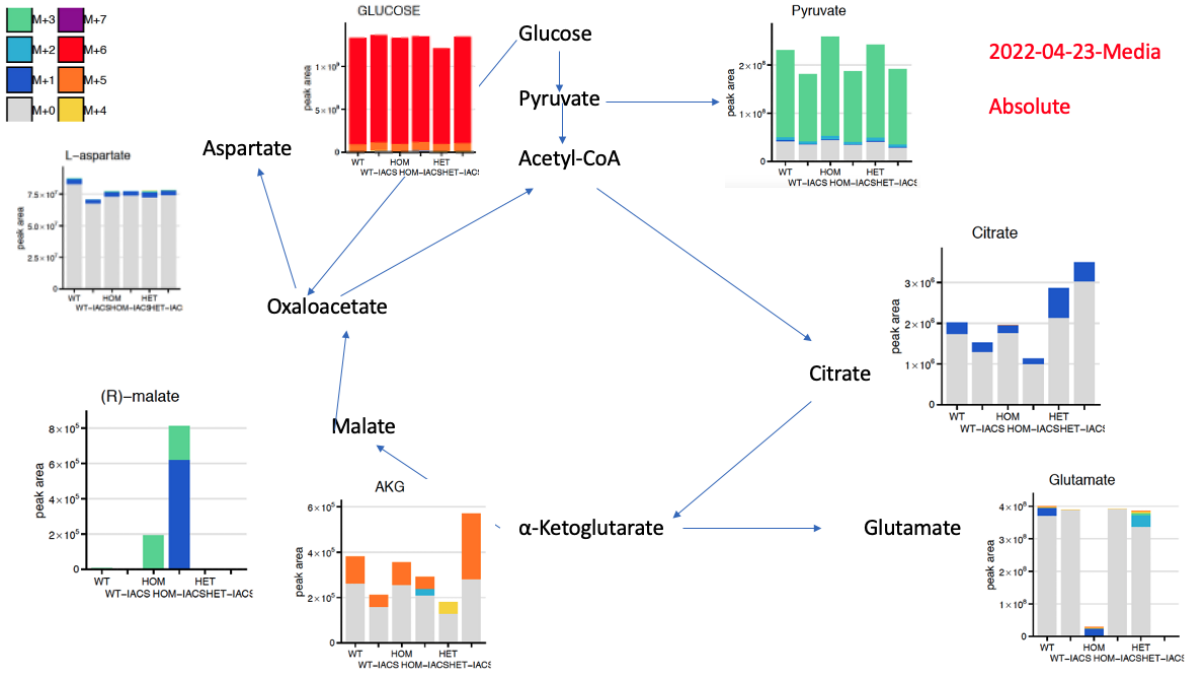

Figure 5.15 Media LC-MS profiles of LSK MPN cells

Absolute isotope distribution of indicated metabolites of TCA cycle in WT, HOM and HET LSK cells media after 24h incubation from experiment

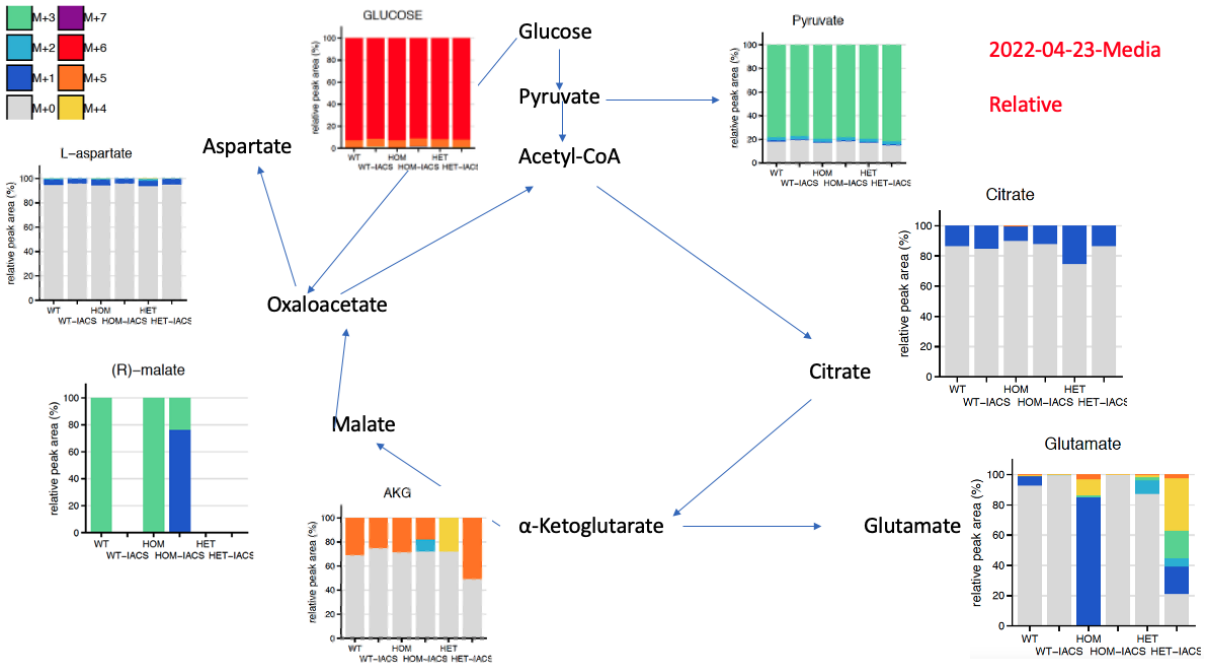

Figure 5.16 Media LC-MS profiles of LSK MPN cells

Relative isotope distribution of indicated metabolites of TCA cycle in WT, HOM and HET LSK cells from media after 24h incubation from experiment 3.

Experiment 4

Table 5.5 Experiment4 cell counting after sorting and O/N culture

LSK cells number	WT1 (M, 10w)	WT2 (M, 10w)	HOM1 (M, 9w)	HOM2 (F, 9w)	HET1 (M,10w)	HET2 (M,10w)	HET3 (F,10w)	HET4 (M,9w)
After Sorting	187,000	120,000	437,000	300,003	342,000	505,000	230,000	152,000
After O/N culture	160,000	60,000	180,000	100,000	140,000	240,000	60,000	60,000

Table 5.6 Experiment4 cell counting before and after [$^{13}C_6$] Glucose* Trace

LSK cells number	WT1	WT1-IACS	WT2	WT2-IACS	HOM1	HOM1-IACS	HOM2	HOM2-IACS	HET1	HET1-IACS	HET2

Before Glucose* Tracing	80,000	80,000	30,000	30,000	90,000	90,000	50,000	50,000	70,000	70,000	120,000
After Glucose* Tracing	64,000	42,000	31,000	13,750	93,000	85,555	25,000	13,750	46,666	37,000	37,000

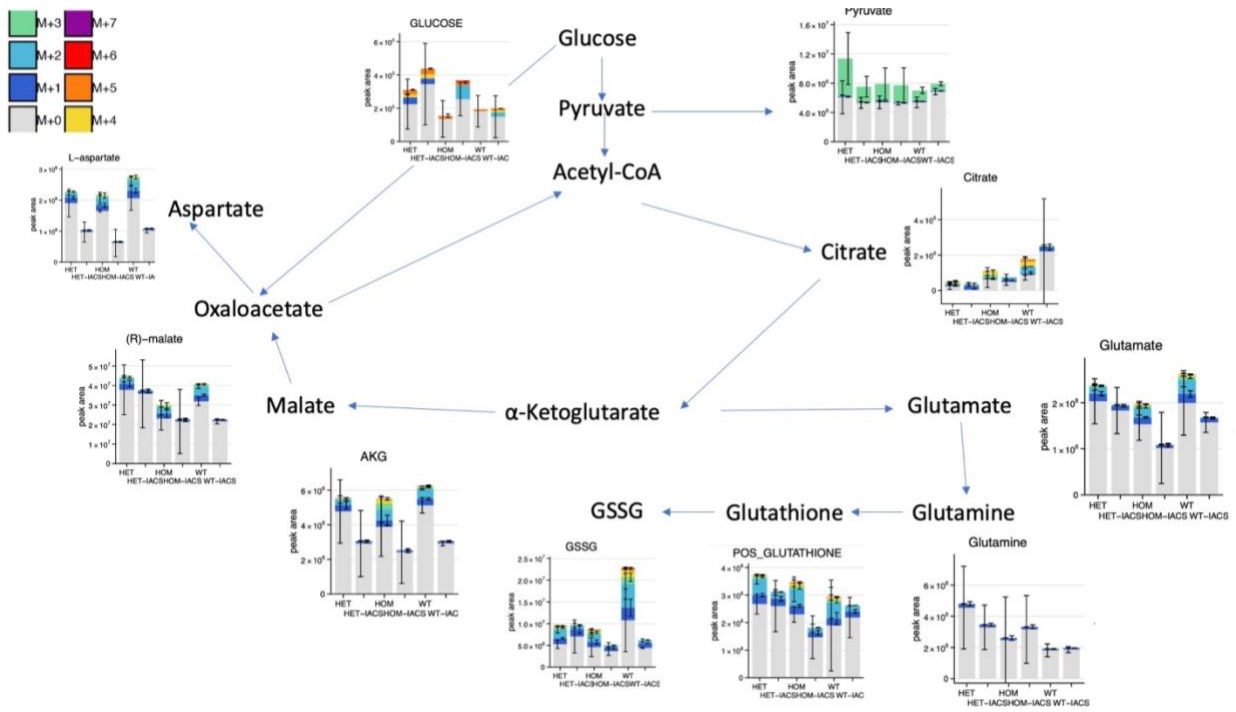

Figure 5.17 Experiment4-LC-MS profiles of c-Kit$^+$ MPN cells

Absolute isotope distribution of indicated metabolites of TCA cycle in WT, HOM and HET LSK cells from experiment 4. WT (n=2), WT IACS (n=2), HOM (n=2), HOM IACS (n=2), HET (n=3), HET IACS (n=3).

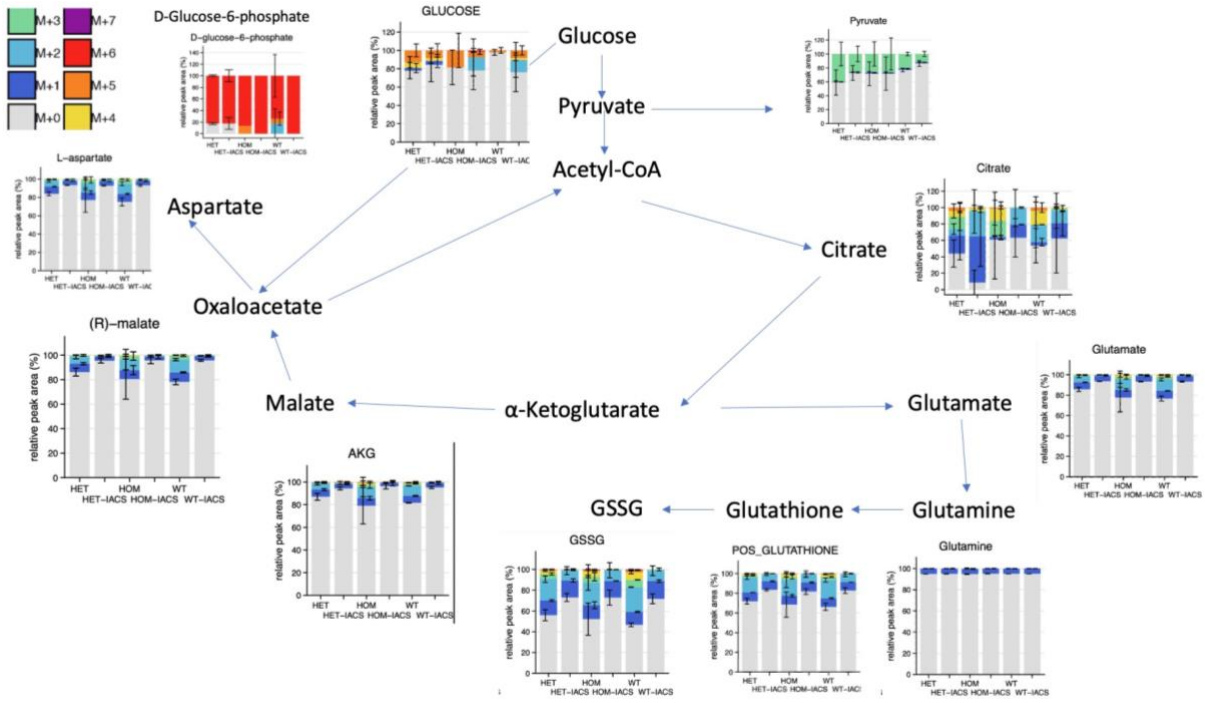

Figure 5.18 Experiment4-LC-MS profiles of LSK MPN cells

Relative isotope distribution of indicated metabolites of TCA cycle in WT, HOM and HET LSK cells from experiment 4. WT (n=2), WT IACS (n=2), HOM (n=2), HOM IACS (n=2), HET (n=3), HET IACS (n=3).

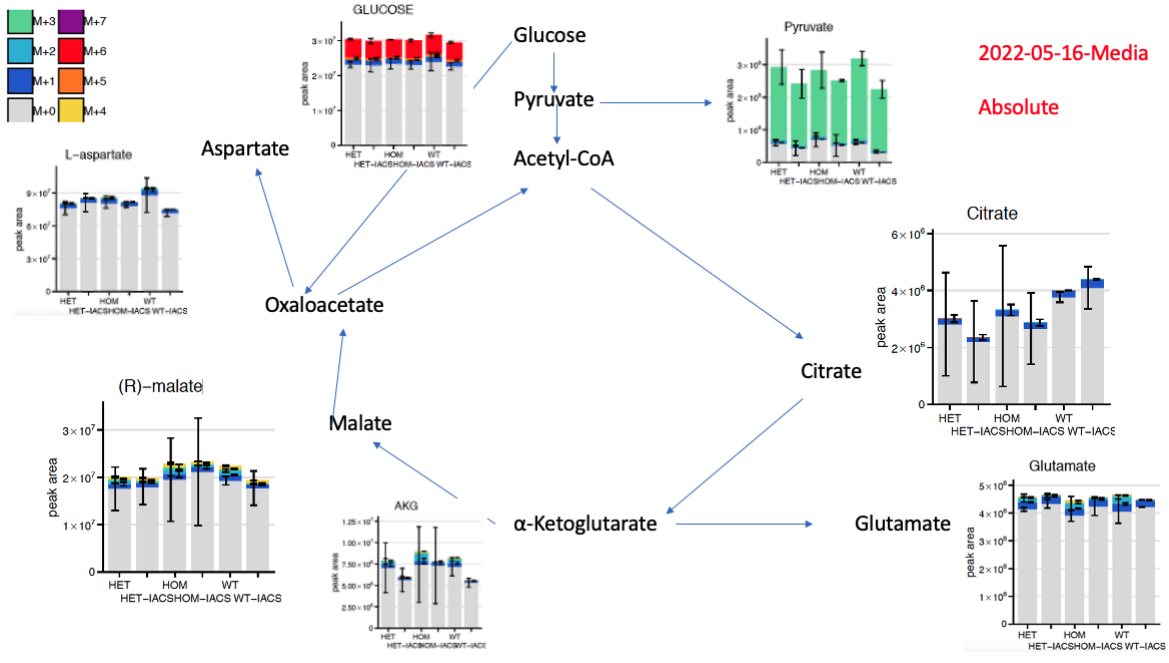

Figure 5.19 LC-MS profiles of LSK MPN cells Medium

Absolute isotope distribution of indicated metabolites of TCA cycle in WT, HOM and HET LSK cells from media after 24h incubation from experiment4.

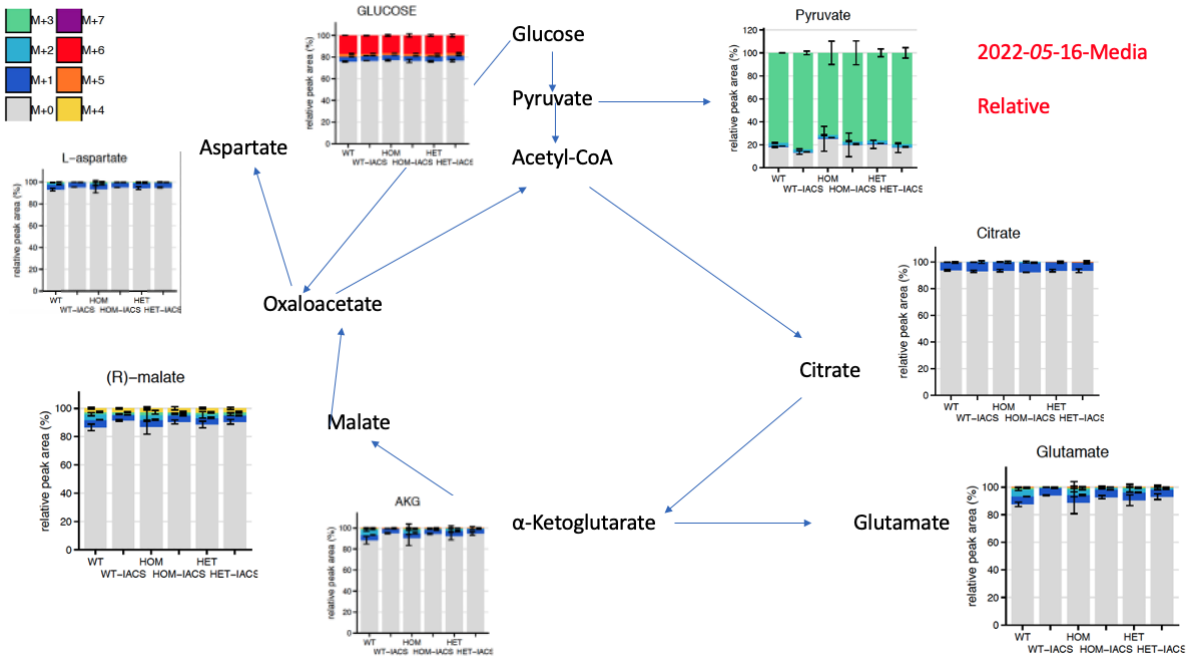

Figure 5.20 Medium LC-MS profiles of LSK MPN cells

Relative isotope distribution of indicated metabolites of TCA cycle in WT, HOM and HET LSK cells from media after 24h incubation from experiment 4.

5.2.4 MPN HET c-Kit$^+$ cells utilized glutamate for anaplerotic pathway to generate glutathione and glutathione disulfide (GSSG)

It is worth noting that glutathione also shows M+1 to M+4 isotopologue, while glutathione disulfide displays from M+1 to M+6, which may originate from various metabolic sources (Burch et al., 2018; Yoo et al., 2020). In the results shown in glutathione disulfide (GSSG) displays an M+7 isotopologue, indicating that it incorporates labelled carbons from a precursor with a high number of labelled carbons, such as labelled glucose or other intermediates substrates introduced into the system. In this experiment, the M+7 labelling likely arises from the incorporation of labelled carbons into the glutamate and glycine residues of glutathione. 13C-labeled glucose-labelled carbons from glucose could be incorporated into glutathione through TCA cycle intermediates, eventually labelling GSSG (Wise and Thompson, 2010).

As GSSG is formed by the oxidation of two reduced glutathione (GSH) molecules, its labelling pattern mirrors that of the GSH pool. The presence of an M+7 label in GSSG indicates that a substantial portion of labelled carbon from the glucose tracer is incorporated into the glutathione synthesis pathway, resulting in significant labelling in both the glycine

and glutamate ultimately contribute labelled carbons to the synthesis of glutathione, resulting in more extensive labelling (such as M+7) in GSSG.

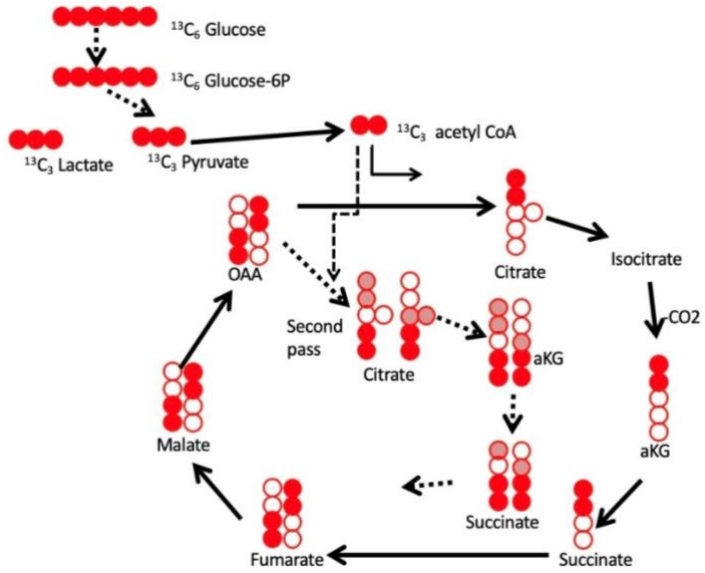

Figure 5.21 Schematic of ^{13}C6 glucose tracing.

5.3 Discussion

After 24 hours of culturing cells in a medium containing uniformly labelled ^{13}Carbon glucose, most glucose is expected to be fully labelled as M+6 (all six carbons labelled with ^{13}C) due to the initial addition of ^{13}C-glucose. However, the presence of M+1 glucose, as well as M+3 pyruvate, indicates that some unlabelled carbon is entering the glucose pool and glycolytic pathway.

The presence of M+1 glucose could result from metabolic recycling. Cells may release unlabelled carbon sources, for example, through the breakdown of other macromolecules or metabolic by-products into the media, where they mix with the labelled glucose (Martin et al., 2016). For instance, cells can synthesize glucose from partially labelled intermediates, which can dilute the fully labelled ^{13}C-glucose pool and produce glucose molecules with one or a few ^{13}C atoms. The presence of M+1 could also indicate some levels of glucose synthesis or exchange with other carbon sources over time, such as through gluconeogenesis pathways or the incorporation of one unlabelled carbon.

M+3 pyruvate is typically produced through glycolysis of M+6 glucose, as each molecule of glucose (6 carbons) splits into two molecules of pyruvate (each with 3 carbons) containing

three ^{13}C atoms. The labelled pyruvate in the media likely reflects incomplete cellular uptake or partial release after glycolysis. Alternatively, it could arise from cells metabolizing glucose and releasing some of the labelled pyruvate back into the media. Another possible explanation is metabolic exchange and release: cells might take up glucose, metabolize it, and release labelled metabolic by-products, which re-enter the media and dilute the isotopic labelling patterns. Over extended culture times, such as 24 hours, this release and re-uptake process can lead to mixed labelling patterns. Finally, the incomplete uptake of M+6 glucose or exchange with media components could also contribute. Some ^{13}C-glucose might remain unconsumed in the media, and exchanges with other metabolic sources (e.g., amino acids or other carbohydrates) could result in mixed isotopologue, such as M+1 glucose or partially labelled pyruvate.

In summary, the observed M+6 and M+1 glucose and M+3 pyruvate after 24 hours in ^{13}C-glucose media suggest a combination of factors, including metabolic recycling and exchange of intermediates, incomplete or variable uptake and utilization of the labelled glucose, and the release of labelled intermediates such as pyruvate back into the media.

These complex interactions between cellular metabolism and media components over time contributed to the mixed isotopologue patterns observed in the extracellular metabolites.

Another finding through those four experiments are the glutamate, glutamine, Gluthothine, GSSG metabolic pathways.

In comparing the metabolic labelling patterns between HET (heterozygous) and HOM (homozygous) conditions, here are some key observations: Glycolytic and TCA Cycle Metabolites: The HET samples generally show higher labelling (e.g., M+2, M+3, etc.) across various intermediates like pyruvate, citrate, and malate compared to the HET samples.

This suggests an increased flux of labelled carbons (possibly from labelled glucose) through glycolysis and the TCA cycle in HOM samples, indicating a possible upregulation in these pathways. In HOM samples, there appears to be a higher incorporation of labelled carbons in both aspartate and AKG compared to HET. This could indicate an enhanced activity of pathways related to amino acid synthesis or anaplerotic reactions (replenishing TCA intermediates). Aspartate, derived from oxaloacetate, shows increased labelling in HOM, which may reflect greater TCA cycle activity or shuttling of intermediates towards amino acid biosynthesis. Both glutamate and glutamine show slightly higher levels of labelled carbons in HOM than in HET samples. Since glutamate and glutamine are closely linked to TCA

cycle intermediates (via α-ketoglutarate), this also supports the idea that HOM samples may have increased TCA cycle activity or altered amino acid metabolism. The increased labelling in GSSG (M+5, M+6, and M+7) in HOM samples compared to HET suggests a higher synthesis rate of glutathione, possibly in response to oxidative stress or increased cellular demand for antioxidant protection. Elevated labelling in GSSG in HOM may imply that HOM cells are under a higher oxidative burden, necessitating more glutathione turnover to manage reactive oxygen species. HOM samples show a broader distribution of labelled isotopologue (e.g., higher M+ forms across multiple metabolites), indicating enhanced metabolic fluxes and possibly a shift in metabolic programming compared to HET samples.

The altered labelling patterns in TCA cycle intermediates and downstream metabolites (like glutamate and GSSG) in HOM suggest that these cells may be adapting their metabolism to meet different bioenergetic or biosynthetic demands, possibly due to genetic differences associated with the homozygous mutation.

In summary, this comparison suggests that HOM cells have an increased metabolic activity, particularly in pathways associated with the TCA cycle, amino acid biosynthesis, and glutathione metabolism, relative to HET cells. This might reflect differences in metabolic reprogramming or stress response due to genetic variation between the two groups.

The labelling patterns and relative intensities of metabolites in this metabolic map indicate metabolic differences. For Glutamate Transporters: Cells have specific transporters for glutamate, such as SLC1A family transporters, particularly EAAT (excitatory amino acid transporters) in neurons and other tissues. These transporters are responsible for the uptake of glutamate into cells, preventing excessive extracellular accumulation, which can be toxic, especially in neural tissue. In non-neuronal cells, other transporters (like SLC7A11, which functions in the antiporter system) mediate the exchange of glutamate with other amino acids, such as cystine. This exchange plays a role in redox regulation and glutathione synthesis. For Glutamine Transporters: Glutamine is transported through various transporters, including SLC1A5 (also known as ASCT2) and SLC38 family transporters (like SNATs). ASCT2 is a prominent transporter involved in glutamine uptake, especially in rapidly proliferating cells (e.g., cancer cells) that use glutamine as a fuel source and nitrogen donor. Some transporters, like SLC7A5/LAT1, function as antiporters that exchange glutamine for other amino acids (like leucine), facilitating nutrient signalling and metabolic regulation. For Glutamate-Glutamine Cycle: In certain tissues, particularly in the brain, there is an essential glutamate-glutamine cycle between neurons and astrocytes.

Neurons release glutamate as a neurotransmitter, which is then taken up by astrocytes. In astrocytes, glutamate is converted to glutamine and subsequently released back to neurons, where it can be converted back to glutamate. This cycle helps regulate neurotransmitter levels and maintain cellular health. In cancer cells and other rapidly proliferating cells, the exchange of glutamine and glutamate across the membrane is especially important. These cells often rely on glutamine for energy production (via glutaminolysis) and biosynthesis. They may release glutamate as a byproduct or exchange it to maintain intracellular glutamine levels, supporting growth and survival. The exchange of glutamate and glutamine across the membrane allows cells to adapt to varying metabolic conditions. For example, during nutrient stress, cells may uptake more glutamine to fuel the TCA cycle and produce α-ketoglutarate, which can be further metabolized into other intermediates.

In summary, glutamate and glutamine are indeed exchanged across the cell membrane, and this process is tightly regulated by various transporters. This exchange allows cells to manage nitrogen metabolism, maintain redox balance, participate in intercellular signalling (particularly in the brain), and support biosynthetic and energy needs in proliferative states.

I first assessed the metabolic effect of the Jak2V617F mutation and IACS using LC-MS. Due to high variability in experimental procedures, I am unable to combine individual experiments into the same graph and chose to therefore show the results of 4 independent experiments.

Firstly, my results showed that 30nM IACS-010759 inhibited the mitochondrial complex I, leading to ATP depletion. All the metabolites in the TCA cycle Citrate, Glutamate, α-ketoglutarate, Aspartate isotopolog distribution showed a decrease in WT-IACS, HOM-IACS, HET-IACS samples. However, it showed a sharp decrease in HET-IACS compared to HOM-IACS or WT-IACS which indicated that HET LSK cells depend on TCA cycle more than HOM or WT LSK cells. In addition, glucose is consistently labelled M+6 with citrate and glutamate are labelled with M+1 to M+5, which suggests that $^{13}C6$ glucose was circulated through the TCA cycle. There might also be alternative pathways such as extracellular glutamate and glutamine exchange. Overall, the LC-MS data show that HET c-Kit^{+} cells depend on TCA cycle more than HOM or WT c-Kit^{+} cells.

Secondly, the media of HOM Lc-kit+ cells after 24h [13C6] glucose tracing showed an increase in glutamate, AKG and malate which indicated the excretion of glutamate, AKG

and malate to the outside of the cell membrane. It may suggest the excretion of glutamate and the existing anaplerotic pathway through glutamate.

Thirdly, the media of HOM-IACS kit+ cells after 24h ^{13}C6 Glucose trace showed a decrease in pyruvate level in all four independent experiments which indicated decreased glycolysis when using IACS inhibition.

The data suggest that HET cells, rather than HOM, exhibit increased metabolic flux through the TCA cycle, higher glutathione turnover, and possibly enhanced amino acid metabolism. This metabolic reprogramming in HET cells could reflect adaptations or responses to unique metabolic demands or stressors associated with their genetic makeup.

From the results generated from several methods already, we have put forward a venture hypothesis that Solute Carrier Family I member (SLC1A1) is a key regulator of glutamate metabolism in HOM and HET hematopoietic stem cells which may build up an alternative pathway to drive the TCA cycle. HOM HSCs have different alternative metabolism pathway compared to HET HSCs although they both tend to have higher oxidative phosphorylation.

The presence of M+1 glucose could result from metabolic recycling. Cells may release unlabelled carbon sources (e.g., through the breakdown of other macromolecules or metabolic by-products) back into the media, where they mix with the labelled glucose (Martin et al., 2016). For instance, cells can synthesize glucose from partially labelled intermediates, which can dilute the fully labelled 13C-glucose pool and produce glucose molecules with one or a few 13C atoms. The presence of M+1 could also indicate some levels of glucose synthesis or exchange with other carbon sources over time, such as through gluconeogenesis pathways or the incorporation of one unlabelled carbon.

As for M+3 Pyruvate, normally, glycolysis of M+6 glucose would produce M+3 pyruvate, as each molecule of glucose (6 carbons) splits into two molecules of pyruvate (each with 3 carbons) containing three 13C atoms. This labelled pyruvate in the media likely reflects incomplete uptake by cells or partial release after glycolysis. Alternatively, it could arise if cells release some of the labelled pyruvate back into the media as they metabolize glucose. Another proper explanation maybe the potential Metabolic Exchange and Release: Cells could be taking up glucose, metabolizing it, and releasing labelled metabolic by-products, which re-enter the media and dilute the isotopic labelling pattern. This release and re-uptake process can lead to mixed labelling patterns, especially over extended culture times

like 24 hours. The third reason for that maybe the incomplete glucose uptake or exchange with the media: Cells might not fully consume the M+6 glucose, leaving some 13C-glucose in the media. Some exchange with other metabolic sources (e.g., amino acids or other carbohydrates) could result in mixed isotopologue, such as M+1 glucose or partially labelled pyruvate.

In summary, the observed M+6 and M+1 glucose and M+3 pyruvate after 24 hours in 13C-glucose media suggest a combination of factors, including: Metabolic recycling and exchange of intermediates, Incomplete or variable uptake and utilization of the labelled glucose, release of labelled intermediates like pyruvate back into the media.

These complex interactions between cellular metabolism and media components over time create mixed isotopologue patterns in the extracellular metabolites.

Another finding through those four experiments is the glutamate, glutamine, Gluthothine, GSSG metabolic pathways.

In comparing the metabolic labelling patterns between HET (heterozygous) and HOM (homozygous) conditions, here are some key observations: Glycolytic and TCA Cycle Metabolites: The HET samples generally show higher labelling (e.g., M+2, M+3, etc.) across various intermediates like pyruvate, citrate, and malate compared to the HET samples.

This suggests an increased flux of labelled carbons (possibly from labelled glucose) through glycolysis and the TCA cycle in HOM samples, indicating a possible upregulation in these pathways. In HOM samples, there appears to be a higher incorporation of labelled carbons in both aspartate and AKG compared to HET. This could indicate an enhanced activity of pathways related to amino acid synthesis or anaplerotic reactions (replenishing TCA intermediates). Aspartate, derived from oxaloacetate, shows increased labelling in HOM, which may reflect greater TCA cycle activity or shuttling of intermediates towards amino acid biosynthesis. Both glutamate and glutamine show slightly higher levels of labelled carbons in HOM than in HET samples. Since glutamate and glutamine are closely linked to TCA cycle intermediates (via α-ketoglutarate), this also supports the idea that HOM samples may have increased TCA cycle activity or altered amino acid metabolism. The increased labelling in GSSG (M+5, M+6, and M+7) in HOM samples compared to HET suggests a higher synthesis rate of glutathione, possibly in response to oxidative stress or increased cellular demand for antioxidant protection. Elevated labelling in GSSG in HOM may imply that HOM cells are under a higher oxidative burden, necessitating more glutathione turnover

to manage reactive oxygen species. HOM samples show a broader distribution of labelled isotopologue (e.g., higher M+ forms across multiple metabolites), indicating enhanced metabolic fluxes and possibly a shift in metabolic programming compared to HET samples.

The altered labelling patterns in TCA cycle intermediates and downstream metabolites (like glutamate and GSSG) in HOM suggest that these cells may be adapting their metabolism to meet different bioenergetic or biosynthetic demands, possibly due to genetic differences associated with the homozygous mutation.

In summary, this comparison suggests that HOM cells have an increased metabolic activity, particularly in pathways associated with the TCA cycle, amino acid biosynthesis, and glutathione metabolism, relative to HET cells. This might reflect differences in metabolic reprogramming or stress response due to genetic variation between the two groups.

The labelling patterns and relative intensities of metabolites in this metabolic map indicate metabolic differences. For Glutamate Transporters: Cells have specific transporters for glutamate, such as SLC1A family transporters, particularly EAAT (excitatory amino acid transporters) in neurons and other tissues. These transporters are responsible for the uptake of glutamate into cells, preventing excessive extracellular accumulation, which can be toxic, especially in neural tissue. In non-neuronal cells, other transporters (like SLC7A11, which functions in the antiporter system) mediate the exchange of glutamate with other amino acids, such as cystine. This exchange plays a role in redox regulation and glutathione synthesis. For Glutamine Transporters: Glutamine is transported through various transporters, including SLC1A5 (also known as ASCT2) and SLC38 family transporters (like SNATs). ASCT2 is a prominent transporter involved in glutamine uptake, especially in rapidly proliferating cells (e.g., cancer cells) that use glutamine as a fuel source and nitrogen donor. Some transporters, like SLC7A5/LAT1, function as antiporters that exchange glutamine for other amino acids (like leucine), facilitating nutrient signalling and metabolic regulation. For Glutamate-Glutamine Cycle: In certain tissues, particularly in the brain, there is an essential glutamate-glutamine cycle between neurons and astrocytes. Neurons release glutamate as a neurotransmitter, which is then taken up by astrocytes. In astrocytes, glutamate is converted to glutamine and subsequently released back to neurons, where it can be converted back to glutamate. This cycle helps regulate neurotransmitter levels and maintain cellular health. In cancer cells and other rapidly proliferating cells, the exchange of glutamine and glutamate across the membrane is especially important. These cells often rely on glutamine for energy production (via

glutaminolysis) and biosynthesis. They may release glutamate as a byproduct or exchange it to maintain intracellular glutamine levels, supporting growth and survival. The exchange of glutamate and glutamine across the membrane allows cells to adapt to varying metabolic conditions. For example, during nutrient stress, cells may uptake more glutamine to fuel the TCA cycle and produce α-ketoglutarate, which can be further metabolized into other intermediates.

In summary, glutamate and glutamine are indeed exchanged across the cell membrane, and this process is tightly regulated by various transporters. This exchange allows cells to manage nitrogen metabolism, maintain redox balance, participate in intercellular signalling (particularly in the brain), and support biosynthetic and energy needs in proliferative states.

6 Chapter 6 Conclusion, general discussion and future directions

In this thesis, I present the first in-depth investigation of the metabolism of MPN HSPC cells.

I identified mitochondrial oxidative metabolism as a metabolic vulnerability in MPN HSPCs. The first conclusion is that JAK2 drives transcriptional changes in genes involved in metabolic pathways. The second conclusion is that solute carrier genes are deregulated in MPN mice HSPCs. The total conclusion is deregulation in metabolic pathway may provide opportunities to selectively target primitive MPN cells.

In the next paragraphs, I will discuss our findings in relation with the current literature in addition to discussing potential implications and future directions of this work.

6.1 Oxidative metabolism in MPN mice models

Previous work from the Skoda lab has demonstrated that JAK2 expression in mouse models of MPNs causes significant metabolic alterations that have previously been overlooked, including sharply increased energy demands and a critical dependence on glucose (Nageswara Rao et al., 2019). In contrast, their JAK2 mutant models showed more pronounced hypoglycemia without signs of insulin resistance, indicating different types and extents of metabolic reprogramming between acute myeloid Leukemia and MPN cells. This hypoglycemia was closely linked to increased erythropoiesis, highlighting the essential role of glucose metabolism in normal erythropoiesis. E12 mice, which primarily exhibit erythroid hyperproliferation, experienced more severe hypoglycemia compared to VF mice, which showed trilineage involvement with a less pronounced erythroid phenotype (Rao et al., 2019). Although research in Skoda lab has demonstrated metabolic changes in MPN MEP and LSK cells, qPCR analysis of mitochondrial DNA revealed differences between LT-HSCs and MEPs, suggesting a potential distinction between these two cell types. Additionally, differences were observed between VF and E12 mice, which have varying JAK2 burdens. Interestingly, despite these variations, the OCR and ECAR trends remained similar, which may imply that not all mitochondria are involved in oxidative phosphorylation.
Surprisingly, their OCR and ECAR show similar trends which may indicate that not all the mitochondria are undergoing oxidative phosphorylation (Nageswara Rao et al., 2019). My work shows the oxidative phosphorylation upregulation in HSPCs of both MPN JAK2 mutant homozygous mice and heterozygous mice which was validated in our Mass-Spectrometry

data. In addition to these alterations, I found in oxidative phosphorylation and glycolysis, I also found the solute carriers for glutamate and glutamine transfer, Slc43a1, Slc2a4 and Slc25a37 are all upregulated in MPN JAK2V617F homozygous mice c-kit^{+} cells.
My findings underline the importance of uncovering MPN-specific metabolic features and provide a strong rationale for testing metabolic inhibitors in MPN treatment. A combined strategy of targeting both altered metabolic dependencies and mutant JAK2 activity may offer a promising therapeutic approach.

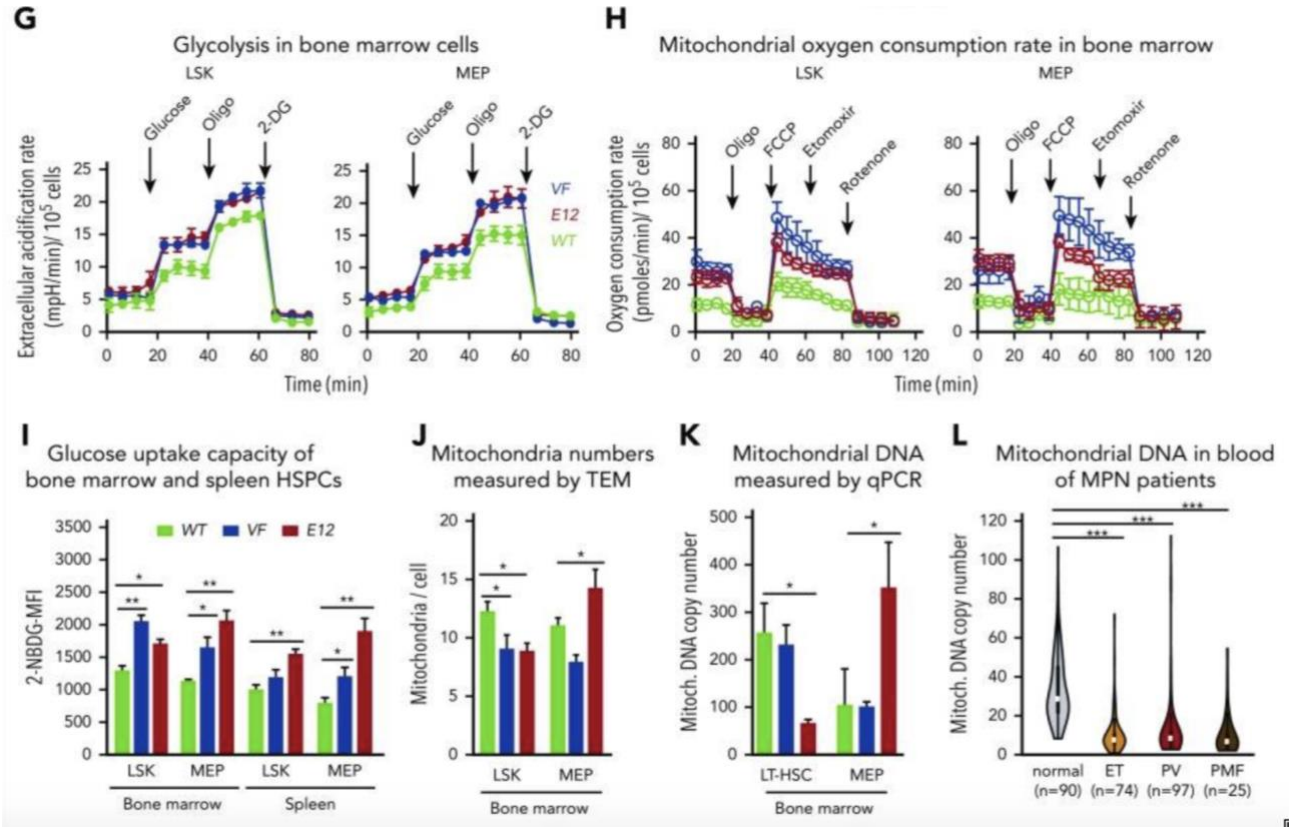

Figure 6.1 OCR and ECAR in MPN mice LSK and MEP cells (Skoda et al, 2019)

6.2 Other solute carrier drugs for treating cancer

Solute carrier (SLC) transporters are a large family of membrane proteins responsible for transporting a variety of metabolites, nutrients, and ions across cell membranes (Najumudeen et al., 2021). In cancer, certain SLC transporters are often overexpressed or dysregulated, making them attractive targets for therapeutic intervention.

SLC43a1

SLC43A1, or solute carrier family 43 member 1, is a gene that produces a protein responsible for transporting large neutral amino acids, such as leucine, across cell membranes. It is part of the solute carrier (SLC) family, a group of proteins that move various substances, including nutrients, ions, and metabolites, within the body.
SLC43A1 operates as a transporter that moves large neutral amino acids like leucine, isoleucine, and valine across cell membranes without relying on sodium. It plays a key role in maintaining amino acid balance and supporting cellular signalling. This gene is active in several tissues, including the brain, liver, kidney, and skeletal muscle, highlighting its importance in nutrient absorption and metabolism. Mutations or irregular activity in SLC43A1 have been linked to certain diseases and metabolic disorders. Inhibition of its function can impair amino acid transport, affecting protein production, energy metabolism, and signaling within cells. SLC43A1 has been proved to accelerate tumor growth by increase the uptake of essential amino acids for cell division. The interactions of amino acid transport is crucial for understanding of SLC434A1's function.

SLC7A11

One example is SLC7A11, which is part of the cystine/glutamate antiporter system (Yan et al., 2023). This transporter imports cystine into cells while exporting glutamate, and overexpressed in several cancers, SLC7A11 supports the synthesis of glutathione, which helps cancer cells cope with oxidative stress. Drugs like sulfasalazine target SLC7A11 to lower glutathione levels, increase reactive oxygen species (ROS) and promote cell death in cancer cells. SLC7A11 inhibitors are currently being explored in preclinical studies, especially for cancers that depend heavily on antioxidant defenses (Yue et al., 2024).

SLC2A1 (GLUT1)

SLC2A1 is a glucose transporter responsible for enabling glucose uptake into cells, GLUT1 is frequently overexpressed in cancer cells, which have high energy demands and rely heavily on glycolysis (known as the Warburg effect) (Galochkina et al., 2019). There are small molecules such as WZB117 and STF-31 as SLC2A1 which are being studied as inhibitors of GLUT1 (Guerrero et al., 2024).
Blocking GLUT1 can limit glucose availability to cancer cells, inhibiting their growth. This strategy is being explored for treating cancers that are highly dependent on glucose.

6.3 Limitations of the methods

The first limitation to my work is that I cannot use MPN patient samples to verify most of my findings because the advanced techniques in this project—such as Seahorse Assays, Mass Spectrometry, and Bulk RNA Sequencing—require a larger quantity of cells than what is obtainable from MPN patients. The second limitation is the lack of LT-HSC data for metabolic analysis, which would have added greater detail and insight to the experiments. The third limitation is that we cannot mimic the physiological bone marrow environment even though we have re-created physiological glutamine and glucose levels in all experiments, but the in vitro metabolism is different from in vivo metabolism. The fourth limitation is the heterogeneity of the mice, because the mice are not easy to get at the same time for wildtype, homozygous and heterozygous, so I cannot eliminate the batch effects through all the experiments. The fifth limitation is the cell numbers I could get for seahorse and Mass-spectrometry, which leads to batch effects of these experiments.

6.4 Future direction

I have identified three solute carriers with available inhibitors, enabling us to combine these with JAK2 inhibitors to study the metabolism of MPN cell lines or c-Kit$^+$ cells from MPN mice. Functional assays like Seahorse or Colony Formation Assays can be employed for these analyses.

Furthermore, specific HSC markers in bulk RNA sequencing could be used to differentiate between LT-HSCs and ST-HSCs, helping us investigate metabolic distinctions between these two cell populations.

Lastly, fatty acid assays on the Seahorse platform could aid in distinguishing oxidative consumption rates originating from the TCA cycle as opposed to fatty acid oxidation.

6.5 Additional remarks

This study would not have been feasible without the access to MPN mice and without the funding from NHS endowment grant.

Bibliography

Achyutuni, S., Nivarthi, H., Majoros, A., Hug, E., Schueller, C., Jia, R., Varga, C., Schuster, M., Senekowitsch, M., Tsiantoulas, D., Kavirayani, A., Binder, C. J., Bock, C., Zagrijtschuk, O., & Kralovics, R. (2021). Hematopoietic expression of a chimeric murine-human CALR oncoprotein allows the assessment of anti-CALR antibody immunotherapies in vivo. *American Journal of Hematology*, *96*(6), 698–707. https://doi.org/10.1002/ajh.26171

Agathocleous, M., Meacham, C. E., Burgess, R. J., Piskounova, E., Zhao, Z., Crane, G. M., Cowin, B. L., Bruner, E., Murphy, M. M., Chen, W., Spangrude, G. J., Hu, Z., DeBerardinis, R. J., & Morrison, S. J. (2017). Ascorbate regulates haematopoietic stem cell function and leukaemogenesis. *Nature*, *549*(7673), 476–481. https://doi.org/10.1038/nature23876

Akada, H., Akada, S., Gajra, A., Bair, A., Graziano, S., Hutchison, R. E., & Mohi, G. (2012). Efficacy of vorinostat in a murine model of polycythemia vera. *Blood*, *119*(16), 3779–3789. https://doi.org/10.1182/blood-2011-02-336743

Akada, H., Yan, D., Zou, H., Fiering, S., Hutchison, R. E., & Mohi, M. G. (2010). Conditional expression of heterozygous or homozygous Jak2V617F from its endogenous promoter induces a polycythemia vera–like disease. *Blood*, *115*(17), 3589–3597. https://doi.org/10.1182/blood-2009-04-215848

Arkoun, B., Robert, E., Boudia, F., Mazzi, S., Dufour, V., Siret, A., Mammasse, Y., Aid, Z., Vieira, M., Aygun, I., Aglave, M., Cambot, M., Petermann, R., Souquere, S., Rameau, P., Catelain, C., Diot, R., Tachdjian, G., Hermine, O., . . . Vainchenker, W. (2022). Stepwise GATA1 and SMC3 mutations alter megakaryocyte differentiation in a Down syndrome leukemia model. *Journal of Clinical Investigation*, *132*(14). https://doi.org/10.1172/jci156290

Asp, J., Skov, V., Bellosillo, B., Kristensen, T., Lippert, E., Dicker, F., Schwarz, J., Wojtaszewska, M., Palmqvist, L., Akiki, S., Aggerholm, A., Andersen, M. T., Girodon, F., Kjær, L., Leibundgut, E. O., Pancrazzi, A., Vorland, M., Andrikovics, H., Kralovics, R., . . . Pallisgaard, N. (2018). International external quality assurance of JAK2 V617F quantification. *Annals of Hematology*, *98*(5), 1111–1118. https://doi.org/10.1007/s00277-018-3570-8

Baldini, C., Moriconi, F. R., Galimberti, S., Libby, P., & De Caterina, R. (2021). The JAK–STAT pathway: an emerging target for cardiovascular disease in rheumatoid arthritis and myeloproliferative neoplasms. *European Heart Journal*, *42*(42), 4389–4400. https://doi.org/10.1093/eurheartj/ehab447

Banker, D. E., Mayer, S. J., Li, H. Y., Willman, C. L., Appelbaum, F. R., & Zager, R. A. (2004). Cholesterol synthesis and import contribute to protective cholesterol increments in acute myeloid leukemia cells. *Blood*, *104*(6), 1816–1824. https://doi.org/10.1182/blood-2004-01-0395

Barbui, T., & Tefferi, A. (2012a). Myeloproliferative neoplasms. In *Springer eBooks*. https://doi.org/10.1007/978-3-642-24989-1

Basso-Valentina, F., Donada, A., Manchev, V. T., Lisetto, M., Balayn, N., Martin, J. E., Muller, D., Oyarzun, C. P. M., Duparc, H., Arkoun, B., Cumin, A., Faivre, L., Droin, N., Biunno, I., Pecci, A., Balduini, A., Debili, N., Antony-Debré, I., Marty, C., . . . Raslova, H. (2023). ANKRD26 is a new regulator of type I cytokine receptor signaling in normal and pathological hematopoiesis. *Haematologica*, *108*(8), 2130–2145. https://doi.org/10.3324/haematol.2022.282049

Baumeister, J., Chatain, N., Hubrich, A., Maié, T., Costa, I. G., Denecke, B., Han, L., Küstermann, C., Sontag, S., Seré, K., Strathmann, K., Zenke, M., Schuppert, A., Brümmendorf, T. H., Kranc, K. R., Koschmieder, S., & Gezer, D. (2019). Hypoxia-inducible factor 1 (HIF-1) is a new therapeutic target in JAK2V617F-positive myeloproliferative neoplasms. *Leukemia*, *34*(4), 1062–1074. https://doi.org/10.1038/s41375-019-0629-z

Beerman, I., Bhattacharya, D., Zandi, S., Sigvardsson, M., Weissman, I. L., Bryder, D., & Rossi, D. J. (2010). Functionally distinct hematopoietic stem cells modulate hematopoietic lineage potential during aging by a mechanism of clonal expansion. *Proceedings of the National Academy of Sciences*, *107*(12), 5465–5470. https://doi.org/10.1073/pnas.1000834107

Belmonte, M., Cabrera-Cosme, L., Øbro, N. F., Li, J., Grinfeld, J., Milek, J., Bennett, E., Irvine, M., Shepherd, M. S., Cull, A. H., Boyd, G., Riedel, L. M., Che, J. L. C., Oedekoven, C. A., Baxter, E. J., Green, A. R., Barlow, J. L., & Kent, D. G. (2024). Increased CXCL10 (IP-10) is associated with advanced myeloproliferative neoplasms and its loss dampens erythrocytosis in mouse models. *Experimental Hematology*, *135*, 104246. https://doi.org/10.1016/j.exphem.2024.104246

Bonelli, M., Kerschbaumer, A., Kastrati, K., Ghoreschi, K., Gadina, M., Heinz, L. X., Smolen, J. S., Aletaha, D., O'Shea, J., & Laurence, A. (2023). Selectivity, efficacy and safety of JAKinibs:

new evidence for a still evolving story. *Annals of the Rheumatic Diseases*, *83*(2), 139–160. https://doi.org/10.1136/ard-2023-223850
Borderon, L., Song, J., Kim, S. J., Marzac, C., Bellanné-Chantelot, C., Papadopoulos, N., Constantinescu, S. N., Vainchenker, W., Plo, I., Prchal, J. T., & Marty, C. (2023). An Atypical Somatic Calr Variant Acquired in Cis to a Germline Calr variant Induces Constitutive Signaling of the Thrombopoietin Receptor and Results in Essential Thrombocythemia. *Blood*, *142*(Supplement 1), 3161. https://doi.org/10.1182/blood-2023-179381
Borsani, O., Jäger, R., Pietra, D., Flieder, I., Riccaboni, G., Kralovics, R., & Rumi, E. (2024). Evaluation of the <i>ATM</i> L2307F germline variant in 121 Italian pedigrees with familial myeloproliferative neoplasms. *Haematologica*. https://doi.org/10.3324/haematol.2024.285539
Bumm, T. G., Elsea, C., Corbin, A. S., Loriaux, M., Sherbenou, D., Wood, L., Deininger, J., Silver, R. T., Druker, B. J., & Deininger, M. W. (2006a). Characterization of murine JAK2V617F-Positive myeloproliferative disease. *Cancer Research*, *66*(23), 11156–11165. https://doi.org/10.1158/0008-5472.can-06-2210
Burch, J. S., Marcero, J. R., Maschek, J. A., Cox, J. E., Jackson, L. K., Medlock, A. E., Phillips, J. D., & Dailey, H. A. (2018b). Glutamine via α-ketoglutarate dehydrogenase provides succinyl-CoA for heme synthesis during erythropoiesis. *Blood*, *132*(10), 987–998. https://doi.org/10.1182/blood-2018-01-829036
Chapeau, E. A., Mandon, E., Gill, J., Romanet, V., Ebel, N., Powajbo, V., Andraos-Rey, R., Qian, Z., Kininis, M., Zumstein-Mecker, S., Ito, M., Hynes, N. E., Tiedt, R., Hofmann, F., Eshkind, L., Bockamp, E., Kinzel, B., Mueller, M., Murakami, M., . . . Radimerski, T. (2019). A conditional inducible JAK2V617F transgenic mouse model reveals myeloproliferative disease that is reversible upon switching off transgene expression. *PLoS ONE*, *14*(10), e0221635. https://doi.org/10.1371/journal.pone.0221635
Chen, K., Liu, J., Heck, S., Chasis, J. A., An, X., & Mohandas, N. (2009). Resolving the distinct stages in erythroid differentiation based on dynamic changes in membrane protein expression during erythropoiesis. *Proceedings of the National Academy of Sciences*, *106*(41), 17413–17418. https://doi.org/10.1073/pnas.0909296106
Choi, Y., & Park, K. (2017a). Targeting glutamine metabolism for cancer treatment. *Biomolecules & Therapeutics*, *26*(1), 19–28. https://doi.org/10.4062/biomolther.2017.178
Collotta, D., Franchina, M. P., Carlucci, V., & Collino, M. (2023a). Recent advances in JAK inhibitors for the treatment of metabolic syndrome. *Frontiers in Pharmacology*, *14*. https://doi.org/10.3389/fphar.2023.1245535
Constantinescu, S. N., & Vainchenker, W. (2024). DNMT3A gates IFN-induced MPN HSC exhaustion. *Blood*, *143*(24), 2445–2446. https://doi.org/10.1182/blood.2024024448
Cui, Y., Riedlinger, G., Miyoshi, K., Tang, W., Li, C., Deng, C., Robinson, G. W., & Hennighausen, L. (2004a). Inactivation of Stat5 in Mouse Mammary Epithelium during Pregnancy Reveals Distinct Functions in Cell Proliferation, Survival, and Differentiation. *Molecular and Cellular Biology*, *24*(18), 8037–8047. https://doi.org/10.1128/mcb.24.18.8037-8047.2004
Dang, L., Yen, K., & Attar, E. (2016). IDH mutations in cancer and progress toward development of targeted therapeutics. *Annals of Oncology*, *27*(4), 599–608. https://doi.org/10.1093/annonc/mdw013
DeBerardinis, R. J., & Cheng, T. (2009a). Q's next: the diverse functions of glutamine in metabolism, cell biology and cancer. *Oncogene*, *29*(3), 313–324. https://doi.org/10.1038/onc.2009.358
DeBerardinis, R. J., Lum, J. J., Hatzivassiliou, G., & Thompson, C. B. (2008). The Biology of Cancer: Metabolic reprogramming fuels cell growth and proliferation. *Cell Metabolism*, *7*(1), 11–20. https://doi.org/10.1016/j.cmet.2007.10.002
DeBerardinis, R. J., Mancuso, A., Daikhin, E., Nissim, I., Yudkoff, M., Wehrli, S., & Thompson, C. B. (2007). Beyond aerobic glycolysis: Transformed cells can engage in glutamine metabolism that exceeds the requirement for protein and nucleotide synthesis. *Proceedings of the National Academy of Sciences*, *104*(49), 19345–19350. https://doi.org/10.1073/pnas.0709747104
Deed - Attribution 4.0 International - Creative Commons. (n.d.). https://creativecommons.org/licenses/by/4.0/
Dodington, D. W., Desai, H. R., & Woo, M. (2017a). JAK/STAT – Emerging Players in Metabolism. *Trends in Endocrinology and Metabolism*, *29*(1), 55–65. https://doi.org/10.1016/j.tem.2017.11.001
Döhner, H., Malcovati, L., Ossenkoppele, G. J., Hochhaus, A., Vannucchi, A. M., Bullinger, L., Cervantes, F., Craddock, C., De Witte, T., Döhner, K., Dombret, H., Fenaux, P., Geissler, J.,

Germing, U., Guilhot, F., Harrison, C., Hellström-Lindberg, E., Passamonti, F., Sierra, J., . . . Wierzbowska, A. (2021). The EHA Research Roadmap: Malignant Myeloid Diseases. *HemaSphere*, *5*(9), e635. https://doi.org/10.1097/hs9.0000000000000635

Doyle, A., McGarry, M. P., Lee, N. A., & Lee, J. J. (2011). The construction of transgenic and gene knockout/knockin mouse models of human disease. *Transgenic Research*, *21*(2), 327–349. https://doi.org/10.1007/s11248-011-9537-3

Duncavage, E. J., Bagg, A., Hasserjian, R. P., DiNardo, C. D., Godley, L. A., Iacobucci, I., Jaiswal, S., Malcovati, L., Vannucchi, A. M., Patel, K. P., Arber, D. A., Arcila, M. E., Bejar, R., Berliner, N., Borowitz, M. J., Branford, S., Brown, A. L., Cargo, C. A., Döhner, H., . . . Cazzola, M. (2022). Genomic profiling for clinical decision making in myeloid neoplasms and acute leukemia. *Blood*, *140*(21), 2228–2247. https://doi.org/10.1182/blood.2022015853

Dunn, W. G., McLoughlin, M. A., & Vassiliou, G. S. (2024a). Clonal hematopoiesis and hematological malignancy. *Journal of Clinical Investigation*, *134*(19). https://doi.org/10.1172/jci180065

Duparc, H., Muller, D., Gilles, L., Chédeville, A. L., Khoury, M. E., Guignard, R., Debili, N., Wittner, M., Kauskot, A., Pasquier, F., Antony-Debré, I., Marty, C., Vainchenker, W., Plo, I., & Raslova, H. (2024). Deregulation of the p19/CDK4/CDK6 axis in Jak2V617F megakaryocytes accelerates the development of myelofibrosis. *Leukemia*. https://doi.org/10.1038/s41375-024-02170-5

Durán, R. V., & Hall, M. N. (2012a). Glutaminolysis feeds mTORC1. *Cell Cycle*, *11*(22), 4107–4108. https://doi.org/10.4161/cc.22632

Dzierzak, E., & Bigas, A. (2018). Blood development: hematopoietic stem cell dependence and independence. *Cell Stem Cell*, *22*(5), 639–651. https://doi.org/10.1016/j.stem.2018.04.015

Emberley, E., Pan, A., Chen, J., Dang, R., Gross, M., Huang, T., Li, W., MacKinnon, A., Singh, D., Sotirovska, N., Steggerda, S. M., Wang, T., & Parlati, F. (2021a). The glutaminase inhibitor telaglenastat enhances the antitumor activity of signal transduction inhibitors everolimus and cabozantinib in models of renal cell carcinoma. *PLoS ONE*, *16*(11), e0259241. https://doi.org/10.1371/journal.pone.0259241

Fahy, E., Cotter, D., Sud, M., & Subramaniam, S. (2011). Lipid classification, structures and tools. *Biochimica Et Biophysica Acta (BBA) - Molecular and Cell Biology of Lipids*, *1811*(11), 637–647. https://doi.org/10.1016/j.bbalip.2011.06.009

Farahzadi, R., Fathi, E., Mesbah-Namin, S. A., & Vietor, I. (2023a). Granulocyte differentiation of rat bone marrow resident C-kit+ hematopoietic stem cells induced by mesenchymal stem cells could be considered as new option in cell-based therapy. *Regenerative Therapy*, *23*, 94–101. https://doi.org/10.1016/j.reth.2023.04.004

Feenstra, J. D. M., Jäger, R., Schischlik, F., Ivanov, D., Eisenwort, G., Rumi, E., Schuster, M., Gisslinger, B., Machherndl-Spandl, S., Bettelheim, P., Krauth, M., Keil, F., Bock, C., Cazzola, M., Gisslinger, H., Kralovics, R., & Valent, P. (2022). PD-L1 overexpression correlates with JAK2-V617F mutational burden and is associated with 9p uniparental disomy in myeloproliferative neoplasms. *American Journal of Hematology*, *97*(4), 390–400. https://doi.org/10.1002/ajh.26461

Feenstra, J. D. M., Rumi, E., Pietra, D., Schönegger, A., Bock, C., Cazzola, M., & Kralovics, R. (2015). Whole Exome sequencing reveals clonal evolution of myeloproliferative neoplasms to acute myeloid leukemia. *Blood*, *126*(23), 1626. https://doi.org/10.1182/blood.v126.23.1626.1626

Filippi, M., & Ghaffari, S. (2019a). Mitochondria in the maintenance of hematopoietic stem cells: new perspectives and opportunities. *Blood*, *133*(18), 1943–1952. https://doi.org/10.1182/blood-2018-10-808873

Folmes, C. D., Dzeja, P. P., Nelson, T. J., & Terzic, A. (2012). Metabolic plasticity in stem cell homeostasis and differentiation. *Cell Stem Cell*, *11*(5), 596–606. https://doi.org/10.1016/j.stem.2012.10.002

Furusawa, A., Sadashivaiah, K., Singh, Z. N., Civin, C. I., & Banerjee, A. (2015). Inefficient megakaryopoiesis in mouse hematopoietic stem–progenitor cells lacking T-bet. *Experimental Hematology*, *44*(3), 194-206.e17. https://doi.org/10.1016/j.exphem.2015.11.003

Gangat, N., Ajufo, H., Abdelmagid, M., Karrar, O., McCullough, K., Badar, T., Foran, J., Palmer, J., Alkhateeb, H., Mangaonkar, A., Kuykendall, A., Rampal, R. K., & Tefferi, A. (2023). IDH1/2 inhibitor monotherapy in blast-phase myeloproliferative neoplasms: A multicentre experience. *British Journal of Haematology*, *203*(3). https://doi.org/10.1111/bjh.19027

Gao, Q., Liang, X., Shaikh, A. S., Zang, J., Xu, W., & Zhang, Y. (2017). JAK/STAT signal transduction: promising attractive targets for immune, inflammatory and hematopoietic diseases. *Current Drug Targets*, *19*(5), 487–500. https://doi.org/10.2174/1389450117666161207163054

Gisslinger, H., Buxhofer-Ausch, V., Thaler, J., Schloegl, E., Gastl, G. A., Wolf, D., Kralovics, R., Gisslinger, B., Lechner, D., Strecker, K., Egle, A., Melchardt, T., Burgstaller, S., Willenbacher, E., Zoerer, M., Zahriychuk, O., Klade, C., & Greil, R. (2013). Efficacy and Safety of AOP2014/P1101, a novel, investigational Mono-Pegylated Proline-Interferon Alpha-2B, in patients with polycythemia Vera (PV): Update on 51 patients from the ongoing Phase I/II PeginVera study. *Blood*, *122*(21), 4046. https://doi.org/10.1182/blood.v122.21.4046.4046

Gisslinger, H., Kralovics, R., Gisslinger, B., Lechner, D., Buxhofer-Ausch, V., Strecker, K., Gastl, G., Willenbacher, E., Greil, R., Egle, A., Melchardt, T., Burgstaller, S., Schloegl, E., Tarmann, F., Zoerer, M., Klade, C., Zahriychuk, O., & Thaler, J. (2012). AOP2014, a Novel Peg-Proline-Interferon Alpha-2b with Improved Pharmacokinetic Properties, Is Safe and Well Tolerated and Shows Promising Efficacy in Patients with Polycythemia Vera (PV). *Blood*, *120*(21), 175. https://doi.org/10.1182/blood.v120.21.175.175

Goessling, W., North, T. E., Loewer, S., Lord, A. M., Lee, S., Stoick-Cooper, C. L., Weidinger, G., Puder, M., Daley, G. Q., Moon, R. T., & Zon, L. I. (2009). Genetic interaction of PGE2 and WNT signaling regulates developmental specification of stem cells and regeneration. *Cell*, *136*(6), 1136–1147. https://doi.org/10.1016/j.cell.2009.01.015

Green, A. (1995). Molecular pathogenesis of myeloproliferative disorders. *Clinical & Laboratory Haematology*, *17*(3), 295–297. https://doi.org/10.1111/j.1365-2257.1995.tb01264.x

Greenfield, G., McMullin, M. F., & Mills, K. (2021). Molecular pathogenesis of the myeloproliferative neoplasms. *Journal of Hematology & Oncology*, *14*(1). https://doi.org/10.1186/s13045-021-01116-z

Griner, L. N., McGraw, K. L., Johnson, J. O., List, A. F., & Reuther, G. W. (2012). JAK2-V617F-mediated signalling is dependent on lipid rafts and statins inhibit JAK2-V617F-dependent cell growth. *British Journal of Haematology*, *160*(2), 177–187. https://doi.org/10.1111/bjh.12103

Gross, M. I., Demo, S. D., Dennison, J. B., Chen, L., Chernov-Rogan, T., Goyal, B., Janes, J. R., Laidig, G. J., Lewis, E. R., Li, J., MacKinnon, A. L., Parlati, F., Rodriguez, M. L., Shwonek, P. J., Sjogren, E. B., Stanton, T. F., Wang, T., Yang, J., Zhao, F., & Bennett, M. K. (2014a). Antitumor activity of the glutaminase inhibitor CB-839 in Triple-Negative breast Cancer. *Molecular Cancer Therapeutics*, *13*(4), 890–901. https://doi.org/10.1158/1535-7163.mct-13-0870

Gu, Z., Liu, Y., Cai, F., Patrick, M., Zmajkovic, J., Cao, H., Zhang, Y., Tasdogan, A., Chen, M., Qi, L., Liu, X., Li, K., Lyu, J., Dickerson, K. E., Chen, W., Ni, M., Merritt, M. E., Morrison, S. J., Skoda, R. C., . . . Xu, J. (2019). Loss of EZH2 reprograms BCAA metabolism to drive leukemic transformation. *Cancer Discovery*, *9*(9), 1228–1247. https://doi.org/10.1158/2159-8290.cd-19-0152

Guerra, M., Pasquer, H., De Oliveira, R. D., Soret-Dulphy, J., Maslah, N., Zhao, L., Marcault, C., Cazaux, M., Gauthier, N., Verger, E., Parquet, N., Vainchenker, W., Raffoux, E., Giraudier, S., Cassinat, B., Kiladjian, J., & Benajiba, L. (2024). Comparative clinical and molecular landscape of primary and secondary myelofibrosis: Superior performance of MIPSS70+ v2.0 over MYSEC-PM. *American Journal of Hematology*, *99*(4), 741–744. https://doi.org/10.1002/ajh.27226

Guglielmelli, P., Nangalia, J., Green, A. R., & Vannucchi, A. M. (2014). CALR mutations in myeloproliferative neoplasms: Hidden behind the reticulum. *American Journal of Hematology*, *89*(5), 453–456. https://doi.org/10.1002/ajh.23678

Guo, Z., Liu, Y., Li, X., Huang, Y., Zhou, Z., & Yang, C. (2024). Reprogramming hematopoietic stem cell metabolism in lung cancer: glycolysis, oxidative phosphorylation, and the role of 2-DG. *Biology Direct*, *19*(1). https://doi.org/10.1186/s13062-024-00514-w

Hadzijusufovic, E., Keller, A., Berger, D., Greiner, G., Wingelhofer, B., Witzeneder, N., Ivanov, D., Pecnard, E., Nivarthi, H., Schur, F. K. M., Filik, Y., Kornauth, C., Neubauer, H. A., Müllauer, L., Tin, G., Park, J., De Araujo, E. D., Gunning, P. T., Hoermann, G., . . . Valent, P. (2020). STAT5 is Expressed in CD34+/CD38− Stem Cells and Serves as a Potential Molecular Target in Ph-Negative Myeloproliferative Neoplasms. *Cancers*, *12*(4), 1021. https://doi.org/10.3390/cancers12041021

Hartwell, K. A., Miller, P. G., Mukherjee, S., Kahn, A. R., Stewart, A. L., Logan, D. J., Negri, J. M., Duvet, M., Järås, M., Puram, R. V., Dancik, V., Al-Shahrour, F., Kindler, T., Tothova, Z., Chattopadhyay, S., Hasaka, T., Narayan, R., Dai, M., Huang, C., . . . Golub, T. R. (2013). Niche-based screening identifies small-molecule inhibitors of leukemia stem cells. *Nature Chemical Biology*, *9*(12), 840–848. https://doi.org/10.1038/nchembio.1367

He, A., Chen, X., Tan, M., Chen, Y., Lu, D., Zhang, X., Dean, J. M., Razani, B., & Lodhi, I. J. (2020). Acetyl-CoA Derived from Hepatic Peroxisomal β-Oxidation Inhibits Autophagy and Promotes

Steatosis via mTORC1 Activation. *Molecular Cell*, *79*(1), 30-42.e4. https://doi.org/10.1016/j.molcel.2020.05.007
Hensley, C. T., Wasti, A. T., & DeBerardinis, R. J. (2013a). Glutamine and cancer: cell biology, physiology, and clinical opportunities. *Journal of Clinical Investigation*, *123*(9), 3678–3684. https://doi.org/10.1172/jci69600
Herault, O., Hope, K. J., Deneault, E., Mayotte, N., Chagraoui, J., Wilhelm, B. T., Cellot, S., Sauvageau, M., Andrade-Navarro, M. A., Hébert, J., & Sauvageau, G. (2012a). A role for GPx3 in activity of normal and leukemia stem cells. *The Journal of Experimental Medicine*, *209*(5), 895–901. https://doi.org/10.1084/jem.20102386
Hermange, G., Rakotonirainy, A., Bentriou, M., Tisserand, A., El-Khoury, M., Girodon, F., Marzac, C., Vainchenker, W., Plo, I., & Cournède, P. (2022). Inferring the initiation and development of myeloproliferative neoplasms. *Proceedings of the National Academy of Sciences*, *119*(37). https://doi.org/10.1073/pnas.2120374119
Hu, X., Li, J., Fu, M., Zhao, X., & Wang, W. (2021a). The JAK/STAT signaling pathway: from bench to clinic. *Signal Transduction and Targeted Therapy*, *6*(1). https://doi.org/10.1038/s41392-021-00791-1
Huang, D., Chen, C., Xie, L., Yu, Z., & Zheng, J. (2019). Hematopoietic stem cell metabolism and stemness. *Blood Science*, *1*(1), 12–18. https://doi.org/10.1097/bs9.0000000000000012
Huang, R., Jaritz, M., Guenzl, P., Vlatkovic, I., Sommer, A., Tamir, I. M., Marks, H., Klampfl, T., Kralovics, R., Stunnenberg, H. G., Barlow, D. P., & Pauler, F. M. (2011). An RNA-SEQ strategy to detect the complete coding and Non-Coding transcriptome including Full-Length imprinted macro NCRNAs. *PLoS ONE*, *6*(11), e27288. https://doi.org/10.1371/journal.pone.0027288
Ito, K., Bonora, M., & Ito, K. (2018). Metabolism as master of hematopoietic stem cell fate. *International Journal of Hematology*, *109*(1), 18–27. https://doi.org/10.1007/s12185-018-2534-z
Ito, K., & Ito, K. (2016a). Metabolism and the control of cell fate decisions and stem cell renewal. *Annual Review of Cell and Developmental Biology*, *32*(1), 399–409. https://doi.org/10.1146/annurev-cellbio-111315-125134
Ito, K., & Ito, K. (2018). Hematopoietic stem cell fate through metabolic control. *Experimental Hematology*, *64*, 1–11. https://doi.org/10.1016/j.exphem.2018.05.005
Ivanov, D., Feenstra, J. D. M., Sadovnik, I., Herrmann, H., Peter, B., Willmann, M., Greiner, G., Slavnitsch, K., Hadzijusufovic, E., Rülicke, T., Dahlhoff, M., Hoermann, G., Machherndl-Spandl, S., Eisenwort, G., Fillitz, M., Sliwa, T., Krauth, M., Bettelheim, P., Sperr, W. R., . . . Valent, P. (2023). Phenotypic characterization of disease-initiating stem cells in JAK2- or CALR-mutated myeloproliferative neoplasms. *American Journal of Hematology*, *98*(5), 770–783. https://doi.org/10.1002/ajh.26889
Jaffredo, T., Balduini, A., Bigas, A., Bernardi, R., Bonnet, D., Canque, B., Charbord, P., Cumano, A., Delwel, R., Durand, C., Fibbe, W., Forrester, L., De Franceschi, L., Ghevaert, C., Gjertsen, B., Gottgens, B., Graf, T., Heidenreich, O., Hermine, O., . . . Schuringa, J. J. (2021). The EHA Research Roadmap: Normal hematopoiesis. *HemaSphere*, *5*(12), e669. https://doi.org/10.1097/hs9.0000000000000669
Jäger, R., Gisslinger, H., Fuchs, E., Bogner, E., Feenstra, J. D. M., Weinzierl, J., Schischlik, F., Gisslinger, B., Schalling, M., Zörer, M., Krejcy, K., Klade, C., & Kralovics, R. (2020). Germline genetic factors influence the outcome of interferon-α therapy in polycythemia vera. *Blood*, *137*(3), 387–391. https://doi.org/10.1182/blood.2020005792
Jak-Stat Signaling : From Basics to disease. (2012). https://doi.org/10.1007/978-3-7091-0891-8
James, C., Ugo, V., Couédic, J. L., Staerk, J., Delhommeau, F., Lacout, C., Garçon, L., Raslova, H., Berger, R., Bennaceur-Griscelli, A., Villeval, J. L., Constantinescu, S. N., Casadevall, N., & Vainchenker, W. (2005). A unique clonal JAK2 mutation leading to constitutive signalling causes polycythaemia vera. *Nature*, *434*(7037), 1144–1148. https://doi.org/10.1038/nature03546
Jia, R., Kutzner, L., Koren, A., Runggatscher, K., Májek, P., Müller, A. C., Schuster, M., Bock, C., Loizou, J. I., Kubicek, S., & Kralovics, R. (2021). High-throughput drug screening identifies the ATR-CHK1 pathway as a therapeutic vulnerability of CALR mutated hematopoietic cells. *Blood Cancer Journal*, *11*(7). https://doi.org/10.1038/s41408-021-00531-2
Kaneko, K., Furuyama, K., Aburatani, H., & Shibahara, S. (2009). Hypoxia induces erythroid-specific 5-aminolevulinate synthase expression in human erythroid cells through transforming growth factor-β signaling. *FEBS Journal*, *276*(5), 1370–1382. https://doi.org/10.1111/j.1742-4658.2009.06878.x

Kauffman, M., Kauffman, M., Traore, K., Zhu, H., Trush, M., Jia, Z., & Li, Y. (2016). MIToSOX-Based flow Cytometry for detecting mitochondrial ROS. *Reactive Oxygen Species*. https://doi.org/10.20455/ros.2016.865

Kiladjian, J., Klade, C., Georgiev, P., Krochmalczyk, D., Gercheva-Kyuchukova, L., Egyed, M., Dulicek, P., Illes, A., Pylypenko, H., Sivcheva, L., Mayer, J., Yablokova, V., Krejcy, K., Empson, V., Hasselbalch, H. C., Kralovics, R., Gisslinger, H., Kiladjian, J., Georgiev, P., . . . Gisslinger, H. (2022). Long-term outcomes of polycythemia vera patients treated with ropeginterferon Alfa-2b. *Leukemia*, *36*(5), 1408–1411. https://doi.org/10.1038/s41375-022-01528-x

Kinder, M., Wei, C., Shelat, S. G., Kundu, M., Zhao, L., Blair, I. A., & Puré, E. (2010). Hematopoietic stem cell function requires 12/15-lipoxygenase–dependent fatty acid metabolism. *Blood*, *115*(24), 5012–5022. https://doi.org/10.1182/blood-2009-09-243139

Klampfl, T., Harutyunyan, A., Berg, T., Gisslinger, B., Passamonti, F., Rumi, E., Pietra, D., Olcaydu, D., JäGer, R., Cazzola, M., Gisslinger, H., & Kralovics, R. (2010a). Chromosomal aberration network in myeloproliferative neoplasms. *Blood*, *116*(21), 318. https://doi.org/10.1182/blood.v116.21.318.318

Kobayashi, H., Watanuki, S., & Takubo, K. (2022). Approaches towards Elucidating the Metabolic Program of Hematopoietic Stem/Progenitor Cells. *Cells*, *11*(20), 3189. https://doi.org/10.3390/cells11203189

Kobayashi, H., Watanuki, S., & Takubo, K. (2023, January 5). *Hematopoietic stem cells and metabolic program*. https://encyclopedia.pub/entry/39779

Kocabas, F., Xie, L., Xie, J., Yu, Z., DeBerardinis, R. J., Kimura, W., Thet, S., Elshamy, A. F., Abouellail, H., Muralidhar, S., Liu, X., Chen, C., Sadek, H. A., Zhang, C. C., & Zheng, J. (2015). Hypoxic metabolism in human hematopoietic stem cells. *Cell & Bioscience*, *5*(1). https://doi.org/10.1186/s13578-015-0020-3

Kollmann, K., Warsch, W., Gonzalez-Arias, C., Nice, F. L., Avezov, E., Milburn, J., Li, J., Dimitropoulou, D., Biddie, S., Wang, M., Poynton, E., Colzani, M., Tijssen, M. R., Anand, S., McDermott, U., Huntly, B., & Green, T. (2016). A novel signalling screen demonstrates that CALR mutations activate essential MAPK signalling and facilitate megakaryocyte differentiation. *Leukemia*, *31*(4), 934–944. https://doi.org/10.1038/leu.2016.280

Kralovics, R., Passamonti, F., Liu, K., Teo, S., Bench, A., Tichelli, A., Lazzarino, M., Green, A. R., Cazzola, M., & Skoda, R. C. (2004). Loss of heterozygosity on chromosome 9P24 is the most frequent chromosomal aberration in polycythemia vera and idiopathic myelofibrosis. *Blood*, *104*(11), 2425. https://doi.org/10.1182/blood.v104.11.2425.2425

Krum, B., Huerta, N., Chiou, V., Welner, R., Patel, S. B., Nemkov, T., & Beaudin, A. E. (2023). Metabolic programming of hematopoietic stem cell function by prenatal folate. *Blood*, *142*(Supplement 1), 5. https://doi.org/10.1182/blood-2023-187431

Kubo, S., Nakayamada, S., Sakata, K., Kitanaga, Y., Ma, X., Lee, S., Ishii, A., Yamagata, K., Nakano, K., & Tanaka, Y. (2018). Janus kinase inhibitor Baricitinib modulates human innate and adaptive immune system. *Frontiers in Immunology*, *9*. https://doi.org/10.3389/fimmu.2018.01510

Kuntz, E. M., Baquero, P., Michie, A. M., Dunn, K., Tardito, S., Holyoake, T. L., Helgason, G. V., & Gottlieb, E. (2017a). Targeting mitochondrial oxidative phosphorylation eradicates therapy-resistant chronic myeloid leukemia stem cells. *Nature Medicine*, *23*(10), 1234–1240. https://doi.org/10.1038/nm.4399

Lacout, C., Pisani, D. F., Tulliez, M., Gachelin, F. M., Vainchenker, W., & Villeval, J. (2006a). JAK2V617F expression in murine hematopoietic cells leads to MPD mimicking human PV with secondary myelofibrosis. *Blood*, *108*(5), 1652–1660. https://doi.org/10.1182/blood-2006-02-002030

Lau, W., Dominicus, C., Hannah, R., Jones, A., Green, A., & Gottgens, B. (2013). JAK/ stat signalling during normal and pathological myelopoiesis with focus on erythropoiesis and megakaryopoiesis. *Experimental Hematology*, *41*(8), S70. https://doi.org/10.1016/j.exphem.2013.05.275

Lee, M. K., Al-Sharea, A., Dragoljevic, D., & Murphy, A. J. (2018). Hand of FATe: lipid metabolism in hematopoietic stem cells. *Current Opinion in Lipidology*, *29*(3), 240–245. https://doi.org/10.1097/mol.0000000000000500

Lee-Six, H., Friesgaard-Oebro, N., Shepherd, M., Grossmann, S., Dawson, K., Belmonte, M., Osborne, R., Martincorena, I., Arias, C. G., Grinfeld, J., Laurenti, E., Huntly, B., Stratton, M., Green, T., Kent, D., & Campbell, P. (2017). Barcoding of human haematopoietic stem and

progenitor cells by whole genome sequencing reveals clonal dynamics of haematopoiesis. *Experimental Hematology*, *53*, S42. https://doi.org/10.1016/j.exphem.2017.06.044
Li, H. Y., Appelbaum, F. R., Willman, C. L., Zager, R. A., & Banker, D. E. (2003). Cholesterol-modulating agents kill acute myeloid leukemia cells and sensitize them to therapeutics by blocking adaptive cholesterol responses. *Blood*, *101*(9), 3628–3634. https://doi.org/10.1182/blood-2002-07-2283
Li, J., Kent, D. G., Chen, E., & Green, A. R. (2011). Mouse models of myeloproliferative neoplasms: JAK of all grades. *Disease Models & Mechanisms*, *4*(3), 311–317. https://doi.org/10.1242/dmm.006817
Li, J., Spensberger, D., Ahn, J. S., Anand, S., Beer, P. A., Ghevaert, C., Chen, E., Forrai, A., Scott, L. M., Ferreira, R., Campbell, P. J., Watson, S. P., Liu, P., Erber, W. N., Huntly, B. J. P., Ottersbach, K., & Green, A. R. (2010). JAK2 V617F impairs hematopoietic stem cell function in a conditional knock-in mouse model of JAK2 V617F–positive essential thrombocythemia. *Blood*, *116*(9), 1528–1538. https://doi.org/10.1182/blood-2009-12-259747
Li, S., Kralovics, R., De Libero, G., Tichelli, A., & Skoda, R. C. (2007). Lineage Distribution of JAK2 Exon12 Mutations and JAK2-V617F in Patients with Polycythemia Vera. *Blood*, *110*(11), 1527. https://doi.org/10.1182/blood.v110.11.1527.1527
Liu, H., Wang, W., Chew, S. K., Lee, S. C., Li, J., Vassiliou, G. S., Green, T., Futreal, P. A., Bradley, A., Zhang, S., & Liu, P. (2011). Stella-Cre mice are highly efficient Cre deleters. *Genesis*, *49*(8), 689–695. https://doi.org/10.1002/dvg.20741
Liu, P., Cheng, H., Roberts, T. M., & Zhao, J. J. (2009). Targeting the phosphoinositide 3-kinase pathway in cancer. *Nature Reviews Drug Discovery*, *8*(8), 627–644. https://doi.org/10.1038/nrd2926
Liu, X., Zhang, Y., Ni, M., Cao, H., Signer, R. a. J., Li, D., Li, M., Gu, Z., Hu, Z., Dickerson, K. E., Weinberg, S. E., Chandel, N. S., DeBerardinis, R. J., Zhou, F., Shao, Z., & Xu, J. (2017). Regulation of mitochondrial biogenesis in erythropoiesis by mTORC1-mediated protein translation. *Nature Cell Biology*, *19*(6), 626–638. https://doi.org/10.1038/ncb3527
Lukes, J., Potuckova, E., Alquezar-Artieda, N., Hermanova, I., Kosanovic, S., Hlozkova, K., Jorda, M. A., Zuna, J., Trka, J., Tennant, D. A., Stanulla, M., Zaliova, M., & Starkova, J. (2023a). Chimeric JAK2 kinases trigger non-uniform changes of cellular metabolism in BCR-ABL1-like childhood ALL. *HemaSphere*, *7*(9), e946. https://doi.org/10.1097/hs9.0000000000000946
Lukes, J., Potuckova, E., Alquezar-Artieda, N., Hermanova, I., Kosanovic, S., Hlozkova, K., Jorda, M. A., Zuna, J., Trka, J., Tennant, D. A., Stanulla, M., Zaliova, M., & Starkova, J. (2023b). Chimeric JAK2 kinases trigger non-uniform changes of cellular metabolism in BCR-ABL1-like childhood ALL. *HemaSphere*, *7*(9), e946. https://doi.org/10.1097/hs9.0000000000000946
Lundberg, P., Karow, A., Nienhold, R., Looser, R., Hao-Shen, H., Nissen, I., Girsberger, S., Lehmann, T., Passweg, J., Stern, M., Beisel, C., Kralovics, R., & Skoda, R. C. (2014). Clonal evolution and clinical correlates of somatic mutations in myeloproliferative neoplasms. *Blood*, *123*(14), 2220–2228. https://doi.org/10.1182/blood-2013-11-537167
Man, J. C. (1983). MPN tables, corrected. *European Journal of Applied Microbiology and Biotechnology*, *17*(5), 301–305. https://doi.org/10.1007/bf00508025
Mansier, O., Kilani, B., Guitart, A. V., Guy, A., Gourdou-Latyszenok, V., Marty, C., Parrens, M., Plo, I., Vainchenker, W., & James, C. (2019). Description of a knock-in mouse model of JAK2V617F MPN emerging from a minority of mutated hematopoietic stem cells. *Blood*, *134*(26), 2383–2387. https://doi.org/10.1182/blood.2019001163
Marty, C., Lacout, C., Martin, A., Hasan, S., Jacquot, S., Birling, M., Vainchenker, W., & Villeval, J. (2010). Myeloproliferative neoplasm induced by constitutive expression of JAK2V617F in knock-in mice. *Blood*, *116*(5), 783–787. https://doi.org/10.1182/blood-2009-12-257063
Marubayashi, S., Koppikar, P., Taldone, T., Abdel-Wahab, O., West, N., Bhagwat, N., Caldas-Lopes, E., Ross, K. N., Gönen, M., Gozman, A., Ahn, J. H., Rodina, A., Ouerfelli, O., Yang, G., Hedvat, C., Bradner, J. E., Chiosis, G., & Levine, R. L. (2010). HSP90 is a therapeutic target in JAK2-dependent myeloproliferative neoplasms in mice and humans. *Journal of Clinical Investigation*, *120*(10), 3578–3593. https://doi.org/10.1172/jci42442
Maslah, N., Roux, B., Kaci, N., Verger, E., De Oliveira, R. D., Pasquer, H., Gauthier, N., Soret, J., Ganesan, S., Gou, P., Ling, F., Parquet, N., Vainchenker, W., Raffoux, E., Padua, R. A., Giraudier, S., Puissant, A., Lobry, C., Kiladjian, J., . . . Benajiba, L. (2022a). JAK inhibition mediates clonal selection of RAS pathway mutations in myeloproliferative neoplasms. *Blood*, *140*(Supplement 1), 795–796. https://doi.org/10.1182/blood-2022-167719

Matsuoka, Y., Sasaki, Y., Nakatsuka, R., Takahashi, M., Iwaki, R., Uemura, Y., & Sonoda, Y. (2011a). Low level of C-Kit expression marks deeply quiescent murine hematopoietic stem cells. *Stem Cells*, *29*(11), 1783–1791. https://doi.org/10.1002/stem.721

McLornan, D. P., Psaila, B., Ewing, J., Innes, A., Arami, S., Brady, J., Butt, N. M., Cargo, C., Cross, N. C. P., Francis, S., Frewin, R., Garg, M., Godfrey, A. L., Green, A., Khan, A., Knapper, S., Lambert, J., McGregor, A., McMullin, M. F., . . . Harrison, C. N. (2023). The management of myelofibrosis: A British Society for Haematology Guideline. *British Journal of Haematology*, *204*(1), 136–150. https://doi.org/10.1111/bjh.19186

Mead, A. J., Milojkovic, D., Knapper, S., Garg, M., Chacko, J., Farquharson, M., Yin, J., Ali, S., Clark, R. E., Andrews, C., Dawson, M. K., & Harrison, C. (2015). Response to ruxolitinib in patients with intermediate-1-, intermediate-2-, and high-risk myelofibrosis: results of the UK ROBUST Trial. *British Journal of Haematology*, *170*(1), 29–39. https://doi.org/10.1111/bjh.13379

Mead, A. J., & Mullally, A. (2017a). Myeloproliferative neoplasm stem cells. *Blood*, *129*(12), 1607–1616. https://doi.org/10.1182/blood-2016-10-696005

Mead, A. J., & Mullally, A. (2017b). Myeloproliferative neoplasm stem cells. *Blood*, *129*(12), 1607–1616. https://doi.org/10.1182/blood-2016-10-696005

Mead, A. J., Neo, W. H., Barkas, N., Matsuoka, S., Giustacchini, A., Facchini, R., Thongjuea, S., Jamieson, L., Booth, C. A., Fordham, N., Di Genua, C., Atkinson, D., Chowdhury, O., Repapi, E., Gray, N., Kharazi, S., Clark, S., Bouriez, T., Woll, P., . . . Jacobsen, S. E. W. (2017). Niche-mediated depletion of the normal hematopoietic stem cell reservoir by Flt3-ITD–induced myeloproliferation. *The Journal of Experimental Medicine*, *214*(7), 2005–2021. https://doi.org/10.1084/jem.20161418

Methods in molecular biology. (n.d.). Springer. http://www.springer.com/series/7651

Metzeler, K. H., Becker, H., Maharry, K., Radmacher, M. D., Kohlschmidt, J., Mrózek, K., Nicolet, D., Whitman, S. P., Wu, Y., Schwind, S., Powell, B. L., Carter, T. H., Wetzler, M., Moore, J. O., Kolitz, J. E., Baer, M. R., Carroll, A. J., Larson, R. A., Caligiuri, M. A., . . . Bloomfield, C. D. (2011). ASXL1 mutations identify a high-risk subgroup of older patients with primary cytogenetically normal AML within the ELN Favorable genetic category. *Blood*, *118*(26), 6920–6929. https://doi.org/10.1182/blood-2011-08-368225

Mistry, J. J., Bowles, K., & Rushworth, S. A. (2022a). HSC-derived fatty acid oxidation in steady-state and stressed hematopoiesis. *Experimental Hematology*, *117*, 1–8. https://doi.org/10.1016/j.exphem.2022.10.003

Morganti, C., Bonora, M., & Ito, K. (2019). Improving the accuracy of flow cytometric assessment of mitochondrial membrane potential in hematopoietic stem and progenitor cells through the inhibition of efflux pumps. *Journal of Visualized Experiments*, *149*. https://doi.org/10.3791/60057

Morganti, C., Cabezas-Wallscheid, N., & Ito, K. (2022a). Metabolic regulation of hematopoietic stem cells. *HemaSphere*, *6*(7), e740. https://doi.org/10.1097/hs9.0000000000000740

Morrison, S. J., & Scadden, D. T. (2014). The bone marrow niche for haematopoietic stem cells. *Nature*, *505*(7483), 327–334. https://doi.org/10.1038/nature12984

Mughal, T. I., Lion, T., Abdel-Wahab, O., Mesa, R., Scherber, R. M., Perrotti, D., Mauro, M., Verstovsek, S., Saglio, G., Van Etten, R. A., & Kralovics, R. (2018). Precision immunotherapy, mutational landscape, and emerging tools to optimize clinical outcomes in patients with classical myeloproliferative neoplasms. *Hematological Oncology*, *36*(5), 740–748. https://doi.org/10.1002/hon.2537

Mullally, A., Lane, S. W., Ball, B., Megerdichian, C., Okabe, R., Al-Shahrour, F., Paktinat, M., Haydu, J. E., Housman, E., Lord, A. M., Wernig, G., Kharas, M. G., Mercher, T., Kutok, J. L., Gilliland, D. G., & Ebert, B. L. (2010a). Physiological Jak2V617F Expression Causes a Lethal Myeloproliferative Neoplasm with Differential Effects on Hematopoietic Stem and Progenitor Cells. *Cancer Cell*, *17*(6), 584–596. https://doi.org/10.1016/j.ccr.2010.05.015

Mullally, A., Lane, S. W., Brumme, K., & Ebert, B. L. (2012a). Myeloproliferative neoplasm animal models. *Hematology/Oncology Clinics of North America*, *26*(5), 1065–1081. https://doi.org/10.1016/j.hoc.2012.07.007

Mullally, A., Poveromo, L., Schneider, R. K., Al-Shahrour, F., Lane, S. W., & Ebert, B. L. (2012). Distinct roles for long-term hematopoietic stem cells and erythroid precursor cells in a murine model of Jak2V617F-mediated polycythemia vera. *Blood*, *120*(1), 166–172. https://doi.org/10.1182/blood-2012-01-402396

Murakami, S., Barroca, V., Perié, L., Bravard, A., Bernardino-Sgherri, J., Tisserand, A., Devanand, C., Edmond, V., Magniez, A., Bento, S. T., Torres, C., Pasquier, F., Plo, I., Vainchenker, W., Villeval, J., Roméo, P., & Lewandowski, D. (2022). In vivo monitoring of polycythemia vera

development reveals carbonic anhydrase 1 as a potent therapeutic target. *Blood Cancer Discovery*, *3*(4), 285–297. https://doi.org/10.1158/2643-3230.bcd-21-0039

Murphy, A. J., Bijl, N., Yvan-Charvet, L., Welch, C. B., Bhagwat, N., Reheman, A., Wang, Y., Shaw, J. A., Levine, R. L., Ni, H., Tall, A. R., & Wang, N. (2013). Cholesterol efflux in megakaryocyte progenitors suppresses platelet production and thrombocytosis. *Nature Medicine*, *19*(5), 586–594. https://doi.org/10.1038/nm.3150

Nangalia, J., & Green, T. R. (2014). The evolving genomic landscape of myeloproliferative neoplasms. *Hematology*, *2014*(1), 287–296. https://doi.org/10.1182/asheducation-2014.1.287

Nieborowska-Skorska, M., Maifrede, S., Dasgupta, Y., Sullivan, K., Flis, S., Le, B. V., Solecka, M., Belyaeva, E. A., Kubovcakova, L., Nawrocki, M., Kirschner, M., Zhao, H., Prchal, J. T., Piwocka, K., Moliterno, A. R., Wasik, M., Koschmieder, S., Green, T. R., Skoda, R. C., & Skorski, T. (2017). Ruxolitinib-induced defects in DNA repair cause sensitivity to PARP inhibitors in myeloproliferative neoplasms. *Blood*, *130*(26), 2848–2859. https://doi.org/10.1182/blood-2017-05-784942

Øbro, N. F., Grinfeld, J., Belmonte, M., Irvine, M., Shepherd, M. S., Rao, T. N., Karow, A., Riedel, L. M., Harris, O. B., Baxter, E. J., Nangalia, J., Godfrey, A., Harrison, C. N., Li, J., Skoda, R. C., Campbell, P. J., Green, A. R., & Kent, D. G. (2020). Longitudinal cytokine profiling identifies GRO-A and EGF as potential biomarkers of disease progression in essential thrombocythemia. *HemaSphere*, *4*(3). https://doi.org/10.1097/hs9.0000000000000371

Oguro, H. (2019). The roles of cholesterol and its metabolites in normal and malignant hematopoiesis. *Frontiers in Endocrinology*, *10*. https://doi.org/10.3389/fendo.2019.00204

Oh, S. T., Verstovsek, S., Gupta, V., Platzbecker, U., Devos, T., Kiladjian, J., McLornan, D. P., Perkins, A., Fox, M. L., McMullin, M. F., Mead, A. J., Egyed, M., Mayer, J., Sacha, T., Kawashima, J., Huang, M., Strouse, B., & Mesa, R. (2024). Changes in bone marrow fibrosis during momelotinib or ruxolitinib therapy do not correlate with efficacy outcomes in patients with myelofibrosis. *eJHaem*. https://doi.org/10.1002/jha2.854

Orsini, M., Chateauvieux, S., Rhim, J., Gaigneaux, A., Cheillan, D., Christov, C., Dicato, M., Morceau, F., & Diederich, M. (2018). Sphingolipid-mediated inflammatory signaling leading to autophagy inhibition converts erythropoiesis to myelopoiesis in human hematopoietic stem/progenitor cells. *Cell Death and Differentiation*, *26*(9), 1796–1812. https://doi.org/10.1038/s41418-018-0245-x

Pasquer, H., De Oliveira, R. D., Soret, J., Maslah, N., Zhao, L., Marcault, C., Cazaux, M., Gauthier, N., Verger, E., Parquet, N., Vainchenker, W., Raffoux, E., Giraudier, S., Cassinat, B., Kiladjian, J., & Benajiba, L. (2022). Distinct Clinico-Molecular Arterial and Venous Thrombotic Scoring Systems for MPN Patients Risk Stratification. *Blood*, *140*(Supplement 1), 830–831. https://doi.org/10.1182/blood-2022-160329

Passegue, E., Wagers, A. J., Giuriato, S., Anderson, W. C., & Weissman, I. L. (2005). Global analysis of proliferation and cell cycle gene expression in the regulation of hematopoietic stem and progenitor cell fates. *The Journal of Experimental Medicine*, *202*(11), 1599–1611. https://doi.org/10.1084/jem.20050967

Paz, D. L., Ashcroft, P., & Skoda, R. C. (2021). Myeloproliferative neoplasms: The long wait for JAK2-Mutant clone expansion. *Cell Stem Cell*, *28*(3), 359–361. https://doi.org/10.1016/j.stem.2021.02.018

Paz, D. L., Bader, M. S., Nienhold, R., Rai, S., Fonseca, T. A., Stetka, J., Hao-Shen, H., Mild-Schneider, G., Passweg, J. R., & Skoda, R. C. (2023). Impact of clonal architecture on clinical course and prognosis in patients with myeloproliferative neoplasms. *HemaSphere*, *7*(5), e885. https://doi.org/10.1097/hs9.0000000000000885

Paz, D. L., Kralovics, R., & Skoda, R. C. (2022a). Genetic basis and molecular profiling in myeloproliferative neoplasms. *Blood*, *141*(16), 1909–1921. https://doi.org/10.1182/blood.2022017578

Pecquet, C., Papadopoulos, N., Balligand, T., Chachoua, I., Tisserand, A., Vertenoeil, G., Nédélec, A., Vertommen, D., Roy, A., Marty, C., Nivarthi, H., Defour, J., El-Khoury, M., Hug, E., Majoros, A., Xu, E., Zagrijtschuk, O., Fertig, T. E., Marta, D. S., . . . Constantinescu, S. N. (2022). Secreted mutant calreticulins as rogue cytokines in myeloproliferative neoplasms. *Blood*, *141*(8), 917–929. https://doi.org/10.1182/blood.2022016846

Pérez-Gómez, C., Campos-Sandoval, J. A., Alonso, F. J., Segura, J. A., Manzanares, E., Ruiz-Sánchez, P., González, M. E., Márquez, J., & Matés, J. M. (2005). Co-expression of glutaminase K and L isoenzymes in human tumour cells. *Biochemical Journal*, *386*(3), 535–542. https://doi.org/10.1042/bj20040996

Perry, S. W., Norman, J. P., Barbieri, J., Brown, E. B., & Gelbard, H. A. (2011a). Mitochondrial membrane potential probes and the proton gradient: a practical usage guide. *BioTechniques*, *50*(2), 98–115. https://doi.org/10.2144/000113610

Poulain, L., Sujobert, P., Zylbersztejn, F., Barreau, S., Stuani, L., Lambert, M., Palama, T. L., Chesnais, V., Birsen, R., Vergez, F., Farge, T., Chenevier-Gobeaux, C., Fraisse, M., Bouillaud, F., Debeissat, C., Herault, O., Récher, C., Lacombe, C., Fontenay, M., . . . Chapuis, N. (2017). High mTORC1 activity drives glycolysis addiction and sensitivity to G6PD inhibition in acute myeloid leukemia cells. *Leukemia*, *31*(11), 2326–2335. https://doi.org/10.1038/leu.2017.81

Prestipino, A., Emhardt, A. J., Aumann, K., O'Sullivan, D., Gorantla, S. P., Duquesne, S., Melchinger, W., Braun, L., Vuckovic, S., Boerries, M., Busch, H., Halbach, S., Pennisi, S., Poggio, T., Apostolova, P., Veratti, P., Hettich, M., Niedermann, G., Bartholomä, M., . . . Zeiser, R. (2018). Oncogenic JAK2 V617F causes PD-L1 expression, mediating immune escape in myeloproliferative neoplasms. *Science Translational Medicine*, *10*(429). https://doi.org/10.1126/scitranslmed.aam7729

Psaila, B., & Mead, A. J. (2019). Single-cell approaches reveal novel cellular pathways for megakaryocyte and erythroid differentiation. *Blood*, *133*(13), 1427–1435. https://doi.org/10.1182/blood-2018-11-835371

Psaila, B., Wang, G., Meira, A. R., Heuston, E. F., Li, R., O'Sullivan, J., Sousos, N., Anderson, S., Senis, Y., Weinberg, O. K., Calicchio, M. L., Iskander, D., Royston, D., Milojkovic, D., Roberts, I., Bodine, D. M., Thongjuea, S., & Mead, A. J. (2019). Single-cell analyses reveal aberrant pathways for megakaryocyte-biased hematopoiesis in myelofibrosis and identify mutant clone-specific targets. *bioRxiv (Cold Spring Harbor Laboratory)*. https://doi.org/10.1101/642819

Psaila, B., Wang, G., Rodriguez-Meira, A., Li, R., Heuston, E. F., Murphy, L., Yee, D., Hitchcock, I. S., Sousos, N., O'Sullivan, J., Anderson, S., Senis, Y. A., Weinberg, O. K., Calicchio, M. L., Iskander, D., Royston, D., Milojkovic, D., Roberts, I., Bodine, D. M., . . . Mead, A. J. (2020). Single-Cell analyses reveal Megakaryocyte-Biased hematopoiesis in myelofibrosis and identify mutant Clone-Specific targets. *Molecular Cell*, *78*(3), 477-492.e8. https://doi.org/10.1016/j.molcel.2020.04.008

Quintás-Cardama, A., Kantarjian, H., Pierce, S., Cortes, J., & Verstovsek, S. (2013). Prognostic model to identify patients with myelofibrosis at the highest risk of transformation to acute myeloid leukemia. *Clinical Lymphoma Myeloma & Leukemia*, *13*(3), 315-318.e2. https://doi.org/10.1016/j.clml.2013.01.001

Rai, S., Zhang, Y., Grockowiak, E., Kimmerlin, Q., Hansen, N., Stoll, C. B., Usart, M., Paz, D. L., Hao-Shen, H., Zhu, Y., Roux, J., Bader, M. S., Dirnhofer, S., Farady, C. J., Schroeder, T., Méndez-Ferrer, S., & Skoda, R. C. (2024). IL-1β promotes MPN disease initiation by favoring early clonal expansion of JAK2-mutant hematopoietic stem cells. *Blood Advances*. https://doi.org/10.1182/bloodadvances.2023011338

Rao, T. N., Hansen, N., Hilfiker, J., Rai, S., Majewska, J., Leković, D., Gezer, D., Andina, N., Galli, S., Cassel, T., Geier, F., Delezie, J., Nienhold, R., Hao-Shen, H., Beisel, C., Di Palma, S., Dimeloe, S., Trebicka, J., Wolf, D., . . . Skoda, R. C. (2019a). JAK2-mutant hematopoietic cells display metabolic alterations that can be targeted to treat myeloproliferative neoplasms. *Blood*, *134*(21), 1832–1846. https://doi.org/10.1182/blood.2019000162

Rao, T. N., Hansen, N., Stetka, J., Paz, D. L., Kalmer, M., Hilfiker, J., Endele, M., Ahmed, N., Kubovcakova, L., Rybarikova, M., Hao-Shen, H., Geier, F., Beisel, C., Dirnhofer, S., Schroeder, T., Brümmendorf, T. H., Wolf, D., Koschmieder, S., & Skoda, R. C. (2021a). JAK2-V617F and interferon-α induce megakaryocyte-biased stem cells characterized by decreased long-term functionality. *Blood*, *137*(16), 2139–2151. https://doi.org/10.1182/blood.2020005563

Ratajczak, M. Z., Lee, H., Wysoczynski, M., Wan, W., Marlicz, W., Laughlin, M. J., Kucia, M., Janowska-Wieczorek, A., & Ratajczak, J. (2010). Novel insight into stem cell mobilization-Plasma sphingosine-1-phosphate is a major chemoattractant that directs the egress of hematopoietic stem progenitor cells from the bone marrow and its level in peripheral blood increases during mobilization due to activation of complement cascade/membrane attack complex. *Leukemia*, *24*(5), 976–985. https://doi.org/10.1038/leu.2010.53

Reis, E., Buonpane, R., Celik, H., Marty, C., Lei, A., Jobe, F., Rupar, M., Zhang, Y., DiMatteo, D., Awdew, R., Vainchenker, W., Zhou, J., Hitchcock, I., Plo, I., Nastri, H., & Mayes, P. (2022). Discovery of INCA033989, a monoclonal antibody that selectively antagonizes mutant calreticulin oncogenic function in myeloproliferative neoplasms (MPNs). *Blood*, *140*(Supplement 1), 14–15. https://doi.org/10.1182/blood-2022-159435

Rimmelé, P., Liang, R., Bigarella, C. L., Kocabas, F., Xie, J., Serasinghe, M. N., Chipuk, J., Sadek, H., Zhang, C. C., & Ghaffari, S. (2015a). Mitochondrial metabolism in hematopoietic stem cells requires functional FOXO 3. *EMBO Reports*, *16*(9), 1164–1176. https://doi.org/10.15252/embr.201439704

Rivera, J., Proia, R. L., & Olivera, A. (2008). The alliance of sphingosine-1-phosphate and its receptors in immunity. *Nature Reviews. Immunology*, *8*(10), 753–763. https://doi.org/10.1038/nri2400

Rodriguez-Meira, A., Norfo, R., Wen, S., Chédeville, A. L., Rahman, H., O'Sullivan, J., Wang, G., Louka, E., Kretzschmar, W. W., Paterson, A., Brierley, C., Martin, J., Demeule, C., Bashton, M., Sousos, N., Moralli, D., Meem, L. S., Carrelha, J., Wu, B., . . . Mead, A. J. (2023). Single-cell multi-omics identifies chronic inflammation as a driver of TP53-mutant leukemic evolution. *Nature Genetics*, *55*(9), 1531–1541. https://doi.org/10.1038/s41588-023-01480-1

Rumi, E., Pietra, D., Ferretti, V., Klampfl, T., Harutyunyan, A. S., Milosevic, J. D., Them, N. C. C., Berg, T., Elena, C., Casetti, I. C., Milanesi, C., Sant'Antonio, E., Bellini, M., Fugazza, E., Renna, M. C., Boveri, E., Astori, C., Pascutto, C., Kralovics, R., & Cazzola, M. (2013). JAK2 or CALR mutation status defines subtypes of essential thrombocythemia with substantially different clinical course and outcomes. *Blood*, *123*(10), 1544–1551. https://doi.org/10.1182/blood-2013-11-539098

Samimi, A., Khodayar, M. J., Alidadi, H., & Khodadi, E. (2020). The dual role of ROS in hematological malignancies: stem cell protection and cancer cell metastasis. *Stem Cell Reviews and Reports*, *16*(2), 262–275. https://doi.org/10.1007/s12015-019-09949-5

Sanjuan-Pla, A., Macaulay, I. C., Jensen, C. T., Woll, P. S., Luis, T. C., Mead, A., Moore, S., Carella, C., Matsuoka, S., Jones, T. B., Chowdhury, O., Stenson, L., Lutteropp, M., Green, J. C. A., Facchini, R., Boukarabila, H., Grover, A., Gambardella, A., Thongjuea, S., . . . Jacobsen, S. E. W. (2013). Platelet-biased stem cells reside at the apex of the haematopoietic stem-cell hierarchy. *Nature*, *502*(7470), 232–236. https://doi.org/10.1038/nature12495

Seif, F., Khoshmirsafa, M., Aazami, H., Mohsenzadegan, M., Sedighi, G., & Bahar, M. (2017). The role of JAK-STAT signaling pathway and its regulators in the fate of T helper cells. *Cell Communication and Signaling*, *15*(1). https://doi.org/10.1186/s12964-017-0177-y

Seitz, G., Boehmler, A. M., Kanz, L., & Möhle, R. (2005). The role of sphingosine 1-Phosphate receptors in the trafficking of hematopoietic progenitor cells. *Annals of the New York Academy of Sciences*, *1044*(1), 84–89. https://doi.org/10.1196/annals.1349.011

Seneviratne, A. K., Xu, M., Henao, J. J. A., Fajardo, V. A., Hao, Z., Voisin, V., Xu, G. W., Hurren, R., Kim, S., MacLean, N., Wang, X., Gronda, M., Jeyaraju, D., Jitkova, Y., Ketela, T., Mullokandov, M., Sharon, D., Thomas, G., Chouinard-Watkins, R., . . . Schimmer, A. D. (2019). The mitochondrial transacylase, tafazzin, regulates AML stemness by modulating intracellular levels of phospholipids. *Cell Stem Cell*, *24*(4), 621-636.e16. https://doi.org/10.1016/j.stem.2019.02.020

Sevin, M., Kubovcakova, L., Pernet, N., Causse, S., Vitte, F., Villeval, J. L., Lacout, C., Cordonnier, M., Rodrigues-Lima, F., Chanteloup, G., Mosca, M., Chrétien, M., Bastie, J. N., Audia, S., Sagot, P., Ramla, S., Martin, L., Gleave, M., Mezger, V., . . . De Thonel, A. (2018). HSP27 is a partner of JAK2-STAT5 and a potential therapeutic target in myelofibrosis. *Nature Communications*, *9*(1). https://doi.org/10.1038/s41467-018-03627-9

Shah, M., Kumar, H., Qiu, S., Li, H., Harris, M., He, J., Abraham, A., Crossman, D. K., Paterson, A., Welner, R. S., & Bhatia, R. (2022). Low c-Kit expression identifies primitive, therapy-resistant CML stem cells. *JCI Insight*, *8*(1). https://doi.org/10.1172/jci.insight.157421

Sharma, V., Wright, K. L., Epling-Burnette, P. K., & Reuther, G. W. (2020). Metabolic vulnerabilities and epigenetic dysregulation in myeloproliferative neoplasms. *Frontiers in Immunology*, *11*. https://doi.org/10.3389/fimmu.2020.604142

Shawky, A. M., Almalki, F. A., Abdalla, A. N., Abdelazeem, A. H., & Gouda, A. M. (2022). A comprehensive overview of globally approved JAK inhibitors. *Pharmaceutics*, *14*(5), 1001. https://doi.org/10.3390/pharmaceutics14051001

Shi, X., Reinstadler, B., Shah, H., To, T., Byrne, K., Summer, L., Calvo, S. E., Goldberger, O., Doench, J. G., Mootha, V. K., & Shen, H. (2022a). Combinatorial GxGxE CRISPR screen identifies SLC25A39 in mitochondrial glutathione transport linking iron homeostasis to OXPHOS. *Nature Communications*, *13*(1). https://doi.org/10.1038/s41467-022-30126-9

Shide, K., Shimoda, H. K., Kumano, T., Karube, K., Kameda, T., Takenaka, K., Oku, S., Abe, H., Katayose, K. S., Kubuki, Y., Kusumoto, K., Hasuike, S., Tahara, Y., Nagata, K., Matsuda, T., Ohshima, K., Harada, M., & Shimoda, K. (2007). Development of ET, primary myelofibrosis

and PV in mice expressing JAK2 V617F. *Leukemia*, *22*(1), 87–95. https://doi.org/10.1038/sj.leu.2405043
Shin, J. Y., Hu, W., Naramura, M., & Park, C. Y. (2014). High c-Kit expression identifies hematopoietic stem cells with impaired self-renewal and megakaryocytic bias. *The Journal of Experimental Medicine*, *211*(2), 217–231. https://doi.org/10.1084/jem.20131128
Shlush, L. I., Mitchell, A., Heisler, L., Abelson, S., Ng, S. W. K., Trotman-Grant, A., Medeiros, J. J. F., Rao-Bhatia, A., Jaciw-Zurakowsky, I., Marke, R., McLeod, J. L., Doedens, M., Bader, G., Voisin, V., Xu, C., McPherson, J. D., Hudson, T. J., Wang, J. C. Y., Minden, M. D., & Dick, J. E. (2017). Tracing the origins of relapse in acute myeloid leukaemia to stem cells. *Nature*, *547*(7661), 104–108. https://doi.org/10.1038/nature22993
Sommerkamp, P., Altamura, S., Renders, S., Narr, A., Ladel, L., Zeisberger, P., Eiben, P. L., Fawaz, M., Rieger, M. A., Cabezas-Wallscheid, N., & Trumpp, A. (2020). Differential alternative polyadenylation landscapes mediate hematopoietic stem cell activation and regulate glutamine metabolism. *Cell Stem Cell*, *26*(5), 722-738.e7. https://doi.org/10.1016/j.stem.2020.03.003
Spivak, J. L. (2017). Myeloproliferative neoplasms. *New England Journal of Medicine*, *376*(22), 2168–2181. https://doi.org/10.1056/nejmra1406186
Stetka, J., & Skoda, R. C. (2021). Mouse models of myeloproliferative neoplasms for pre-clinical testing of novel therapeutic agents. *Biomedical Papers*, *165*(1), 26–33. https://doi.org/10.5507/bp.2021.004
Stetka, J., Usart, M., Kubovcakova, L., Rai, S., Rao, T. N., Sutter, J., Hao-Shen, H., Dirnhofer, S., Geier, F., Bader, M. S., Passweg, J. R., Manolova, V., Dürrenberger, F., Ahmed, N., Schroeder, T., Ganz, T., Nemeth, E., Silvestri, L., Nai, A.,Skoda, R. C. (2023). Iron is a modifier of the phenotypes of JAK2-mutant myeloproliferative neoplasms. *Blood*. https://doi.org/10.1182/blood.2022017976
Suda, T., Takubo, K., & Semenza, G. L. (2011). Metabolic regulation of hematopoietic stem cells in the hypoxic niche. *Cell Stem Cell*, *9*(4), 298–310. https://doi.org/10.1016/j.stem.2011.09.010
Sun, X., Cao, B., Naval-Sanchez, M., Pham, T., Sun, Y. B. Y., Williams, B., Heazlewood, S. Y., Deshpande, N., Li, J., Kraus, F., Rae, J., Nguyen, Q., Yari, H., Schröder, J., Heazlewood, C. K., Fulton, M., Hatwell-Humble, J., Gupta, K. D., Kapetanovic, R., . . . Nilsson, S. K. (2021). Nicotinamide riboside attenuates age-associated metabolic and functional changes in hematopoietic stem cells. *Nature Communications*, *12*(1). https://doi.org/10.1038/s41467-021-22863-0
Takubo, K., Nagamatsu, G., Kobayashi, C. I., Nakamura-Ishizu, A., Kobayashi, H., Ikeda, E., Goda, N., Rahimi, Y., Johnson, R. S., Soga, T., Hirao, A., Suematsu, M., & Suda, T. (2013). Regulation of glycolysis by PDK functions as a metabolic checkpoint for cell cycle quiescence in hematopoietic stem cells. *Cell Stem Cell*, *12*(1), 49–61. https://doi.org/10.1016/j.stem.2012.10.011
Tefferi, A., Ianotto, J., Mathews, V., Samuelsson, J., Szuber, N., Xiao, Z., & Hokland, P. (2022). Myeloproliferative neoplasms – a global view. *British Journal of Haematology*, *198*(6), 953–964. https://doi.org/10.1111/bjh.18213
Thomas, S. J., Snowden, J. A., Zeidler, M. P., & Danson, S. J. (2015). The role of JAK/STAT signalling in the pathogenesis, prognosis and treatment of solid tumours. *British Journal of Cancer*, *113*(3), 365–371. https://doi.org/10.1038/bjc.2015.233
Thorsten, K., Gisslinger, H., Harutyunyan, A. S., Nivarthi, H., Rumi, E., Milosevic, J. D., Them, N. C., Berg, T., Gisslinger, B., Pietra, D., Chen, D., Vladimer, G. I., Bagienski, K., Milanesi, C., Casetti, I. C., Sant'Antonio, E., Ferretti, V., Elena, C., Schischlik, F., . . . Kralovics, R. (2013). Frequent mutations in the calreticulin gene CALR in myeloproliferative neoplasms. *Blood*, *122*(21), LBA-https://doi.org/10.1182/blood.v122.21.lba-1.lba-1
Tiedt, R., Hao-Shen, H., Sobas, M. A., Looser, R., Dirnhofer, S., Schwaller, J., & Skoda, R. C. (2007). Ratio of mutant JAK2-V617F to wild-type Jak2 determines the MPD phenotypes in transgenic mice. *Blood*, *111*(8), 3931–3940. https://doi.org/10.1182/blood-2007-08-107748
Tripolt, S., Porpaczy, E. A., Hoelbl-Kovacic, A., Gisslinger, B., Bago-Horvath, Z., Casanova, E., Decker, T., Fux, D., Heller, G., Herkner, H., Kolbe, T., Kornauth, C., Mueller, M., Prchal-Murphy, M., Schiefer, A. I., Schneckenleithner, C., Skrabs, C., Sperr, W. R., Staber, P. B., . . . Gisslinger, H. (2017). JAK2-Inhibitor Therapy Associated lymphomas in myelofibrosis: distinct Clinico-Pathological features recapitulated in a mouse model. *Blood*, *130*, 1643. https://doi.org/10.1182/blood.v130.suppl_1.1643.1643
Tyner, J. W., Bumm, T. G., Deininger, J., Wood, L., Aichberger, K. J., Loriaux, M. M., Druker, B. J., Burns, C. J., Fantino, E., & Deininger, M. W. (2010). CYT387, a novel JAK2 inhibitor, induces

hematologic responses and normalizes inflammatory cytokines in murine myeloproliferative neoplasms. *Blood*, *115*(25), 5232–5240. https://doi.org/10.1182/blood-2009-05-223727
Usart, M., Hansen, N., Stetka, J., Fonseca, T. A., Guy, A., Kimmerlin, Q., Rai, S., Hao-Shen, H., Roux, J., Dirnhofer, S., & Skoda, R. C. (2024a). The glutaminase inhibitor CB-839 targets metabolic dependencies of JAK2-mutant hematopoiesis in MPN. *Blood Advances*, *8*(9), 2312–2325. https://doi.org/10.1182/bloodadvances.2023010950
Usart, M., Stetka, J., Paz, D. L., Hansen, N., Kimmerlin, Q., Fonseca, T. A., Lock, M., Kubovcakova, L., Karjalainen, R., Hao-Shen, H., Börsch, A., Taher, A. E., Schulz, J., Leroux, J., Dirnhofer, S., & Skoda, R. C. (2024). Loss of Dnmt3a increased self-renewal and resistance to pegIFNα in JAK2-V617F-positive myeloproliferative neoplasms. *Blood*. https://doi.org/10.1182/blood.2023020270
Vainchenker, W., Delhommeau, F., Constantinescu, S. N., & Bernard, O. A. (2011). New mutations and pathogenesis of myeloproliferative neoplasms. *Blood*, *118*(7), 1723–1735. https://doi.org/10.1182/blood-2011-02-292102
Vainchenker, W., & Kralovics, R. (2016). Genetic basis and molecular pathophysiology of classical myeloproliferative neoplasms. *Blood*, *129*(6), 667–679. https://doi.org/10.1182/blood-2016-10-695940
Vainchenker, W., Yahmi, N., Havelange, V., Marty, C., Plo, I., & Constantinescu, S. N. (2023). Recent advances in therapies for primary myelofibrosis. *Faculty Reviews*, *12*. https://doi.org/10.12703/r/12-23
Verstovsek, S., & Tefferi, A. (2010). Myeloproliferative neoplasms. In *Humana Press eBooks*. https://doi.org/10.1007/978-1-60761-266-7
Vetrie, D., Helgason, G. V., & Copland, M. (2020). The leukaemia stem cell: similarities, differences and clinical prospects in CML and AML. *Nature Reviews. Cancer*, *20*(3), 158–173. https://doi.org/10.1038/s41568-019-0230-9
Warr, M. R., Binnewies, M., Flach, J., Reynaud, D., Garg, T., Malhotra, R., Debnath, J., & Passegué, E. (2013). FOXO3A directs a protective autophagy program in haematopoietic stem cells. *Nature*, *494*(7437), 323–327. https://doi.org/10.1038/nature11895
Watanuki, S., Kobayashi, H., Sugiura, Y., Yamamoto, M., Karigane, D., Shiroshita, K., Sorimachi, Y., Fujita, S., Morikawa, T., Koide, S., Oshima, M., Nishiyama, A., Murakami, K., Haraguchi, M., Tamaki, S., Yamamoto, T., Yabushita, T., Tanaka, Y., Nagamatsu, G., . . . Takubo, K. (2023). Context-dependent modification of PFKFB3 in hematopoietic stem cells promotes anaerobic glycolysis and ensures stress hematopoiesis. *eLife*, *12*. https://doi.org/10.7554/elife.87674
Weigert, O., Lane, A. A., Bird, L., Kopp, N., Chapuy, B., Van Bodegom, D., Toms, A. V., Marubayashi, S., Christie, A. L., McKeown, M., Paranal, R. M., Bradner, J. E., Yoda, A., Gaul, C., Vangrevelinghe, E., Romanet, V., Murakami, M., Tiedt, R., Ebel, N., . . . Weinstock, D. M. (2012). Genetic resistance to JAK2 enzymatic inhibitors is overcome by HSP90 inhibition. *The Journal of Experimental Medicine*, *209*(2), 259–273. https://doi.org/10.1084/jem.20111694
Wen, Q. J., Yang, Q., Goldenson, B., Malinge, S., Lasho, T., Schneider, R. K., Breyfogle, L. J., Schultz, R., Gilles, L., Koppikar, P., Abdel-Wahab, O., Pardanani, A., Stein, B., Gurbuxani, S., Mullally, A., Levine, R. L., Tefferi, A., & Crispino, J. D. (2015). Targeting megakaryocytic-induced fibrosis in myeloproliferative neoplasms by AURKA inhibition. *Nature Medicine*, *21*(12), 1473–1480. https://doi.org/10.1038/nm.3995
Wernig, G., Kharas, M. G., Okabe, R., Moore, S. A., Leeman, D. S., Cullen, D. E., Gozo, M., McDowell, E. P., Levine, R. L., Doukas, J., Mak, C. C., Noronha, G., Martin, M., Ko, Y. D., Lee, B. H., Soll, R. M., Tefferi, A., Hood, J. D., & Gilliland, D. G. (2008). Efficacy of TG101348, a selective JAK2 inhibitor, in treatment of a murine model of JAK2V617F-Induced polycythemia Vera. *Cancer Cell*, *13*(4), 311–320. https://doi.org/10.1016/j.ccr.2008.02.009
Wernig, G., Mercher, T., Okabe, R., Levine, R. L., Lee, B. H., & Gilliland, D. G. (2006a). Expression of Jak2V617F causes a polycythemia vera–like disease with associated myelofibrosis in a murine bone marrow transplant model. *Blood*, *107*(11), 4274–4281. https://doi.org/10.1182/blood-2005-12-4824
Westerterp, M., Gourion-Arsiquaud, S., Murphy, A. J., Shih, A., Cremers, S., Levine, R. L., Tall, A. R., & Yvan-Charvet, L. (2012). Regulation of hematopoietic stem and progenitor cell mobilization by cholesterol efflux pathways. *Cell Stem Cell*, *11*(2), 195–206. https://doi.org/10.1016/j.stem.2012.04.024
Wildschut, M. H. E., Mena, J., Dördelmann, C., Van Oostrum, M., Hale, B. D., Settelmeier, J., Festl, Y., Lysenko, V., Schürch, P. M., Ring, A., Severin, Y., Bader, M. S., Pedrioli, P. G. A., Goetze, S., Van Drogen, A., Balabanov, S., Skoda, R. C., Lopes, M., Wollscheid, B., . . . Snijder, B.

(2023). Proteogenetic drug response profiling elucidates targetable vulnerabilities of myelofibrosis. *Nature Communications*, *14*(1). https://doi.org/10.1038/s41467-023-42101-z
Willekens, C., Laplane, L., Dagher, T., Benlabiod, C., Papadopoulos, N., Lacout, C., Rameau, P., Catelain, C., Alfaro, A., Edmond, V., Signolle, N., Marchand, V., Droin, N., Hoogenboezem, R., Schneider, R. K., Penson, A., Abdel-Wahab, O., Giraudier, S., Pasquier, F., . . . Solary, E. (2023). SRSF2-P95H decreases JAK/STAT signaling in hematopoietic cells and delays myelofibrosis development in mice. *Leukemia*, *37*(6), 1287–1297. https://doi.org/10.1038/s41375-023-01878-0
Wills, Q. F., & Mead, A. J. (2015). Application of single-cell genomics in cancer: promise and challenges. *Human Molecular Genetics*, *24*(R1), R74–R84. https://doi.org/10.1093/hmg/ddv235
Wisniewski, D., Affer, M., Willshire, J., & Clarkson, B. (2011). Further phenotypic characterization of the primitive lineage− CD34+CD38−CD90+CD45RA− hematopoietic stem cell/progenitor cell sub-population isolated from cord blood, mobilized peripheral blood and patients with chronic myelogenous leukemia. *Blood Cancer Journal*, *1*(9), e36. https://doi.org/10.1038/bcj.2011.35
Wolf, D., & Pircher, A. (2024a). Targeting metabolic dependencies in JAK2-V617F–driven MPNs. *Blood Advances*, *8*(9), 2310–2311. https://doi.org/10.1182/bloodadvances.2024012837
Xing, S., Wanting, T. H., Zhao, W., Ma, J., Wang, S., Xu, X., Li, Q., Fu, X., Xu, M., & Zhao, Z. J. (2008). Transgenic expression of JAK2V617F causes myeloproliferative disorders in mice. *Blood*, *111*(10), 5109–5117. https://doi.org/10.1182/blood-2007-05-091579
Xu, Y., Anjaneyulu, M., Donelian, A., Yu, W., Greenberg, M. L., Ren, M., Owusu-Ansah, E., & Schlame, M. (2019). Assembly of the complexes of oxidative phosphorylation triggers the remodeling of cardiolipin. *Proceedings of the National Academy of Sciences*, *116*(23), 11235–11240. https://doi.org/10.1073/pnas.1900890116
Yan, D., Hutchison, R. E., & Mohi, G. (2011). Critical requirement for Stat5 in a mouse model of polycythemia vera. *Blood*, *119*(15), 3539–3549. https://doi.org/10.1182/blood-2011-03-345215
Yang, F., Nourse, C., Helgason, G. V., & Kirschner, K. (2023). Unraveling heterogeneity in the aging hematopoietic stem cell compartment: An insight from single-cell approaches. *HemaSphere*, *7*(6), e895. https://doi.org/10.1097/hs9.0000000000000895
Yvan-Charvet, L., Pagler, T., Gautier, E. L., Avagyan, S., Siry, R. L., Han, S., Welch, C. L., Wang, N., Randolph, G. J., Snoeck, H. W., & Tall, A. R. (2010). ATP-Binding cassette transporters and HDL suppress hematopoietic stem cell proliferation. *Science*, *328*(5986), 1689–1693. https://doi.org/10.1126/science.1189731
Zaleskas, V. M., Krause, D. S., Lazarides, K., Patel, N., Hu, Y., Li, S., & Van Etten, R. A. (2006a). Molecular pathogenesis and therapy of polycythemia induced in mice by JAK2 V617F. *PLoS ONE*, *1*(1), e18. https://doi.org/10.1371/journal.pone.0000018
Zenobi, R. (2013). Single-Cell Metabolomics: Analytical and Biological perspectives. *Science*, *342*(6163). https://doi.org/10.1126/science.1243259
Zhang, Y., Gao, S., Xia, J., & Liu, F. (2018). Hematopoietic Hierarchy – an updated roadmap. *Trends in Cell Biology*, *28*(12), 976–986. https://doi.org/10.1016/j.tcb.2018.06.001
Zhang, Y. W., Schönberger, K., & Cabezas-Wallscheid, N. (2023). Bidirectional interplay between metabolism and epigenetics in hematopoietic stem cells and leukemia. *The EMBO Journal*, *42*(24). https://doi.org/10.15252/embj.2022112348